NASA Contractor Report 177645

A High-Performance Constant-Temperature Hot-Wire Anemometer

Jonathan H. Watmuff

MCAT Institute
3933 Blue Gum Dr.
San Jose, CA 95127

Prepared for
Ames Research Center
CONTRACT NCC2-698
August 1994

National Aeronautics and
Space Administration

Ames Research Center
Moffett Field, California 94035-1000

TABLE OF CONTENTS

NOMENCLATURE

$A_j(s)$	Polynomial for Zeros of amplifier j
$B_j(s)$	Polynomial for Poles of amplifier j
c	Temperature coefficient of resistivity of wire filament
C_b	Balance capacitor
C_w	Lumped capacitor for modeling probe cable capacitance
d	Diameter of wire filament
ϵ_i	Small perturbation input voltage
ϵ_o	Small perturbation output voltage
ϵ_S	Small perturbation offset voltage
ϵ_{wire}	Small perturbation voltage across wire
ϵ_w	Small perturbation voltage across wire arm of bridge
E_{off}	Offset voltage of output amplifier
E_{o_n}	d.c. output of n^{th} amplifier (see figure 5.1)
E_{qi}	d.c. component of offset voltage
f_A	Frequency response of feedback amplifier
f_o	Frequency response of system
$F_u(s)$	Normalized frequency response of wire for velocity
G	Gain of output amplifier
I_1, I_2	d.c. bridge currents (see figure 5.1)
i_1, i_2	Bridge current fluctuations
K	Overall Gain of feedback amplifier
K_a	Gain of first equivalent amplifier
K_b	Gain of second equivalent amplifier
K_g	Thermal conductivity of fluid
l	Length of wire filament
L_b	Balance inductor
L_{b0}	L_b for a.c. balance $= (R_c/R_a)L_w$
L_w	Lumped inductor for modeling probe cable inductance
M, M_1, M_2, M_3	Time constants of the feedback amplifier
Nu	Nusselt number
$P(s)$	Polynomial for system Poles
$Q_e(s)$	Polynomial for system Zeros for Offset Voltage perturbations
$Q_u(s)$	Polynomial for system Zeros for Velocity perturbations
R	Resistance ratio $= R_w/R_g$
R_a, R_b, R_c	Resistive components of $Z_a(s)$, $Z_b(s)$ and $Z_c(s)$
R_g	Cold resistance of wire filament
R_w	Hot resistance of wire filament
R_{wa}	Asymptotic value of R_w as $E_{qi} \rightarrow 0$
$\overset{\circ}{\text{R}}$	Bridge imbalance$=R_wR_c - R_aR_b$
s	Laplace variable $s = \sigma + j\omega$
S_u	d.c. sensitivity to velocity fluctuations

T_w	Lumped time constant of hot-wire filament
u	Small perturbation velocity
U	Steady component of velocity
$Z_a(s)$, $Z_b(s)$, $Z_c(s)$	Bridge impedances (see fig 5.1)
$Z_p(s)$	Impedance in parallel with wire and $Z_s(s)$
$Z_s(s)$	Impedance in series with wire
$Z_w(s)$	Total impedance of wire arm of bridge
$Z_{wire}(s)$	Impedance of wire
$Z_1(s)$, $Z_2(s)$, $Z_3(s)$	Polynomials appearing in system transfer functions
α	$= R_w(R_w - R_g)/R_g$
σ	Real component of s
ω	Imaginary component of s
τ_o	System time constant
τ_r	Period of square-wave response oscillations
ζ	Damping of complex conjugate poles given by $(T^2s^2 + 2\zeta Ts + 1)$

SUMMARY

A high-performance constant-temperature hot-wire anemometer has been designed based on a system theory analysis that can be extended to arbitrary order. A motivating factor behind the design was to achieve the highest possible frequency response while ensuring overall system stability. Based on these considerations, the design of the circuit and the selection of components is discussed in depth. Basic operating instructions are included in an operator's guide. The analysis is used to identify operating modes, observed in all anemometers, that are misleading, in the sense that the operator can be deceived by interpreting an erroneous frequency response. Unlike other anemometers, this instrument provides front panel access to all the circuit parameters which affect system stability and frequency response. Instructions are given on how to identify and avoid these rather subtle and undesirable operating modes by appropriate adjustment of the controls. Details, such as fabrication drawings and a parts list, are provided to enable the instrument to be constructed by others.

ACKNOWLEDGMENTS

The development and construction of the constant-temperature hot-wire anemometer described in this Contractor's Report was supported by the Fluid Mechanics Laboratory (FML) Branch of NASA Ames Research Center. The project was initiated at the insistence of Dr. R.V. Westphal. Mr. James Fogarty and Mr. Stanley Mason of Raman Aeronautics were responsible for the layout and testing of prototypes as well as the final PCB and chassis and for sorting out problems when production instruments were delivered. Feedback resulting from testing was received from members of the FML including Dr. James Bell, Dr. Rabindra Mehta and Mr. Gregory Zilliac. Dr. Bell assumed responsibility for the project while the author was absent for short periods. Mr. Zilliac's help with the ordering of components, arranging for their storage and delivery to vendors for fabrication is much appreciated. Mr. Michael Stock of code ETI negotiated the pricing and oversaw the fabrication. His professional approach and knowledge were indispensable along with his promptness in dealing with last minute changes and other issues that arose during the fabrication phase. The help of Stefan Long, an undergraduate engineering student at Santa Clara University, and Tara Naughton, a summer student supported by the Sharp Program, were greatly appreciated during the preliminary testing phase when the first batch of twenty anemometers were delivered. Special thanks must go to the Branch Chief, Dr. Sanford Davis, for supporting the project at the outset and for continued support during the design stage when it appeared that the development cycle would never converge.

1. BACKGROUND

A hot-wire anemometer is an electronic device which passes an electric current through a fine filament which is exposed to the flow. The filament consists of a material which possesses a temperature coefficient of resistivity i.e. as the temperature changes, so also does the resistance and hence the Joule heating. The variation of resistance is used to generate signals which are related to the flow velocity or temperature. The instrument is therefore a thermal transducer which is capable of measuring instantaneous velocities and/or temperatures.

There are two modes of operation of a hot-wire system. The first mode is called the *constant current* mode in which the wire current is kept very nearly constant. The variations in wire temperature (and hence wire resistance) caused by the flow are measured by monitoring the voltage drop across the filament. The second mode is called the *constant temperature* mode. The filament is placed in a Wheatstone bridge and a feedback amplifier is used to maintain the wire at very nearly constant resistance (and hence temperature). Fluctuations in the cooling of the filament cause fluctuations in the wire current which lead to voltage fluctuations which are measured at the top of the bridge. As the title suggests, this report is solely concerned with the constant temperature mode of operation.

Many workers have the preconceived idea that the hot-wire technique is fully developed and that useful measurements can be obtained by simply purchasing a commercially available system and following the instruction manuals. After all the instrument has been used for more than 50 years and the operating principle appears to be quite simple. However this attitude is rather naive and it can often lead to inconsistent measurements or results that differ from those obtained by others elsewhere in supposedly identical flows. One source for this disparity is that hot-wire measurements are indirect in the sense that variation in fluid flow properties are translated into electrical signals via a rather complicated heat transfer process which is not yet completely understood. Furthermore, the filament has thermal inertia with an associated time constant. The electronic circuitry also has its own set of time constants and complicated interactions can occur between the filament and the circuitry. In summary, the hot-wire anemometer is a complex instrument and departures from correct operation can be insidious and subtle in nature.

In the late 1960s low-cost high-performance integrated circuit amplifiers became widely available and it became relatively simple and inexpensive to construct in-house constant-temperature hot-wire anemometers. One example of these 'new' anemometer designs was implemented at the University of Melbourne, based on the ideas of Perry and Morrison (1971). The motivation for building these instruments was because of the cost of, and the anomalous data obtained with, commercially available instruments. The results of various tests and other observations provided convincing evidence that the behavior of this particular design was thoroughly understood. In the first year of his Ph.D. (1976) the author undertook the task of updating this design e.g. by utilizing up-to-date amplifiers which offered higher performance. During the course of this exercise many phenomena were observed that were inexplicable in terms of existing theories. These phenomena were identified as being of higher than the model of Perry and Morrison. Fortunately they could

be recognized during a square-wave test. The operating point could then be changed by adjusting the anemometer controls so that these undesirable phenomena could be avoided.

While at Princeton University during 1986-87 the author worked on methods for increasing the frequency response of this type of anemometer design for use in supersonic flow. A frequency response requirement of 500 kHz is not uncommon in these high speed flows e.g. to maintain a spatial resolution of 1mm when the mean velocity is 500 m/s. Yet with extremely careful tuning of the system controls by the most highly-skilled operators and under the most favorable of circumstances a barely adequate frequency response of around 250kHz can be obtained with commercially available equipment. However the so-called phenomena of strain-gauging (in the form of small amplitude high frequency oscillations) was responsible for contamination of about 3 out of every 4 experimental runs (A.J. Smits, private communication). Sometimes the oscillations could be made to disappear by adjusting the anemometer controls. This observation led the author to propose that strain-gauging is a purely electronic, rather than an electro-mechanical phenomenon and that a more sophisticated model of the system behavior could lead to further understanding and possible control of this frustrating problem as well as leading to methods for increasing the frequency response. In order to explore this and other ideas the theory of operation of the constant-temperature hot-wire anemometer was extended from 3^{rd}-order to 7^{th}-order by Watmuff (1987) by including the effects of bridge capacitance and the frequency response characteristics of the feedback amplifier. A computer model was created based on this analysis. The results of an extensive set of simulations using a wide range of parameters led to the conclusion that incorporation of additional controls into the anemometer could allow the system frequency response to be increased substantially while maintaining system stability. These ideas were not translated into hardware at Princeton.

In late 1987 the author was sponsored by the Center for Turbulence Research to work with R.V. Westphal in the Fluid Mechanics Laboratory at NASA Ames Research Center on a project concerning turbulent boundary layers. Westphal had experienced frustration with system instabilities when using subminiature hot-wires (e.g. 0.6μm diameter). The computer simulation was used to demonstrate that inadequate frequency response of the feedback amplifier was the most likely cause for these instabilities. On the basis of all of these findings the development of a new high-performance constant-temperature anemometer was designed and built which is the subject of this report.

More recently, a completely general analysis has been performed in which the derivation of the system transfer functions have been "algorithmized". Transfer functions can be derived for systems of arbitrary complexity. This work is published here for the first time.

An effort has been made to include operating instructions. The hot-wire anemometer is a difficult instrument to operate properly and detection of an incorrect mode of operation can be quite subtle. Examples are given of incorrect operation modes which draw on the analysis mentioned above for an explanation. Finally, the report contains a description and a schematic of the circuit together with a parts list with suppliers. This information is sufficient to enable the anemometer to be constructed by others.

2. CIRCUIT BOARD DESIGN

2.1 Introduction

Prototype layout and testing of subsets of the circuit design was carried out by Mr James Fogarty and Mr. Stanley Mason working for Raman Aeronautics. Raman Aeronautics was an electronics design and fabrication company contracted to work for NASA Ames Research Center over a period of many years. Although Raman Aeronautics is no longer in business. Mr. Fogarty and Mr. Mason are presently working at NASA Ames Research Center as contractors with Calspan. Testing was also performed by many of the FML personnel, in addition to the author. In particular, Mr. Gregory Zilliac performed extensive tests on the output amplifier section and was responsible for the discovery of a small 2^{nd}-order nonlinearity. A simplified schematic of the printed circuit board (PCB) and controls is shown in figure 2.1. The complete schematic is shown in figure 2.2.

2.2 Wheatstone Bridge

The resistors forming the upper half of the Wheatstone Bridge are mounted on the PCB and are shown in the upper left hand corner of the detailed schematic in figure 2.2. An important design consideration was to minimize the change in bridge resistance with temperature as part of an effort to reduce the overall drift of the instrument to a negligible level. A relatively large power rating of one watt for the resistors is specified to minimize the temperature rise above ambient owing to Joule heating. The resistors are metal film with a temperature coefficient of 50ppm per $^{\circ}C$ so that the drift is even further reduced.

The standard cross-bridge ratio of 10:1 (i.e. R_c/R_a=10) is implemented by inserting jumper $J3$ while ensuring that jumper $J4$ is omitted. The ten $1k\Omega$ resistors labeled $RB1...RB10$ act in parallel to form the bridge resistor $R_a = 100\Omega$. The resistor labeled $RB11$ forms the bridge resistor $R_c = 1k\Omega$. Using ten resistors for R_a and a single resistor of the same type for R_c means that the temperature rise of each resistor should be almost identical as well as being quite small which will further aid in the reduction of drift. The optional symmetric bridge is configured by removing the resistor labeled $RB11$, removing the jumper $J3$ and installing jumper $J4$. These operations lead to $R_a = R_c = 200\Omega$. In the standard 10:1 cross-bridge ratio configuration the current flow through the passive arm of the bridge is around 10% of the wire current. With the optional cross-bridge ratio of unity the total current capacity of the power supply may need to be increased since the current in the passive arm of the bridge will be approximately equal to the wire current.

The components R_b and L_b which form the balance arm for the standard 10:1 bridge are located on the front panel. A group of resistor decade (1-2-2-2 code) thumbwheel switches is used to set the hot resistance of the probe. The switch is labeled on the sketch of the front panel controls (see figure 3.1) and it is configured such that the setting corresponds to the balance resistor setting in ohms i.e. the setting shown in figure 3.1 corresponds to $R_b = 123.0\Omega$. For the standard cross-bridge ratio of 10:1 this setting corresponds to a hot operating resistance of $R_w = 12.3\Omega$ for the wire. The tunable Cable Compensation Inductor L_b was selected for use with a co-axial probe cable of total length approximately 5 meters. The adjustment range is satisfactory for systems with a frequency response

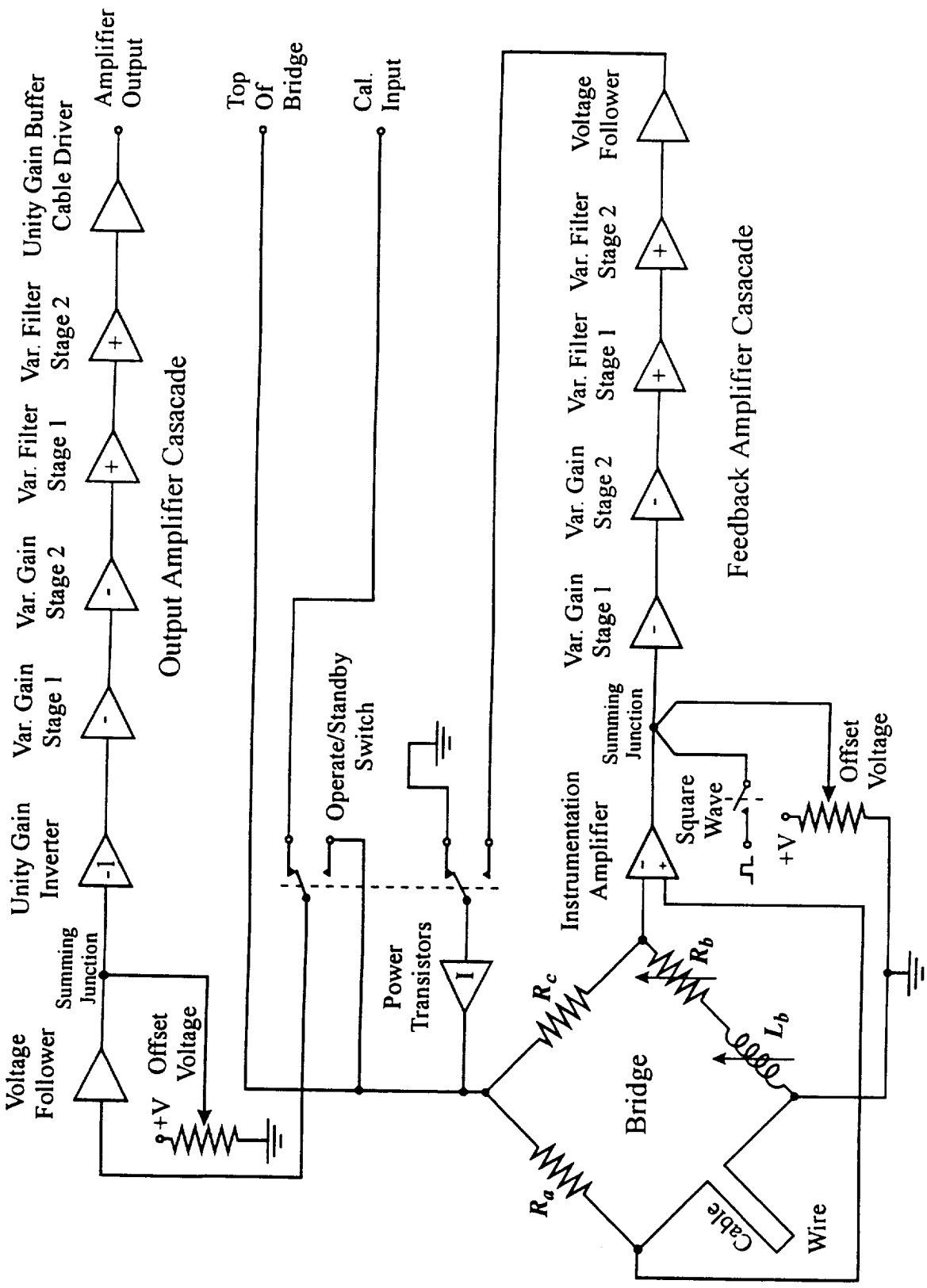

FIGURE 2.1 Simplified schematic of circuit.

of 20kHz to 30kHz, but smaller values of the inductor may be required for optimum frequency response when smaller wires are used since they have a higher frequency response. (Refer to section 6.5 for suggestions and examples for improving the stability when using subminiature wires). One simple solution in this situation is to use a longer cable rather than substitute a smaller inductor. However the overall performance of the system will be improved if a smaller inductor is used. In this case the benefits of reducing the cable length to a practical minimum should be considered in conjunction with the substitution of the inductor since performance is improved when the total inductance is reduced. The scaling for selection of a suitable replacement inductor can be based on the ratio of the cable lengths.

The BNC connector labeled EXT RB is used for the optional configuration in which the cross-bridge ratio is set to unity. For this optional symmetrical bridge configuration the Hot-Wire Resistance Thumbwheel switch and balance inductor must be removed from the bridge. The balance resistor R_b should be located at the end of a length of co-axial cable that has been carefully chosen to match the probe cable. This configuration offers superior compensation to the simple lumped inductor (by using an actual length of cable instead). Once again, it is emphasized that the bridge must be symmetrical for this option to work properly.

2.3 Feedback Amplifier

As mentioned previously many of the ideas for this design were based on the findings of the analysis described in section 5. In particular, front panel control would be required for the gain and frequency response of the feedback amplifier in addition to the offset voltage. In some situations it is possible for the overall frequency response of the anemometer to exceed the open-loop frequency response of the feedback amplifier alone. However this is not always the case and the feedback amplifier should have the potential for both a high gain and a high frequency response in order for the anemometer as a whole to achieve a high frequency response. A realistic maximum frequency response for a constant-temperature hot-wire anemometer was taken to be 500kHz as could be required in a supersonic flow for example. The specification for the feedback amplifier was set at twice that frequency (i.e. 1MHz) at the representative gain of K=1000. To achieve such a large gain-bandwidth product (i.e. $GBW = 10^9$) it was recognized that the feedback amplifier would have to consist of a cascade of individual amplifiers.

At the outset, the feedback amplifier was designed to consist entirely of operational amplifiers conforming to the industry standard 8-pin configuration e.g. LM741. This would provide the largest possible choice of devices at present as well as allowing for upgrades in the future as higher performance devices become available. The high input impedance of instrumentation amplifiers makes them attractive for the first stage of the feedback amplifier cascade and a prototype was constructed using three distinct operational amplifiers. Unfortunately the noise level was less than satisfactory. The magnitude of the noise was found to be dependent on the individual amplifiers even though a variety of high quality devices were tried e.g. Analog Devices AD744. Further, the noise level would change by up to a factor of five upon substitution of a supposedly identical amplifier i.e. one with the same part number from the same manufacturer. Therefore a number of

carefully matched integrated instrumentation amplifiers were tested in an effort to reduce the noise level. The best combination of performance and low noise was obtained with the high performance Burr Brown INA103 Instrumentation Amplifier. The advertised gain-bandwidth product is 100MHz at a gain K =1000 and the noise level is very low at 1.5 $nV/\sqrt{Hz}$ at 1kHz. The instrumentation amplifier is labeled $U1$ in figure 2.2. Jumpers $J6$ and $J7$ are used to connect the bridge to the amplifier and they are easily removed for testing purposes. The default configuration for $U1$ is for a gain of 100 which is imposed by inserting jumper $J5$ on the PCB. The amplifier will have unity gain if the jumper is omitted. The gain may be adjusted to a nonstandard value by inserting a resistor $R1$ which is selected according to $R1 = 6/(K-1)k\Omega$. Integrated Circuit numbers $U2$, $U3$ and $U4$ were originally used for the discrete amplifier components of the instrumentation amplifier. These numbers are no longer used since the amplifiers were replaced by the single IC $U1$.

The rest of the feedback amplifier cascade consists of four operational amplifiers that conform to the industry standard 8-pin layout. The first two amplifiers are AD744 ($U5$ and $U7$) and they are configured as variable gain blocks while the other two ($U9$ and $U12$) are JFET input LF356 which form the low-pass filter section. The roll-off frequency of each variable gain block operational amplifier is adjusted by switching the feedback components i.e. the resistors and capacitors which connect the output to the summing junction. The roll-off frequency of each filter block is adjusted by switching the resistor which is part of an RC network forming the input impedance of the amplifier. One way of performing these switching operations is to place the components directly on a front panel switch. However this is bad design practice since either long routing distances or long leads would be required for the connection from the amplifier to the switch and back. The feedback components should be positioned as close as possible to the amplifier for minimum noise and for best performance. This objective was achieved in the current design by connecting the feedback components with LF13508 analog switches ($U6$, $U8$, $U10$ and $U11$) which are mounted on the PCB close to each operational amplifier. The analog switches are in turn controlled by the front panel switches which generate the digital logic control signals.

The BCD rotary switch labeled GAIN is used to control the overall gain of the feedback amplifier. The BCD outputs drive a logic circuit consisting of the integrated circuits $U24$, $U25$ and $U26$. The logic circuit controls the analog switches in a manner such that the gain of each stage follows the sequence listed in the table on the schematic in figure 2.2. This arrangement tends to distribute the total gain requirement evenly among the two amplifiers. The advertised gain-bandwidth product of the Analog Devices AD744 operational amplifier is 13MHz so that the frequency response would only just fall short of the design specification of 1MHz at the maximum gain level of 16. This corresponds to an overall gain K =25,600 for the feedback amplifier. Tunable capacitors are provided for the input impedance (e.g. $C2$) and in the feedback loop (e.g. $C6$) so that adjustments can be made to ensure that the Bode diagram is flat with frequency. The Bode diagram (frequency response) cannot be guaranteed to be flat out to these -3dB points unless these capacitors have been tuned manually. (See sections 3.4 and 3.5 for tuning instructions). The BCD rotary switch labeled FILTER is used to control the roll-off frequency of the feedback amplifier. Only the first three BCD outputs are used which means that only

the first 8 positions are sequential i.e. switch positions 9 and 10 have the same effect as positions 1 and 2. The switch drives the logic inputs of both analog switches directly. The approximate -3dB roll-off frequency of the amplifiers follows the logarithmic sequence listed in the table on the schematic in figure 2.2. Note that the LF356 operational amplifiers $U9$ and $U12$ are essentially acting as buffer amplifiers. This arrangement isolates the second AD744 gain block from the capacitance of the second filter block. Without this feature the capacitive load of the second filter block could cause the AD744 to undergo high frequency oscillations. A simple pole of fixed frequency is incorporated into the feedback loop of each LF356 amplifier to ensure stability. The roll-off frequency of the pole is around 2.1 MHz which is well beyond the design specification so that it does not interfere with the overall performance objective.

The d.c. offset voltage E_{qi} and the square-wave perturbation voltage ϵ_S are injected into the first gain stage. The d.c. offset is adjusted using the front panel potentiometer labeled $RV4$. The square-wave input is derived using the logic circuit consisting of integrated circuits labeled $U30$, $U31$ and $U32$. A toggle switch is used to provide power to the logic circuit and a LED is used to indicate the On position. The circuit is powered down when the square-wave is not being used because this helps minimize the noise. The amplitude of the square-wave is adjusted using the potentiometer labeled $RV2$ which is located on the printed circuit board. The square-wave amplitude should be small enough to avoid nonlinear behavior i.e. the response to positive and negative fluctuations should be symmetrical. A square-wave amplitude of approximately $\pm$100mV has been found to be satisfactory. The frequency of the square-wave is adjusted using the rotary switch labeled FREQUENCY on the front panel. The square-wave frequency is not a critical parameter and control is provided for convenience of observation on an oscilloscope.

The last LF356 operational amplifier in the feedback amplifier cascade ($U12$) cannot provide the current required to drive the Wheatstone Bridge. The power transistors $T1$ and $T2$ are included for this purpose. The transistors are configured as a Darlington pair and testing has indicated that they are capable of supplying a current of 100 mA while maintaining a frequency response in excess of 1MHz. The output of $U12$ is connected to the power transistors via the LF13508 analog switch $U14$ which is toggled by the front panel Standby/Operate switch. The arrangement of these components can be seen on the second page of the schematic shown in figure 2.2. A LED is used to indicate when the switch is in the Operate position in which case the output of $U12$ is connected to the base of $T1$. When the switch is in the Standby the position the input to the power transistors is grounded and the anemometer is disabled. The switch should be in the Standby position when the probe is connected or removed from the instrument otherwise transient currents may cause the probe to burn out. The output of the power transistor $T2$ is available at the front panel BNC connector labeled TOB (Top Of Bridge).

2.4 Output Amplifier

Typically, the output voltage of a constant-temperature hot-wire anemometer consists of a relatively large d.c. component upon which are superimposed the small fluctuations which are of interest. It is common practice to utilize a separate "buck and gain" amplifier to subtract a d.c. voltage from the anemometer output and to amplify the resultant signal

so that it fills the voltage window of an analog-to-digital converter. For convenience, an output amplifier has been incorporated into the instrument for this purpose. The output amplifier is essentially an analog computer circuit which is hardwired to perform the following linear transformation,

$$E_o = -G(E_i + E_{\text{off}}) \tag{2.1}$$

where G is the gain, E_i is an input voltage and E_{off} is the offset voltage. It is configured as an inverting amplifier because the sensitivity of the anemometer (TOB) output voltage is negative. With this arrangement the overall sensitivity of E_o is positive with respect to velocity.

The front panel Standby/Operate switch is also used to toggle the LF13508 analog switch labeled $U13$ which connects one of two signals to the output amplifier. When the switch is in the Operate position, the input voltage E_i consists of the output of $T2$ i.e. the TOB output voltage of the anemometer. When the switch is in the Standby position the input voltage E_i consists of the signal applied to the Calibration Input BNC connector located on the front panel. The gains of the output amplifier listed in the table in figure 2.2 are only approximate. Careful matching of the resistors would be required for the gain values listed in the table to be realized with precision. However in most situations this is unnecessary. The ability to apply known voltages to the Calibration Input allows the constants G and E_{off} in equation (2.1) to be determined by direct calibration. One reason for wanting these constants with high precision is to enable the recalculation in software of the TOB voltages from the digitized values of the output amplifier signals. This would be the case for a hot-wire calibration scheme based on King's Law, for example. However in other circumstances it is not even necessary to know the magnitude of the constants since the calibration of the output amplifier can be absorbed into the hot-wire calibration as a whole. This would be the case with polynomial based calibration schemes, for example.

The operational amplifier $U34$ serves as a voltage follower buffer between the output of the LF13508 analog switch $U13$ and the unity-gain inverting amplifier $U15$. In the prototype design the analog switch was directly connected to the inverting amplifier $U15$. The input impedance of amplifier $U15$ is only $5k\Omega$ and it was discovered that the small nonlinearity associated with the impedance of the analog switch introduced a small 2^{nd}-order nonlinearity into equation (2.1). Using a larger input impedance of $100k\Omega$ for $U15$ reduced the nonlinearity but unfortunately had the side effect of increasing the noise. The best solution consisted of the introduction of the buffer $U34$ since the extremely high input impedance reduced the nonlinearity to a negligible value. This also allowed the low $5k\Omega$ input impedance to be retained with $U15$ thereby maintaining the lower noise level.

The offset voltage E_{off} is adjusted using the locking counting dial mounted on the panel to set the potentiometer labeled $RV3$. Unlike the feedback amplifier, the offset and input voltages are introduced into the separate unity gain inverting amplifier $U15$ rather than the first of the variable gain stages. The extra inverting amplifier is available because of the requirement of producing an overall negative sensitivity as per equation (2.1). The gain G is adjusted using the BCD rotary switch labeled GAIN in the output amplifier section on the front panel. The BCD outputs drive a logic circuit consisting of the integrated circuits $U27$, $U28$ and $U29$. The logic circuit, the analog switches $U17$ and $U19$ and the amplifiers

$U16$ and $U18$ are essentially a duplicate of variable gain blocks of the feedback amplifier. The overall gain corresponding to the switch positions follows the logarithmic sequence listed in the table in figure 2.2. Also in a duplicate manner to the feedback amplifier, the front panel rotary BCD switch labeled FILTER, the analog switches $U21$ and $U23$ and the operational amplifiers $U20$ and $U22$ serve as simple pole filters for the output amplifier. The approximate roll-off frequency of the amplifiers, as defined by the -3dB point, follows the logarithmic sequence listed in the table on the schematic in figure 2.2. In an earlier version of the circuit the output consisted of amplifier $U22$ which was found to undergo oscillations when driving long cables. The final stage of the output amplifier now consists of an $OPA633$ buffer amplifier $U33$ which avoids this problem. It should be noted that this device is capable of supplying a large current. The 100Ω current limiting resistor $R97$ is placed between the output and the BNC connector for protection purposes. In many circumstances it may be possible to use the last filter stage amplifier $U22$ for the output without any problems and $U33$ may be replaced with an appropriate jumper.

2.5 Power supply and PCB layout

As mentioned previously, the intention was to create a high performance anemometer design. Part of this overall objective was the desire to minimize electronic noise. For this reason the PCB can be configured with dual power supplies. Testing has revealed that the broad-band noise level at the TOB is halved when dual supplies are used. Dual power supply operation also may be necessary in situations where the bridge requires relatively large currents. This could be the case with the optional symmetric bridge configuration and/or if probes are used that require a larger current e.g. hot films. Jumpers $J1$ and $J2$ must be installed if only a single $\pm$15V power supply is to be used. It is recommended that the lowest noise modular $\pm$15V power supplies be used. Note that the front panel toggle switch labeled POWER does not switch the 110V 60Hz a.c. power. The switch is responsible for connection of $\pm$15V power to the PCB. From the viewpoint of minimizing noise the advantage of the dual supply configuration is that one supply is dedicated to the anemometer section alone (i.e. the bridge, feedback amplifier and power transistors) while other $\pm$15V supply is used for the output amplifier where the susceptibility to contamination by noise is much less. This second $\pm$15V power supply also feeds a single +5V voltage regulator for powering the logic circuits and the front panel indicator LEDs. Bypass capacitors are located between the supply and ground rails as close as possible to each active device mounted on the PCB. All operational amplifiers use 2.2μF capacitors while 0.1μF capacitors are used for the digital I.C.s and analog switches.

FOLDOUT FRAME

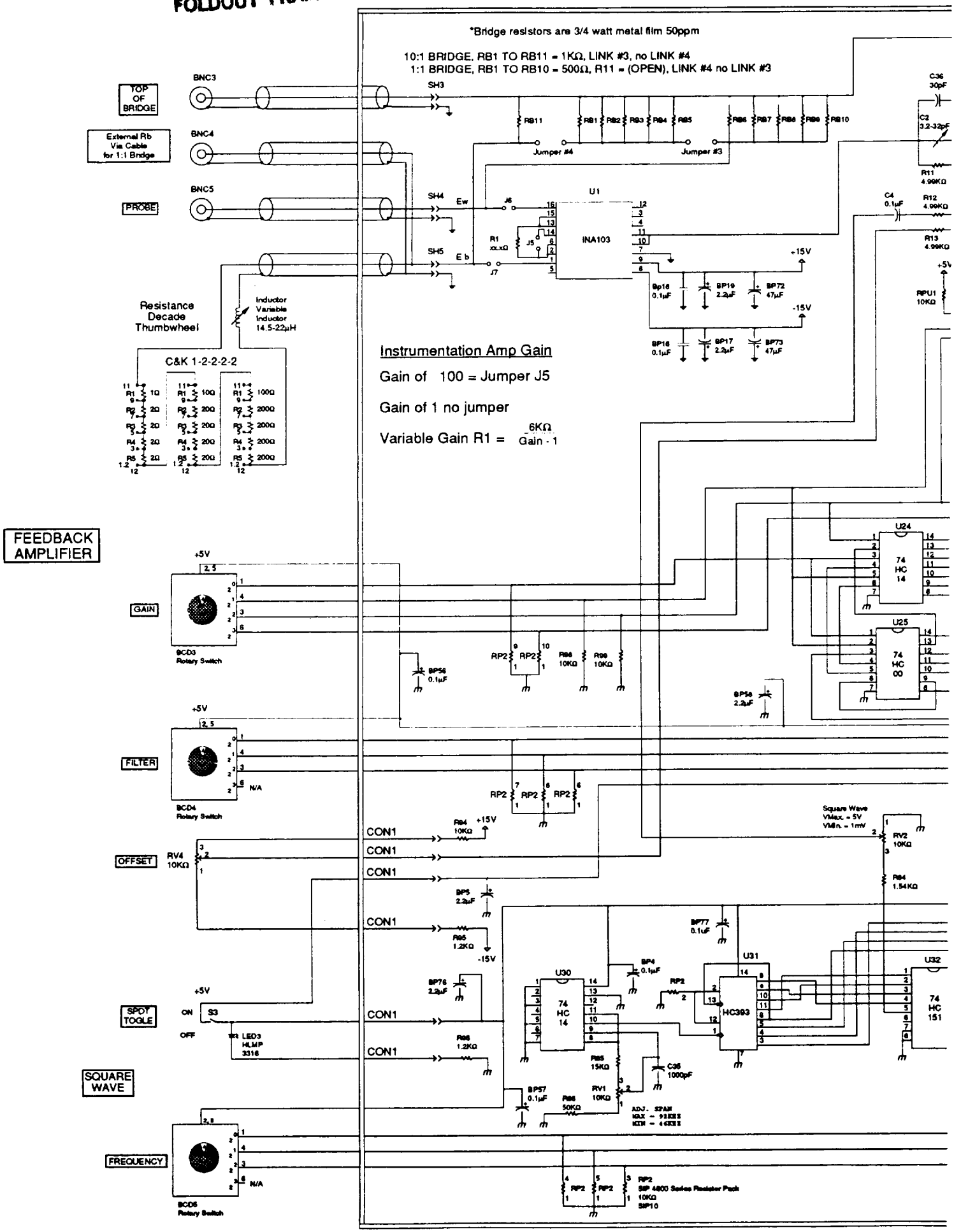

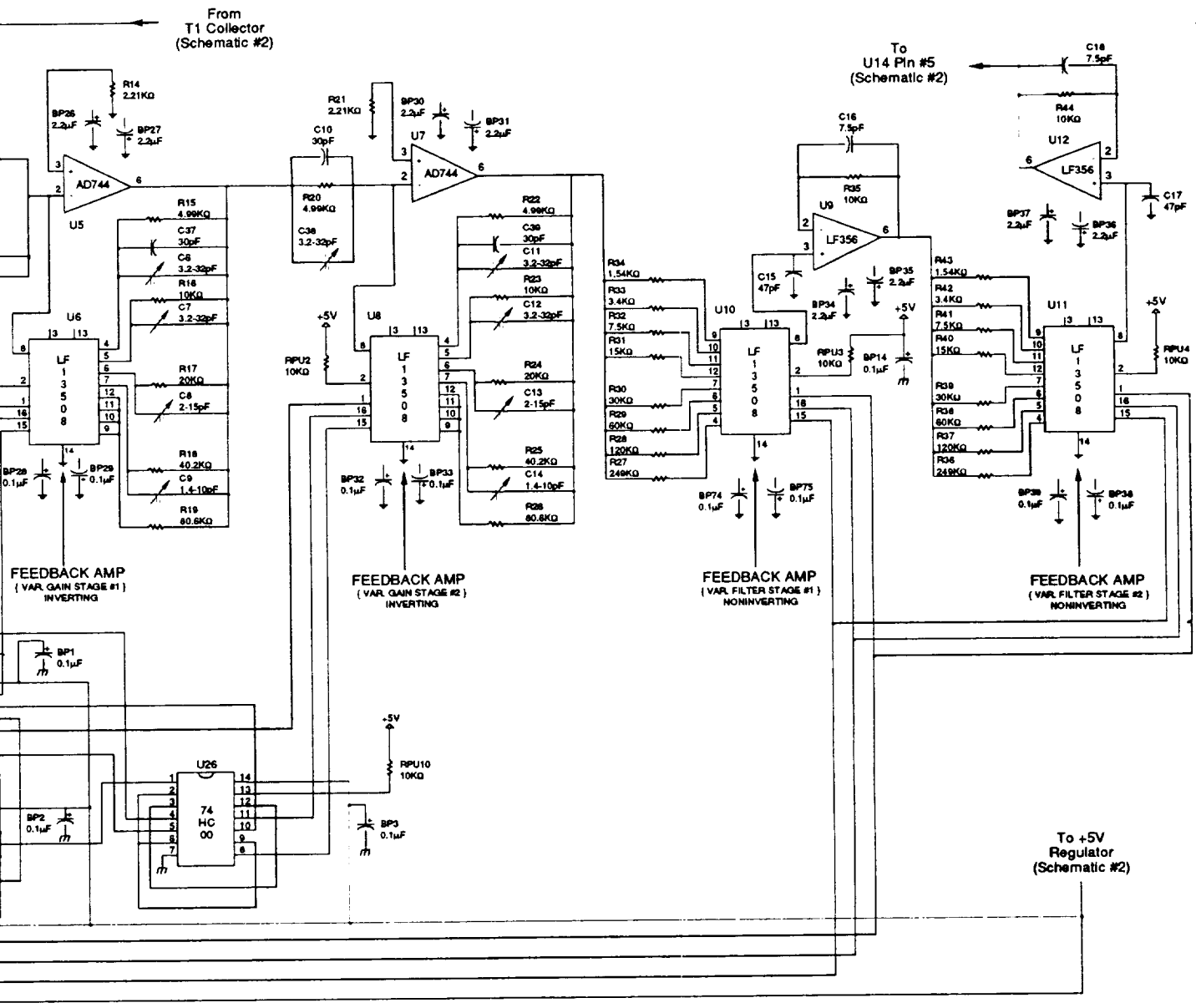

FEEDBACK AMPLIFIER

ROTARY SWITCH BCD3	GAIN OF STAGE #1	GAIN OF STAGE #2	TOTAL GAIN TO BRIDGE
1	1	1	100
2	1	2	200
3	2	2	400
4	2	4	800
5	4	4	1600
6	4	8	3200
7	8	8	6400
8	8	16	12800
9	16	16	25600
10	16	16	25600

FEEDBACK AMPLIFIER FILTER

ROTARY SWITCH BCD2	R(KΩ)	APPROX. FILTER -6db(KHz)
1	249	13.6
2	120	28.2
3	60	56
4	30	112
5	15	225
6	7.5	450
7	3.4	1000
8	1.54	2200

Frenquency Select	Square Wave Output
000	256Hz
001	512Hz
010	1024Hz
011	2048Hz
100	4096Hz
101	8192Hz
110	16384Hz
111	32768Hz

FIGURE 2.2 Schematic of PCB and front panel.

Schematic Page #1

CONSTANT TEMPERATURE
HOT WIRE ANEMOMETER

DESIGN BY:	JON WATMUFF	
DRAWN BY:	RAMAN AERO.	6/7/91
DESIGNED FOR:	FML	

FOLDOUT FRAME /.

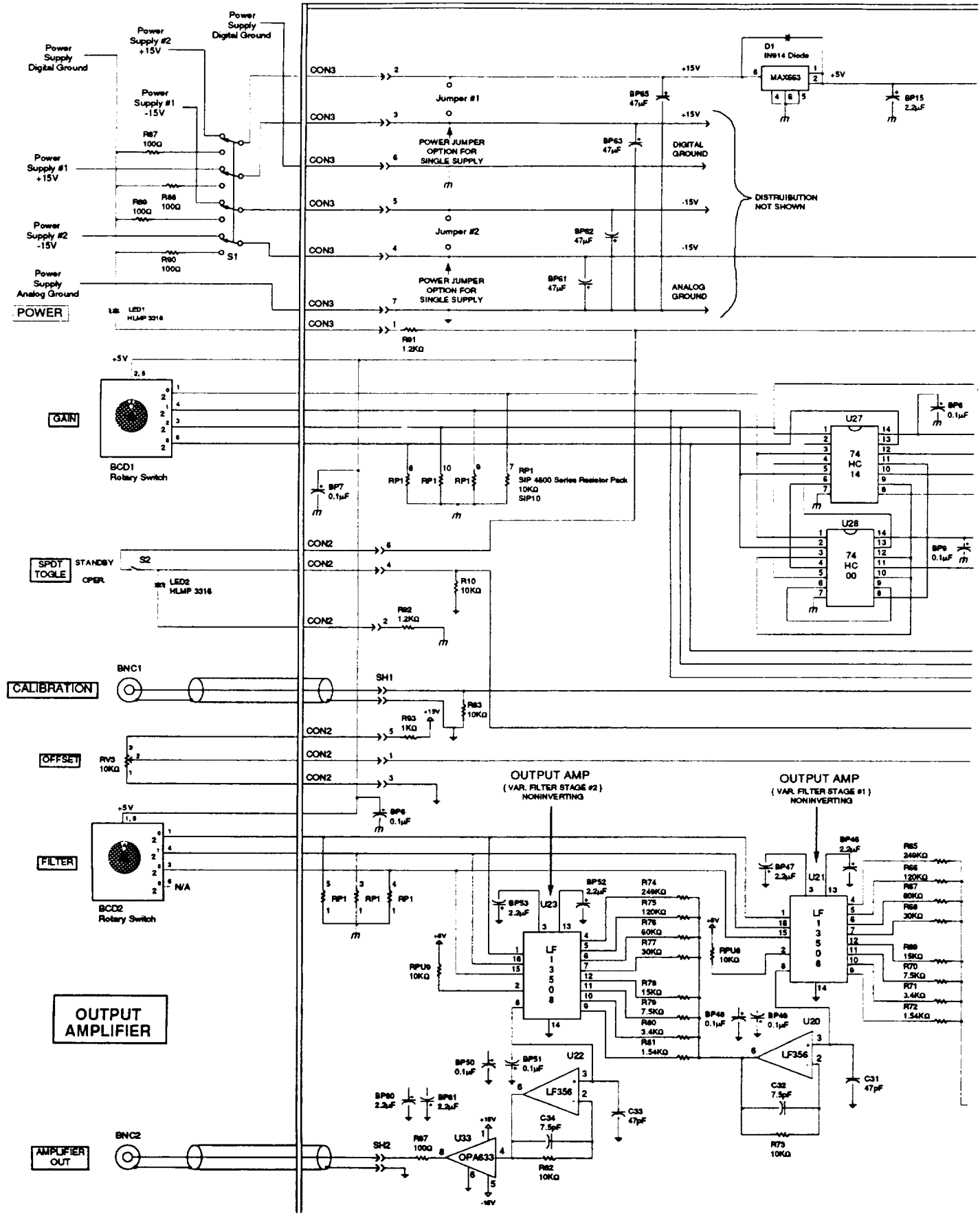

FIGURE 2.2 Schematic of PCB and front panel (continued).

Schematic Page #2

CONSTANT TEMPERATURE HOT WIRE ANEMOMETER		
DESIGN BY:	JON WATMUFF	
DRAWN BY:	RAMAN AERO.	6/7/91
DESIGNED FOR:	FML	

OUTPUT AMPLIFIER FILTER

ROTARY SWITCH BCD2	R(KΩ)	APPROX. FILTER -6db(KHz)
1	249	13.6
2	120	28.2
3	60	56
4	30	112
5	15	225
6	7.5	450
7	3.4	1000
8	1.54	2200

OUTPUT AMPLIFIER

ROTARY SWITCH BCD3	GAIN OF STAGE #1	GAIN OF STAGE #2	TOTAL GAIN
1	1	1	1
2	1	2	2
3	2	2	4
4	2	4	8
5	4	4	16
6	4	8	32
7	8	8	64
8	8	16	128
9	16	16	256
10	16	16	256

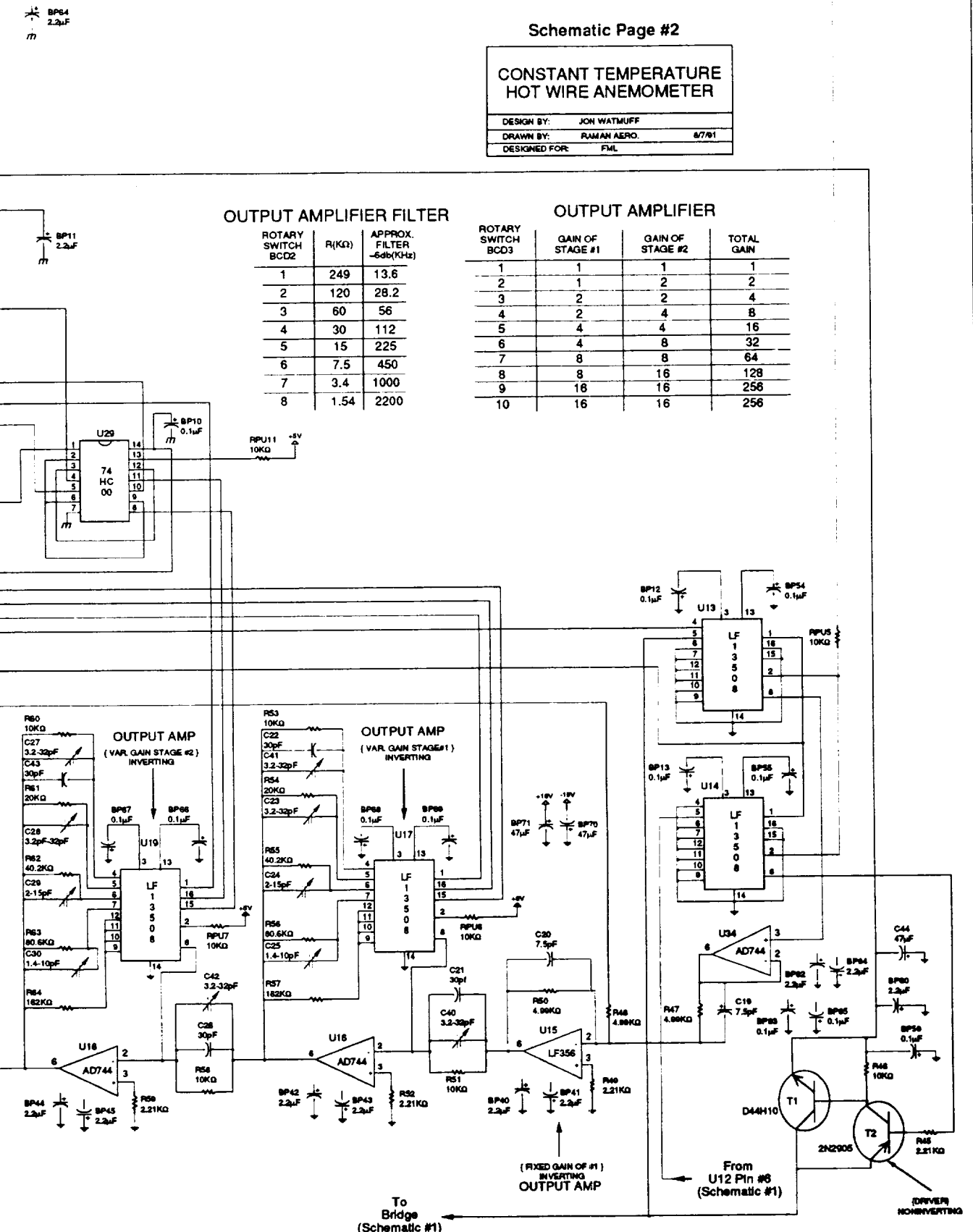

3. FABRICATION

3.1 Chassis and Panels

Complete assembled bare chassis of the required size are not available commercially but the chassis is easily manufactured. The front panel is integral with the PCB since the BCD rotary switches are soldered onto the board and the spindles and knobs must align with holes in the front panel.

The top and bottom of the chassis consist of two inch wide aluminum extrusions available under part number SR2-0625s-41 from Vector Electronic Company (see Table 1). and must be cut to 16 inches length. The edges of the PCB are supported by slots in the extrusions as shown in figure 3.2. The extrusions also have holes for fixing the front and rear panels.

The left and right side panels are cut from 16 gauge aluminum sheet. The right side is plain but the left side contains holes for supporting the PCB via standoffs and mounting the modular power supplies. The dimensions and location of the holes are shown in figure 3.6. The side panels engage slots in the top and bottom extrusions and they are free to slide, being constrained by only the front and rear panels. Blanks for the front and rear panels must be cut to external size from 3/32 inch thick aluminum sheet. After drilling the four mounting holes as shown in figure 3.3 the bare chassis can be assembled.

Figure 3.1 is a drawing of the assembled front panel. The relationship between the chassis, PCB and front panel components is shown in figure 3.2. Figure 3.3 shows the position of all the holes in the front panel. The location and size of the front panel holes is shown in figures 3.4. The specifications for the rear panel holes are shown in figure 3.5.

3.2 Printed Circuit Board (PCB)

A complete schematic of the PCB and associated front panel controls is shown in figure 2.2. The PCB is relatively simple and cheap to manufacture because it has only two layers, although it is double-sided. Photocopies of the four photoplots used to fabricate the PCB are shown in figures 3.7. The specifications for photoplots and construction of the PCB are contained in a set of Gerber files which are industry standard files used by PCB manufacturers. The following list of files are required to construct the PCB. The files are available on a 3.5 inch DOS formatted disk, by sending a written request to:

Branch Chief
Fluid Mechanics Research Laboratory Branch
M/S 260-1
NASA Ames Research Center
Moffett Field, CA 94035

Files for Photoplot Fabrication

ap_photo.txt	Text File	Aperture for photo plots only
gpb_cs.ger	Gerber File	Component Side Ground Plane
gpb_ss.ger	Gerber File	Solder Side Ground Plane
pt_cs.ger	Gerber File	Component Side Pads and Traces
pt_ss.ger	Gerber File	Solder Side Pads and Traces

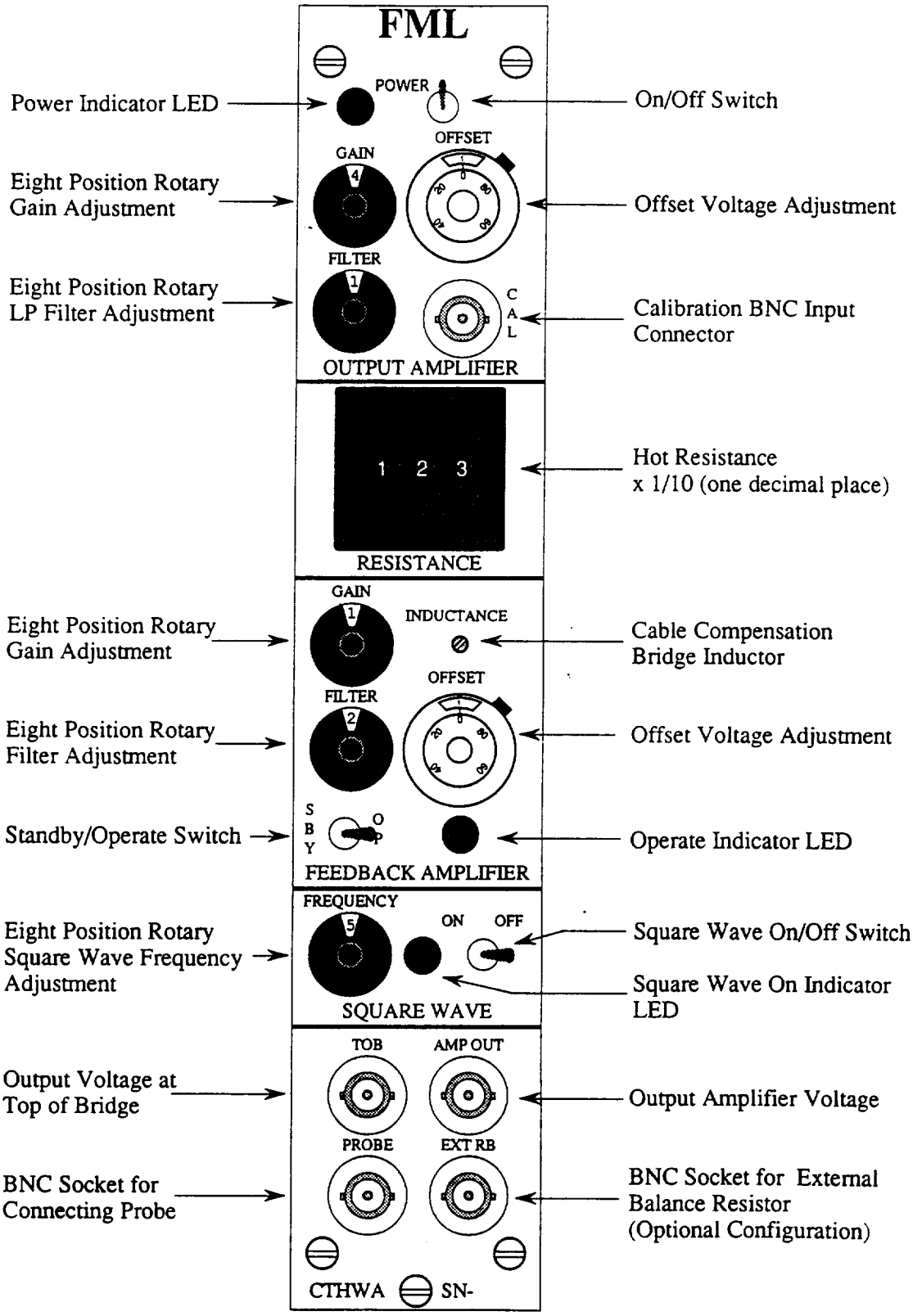

FIGURE 3.1 Layout of assembled front panel with controls labeled.

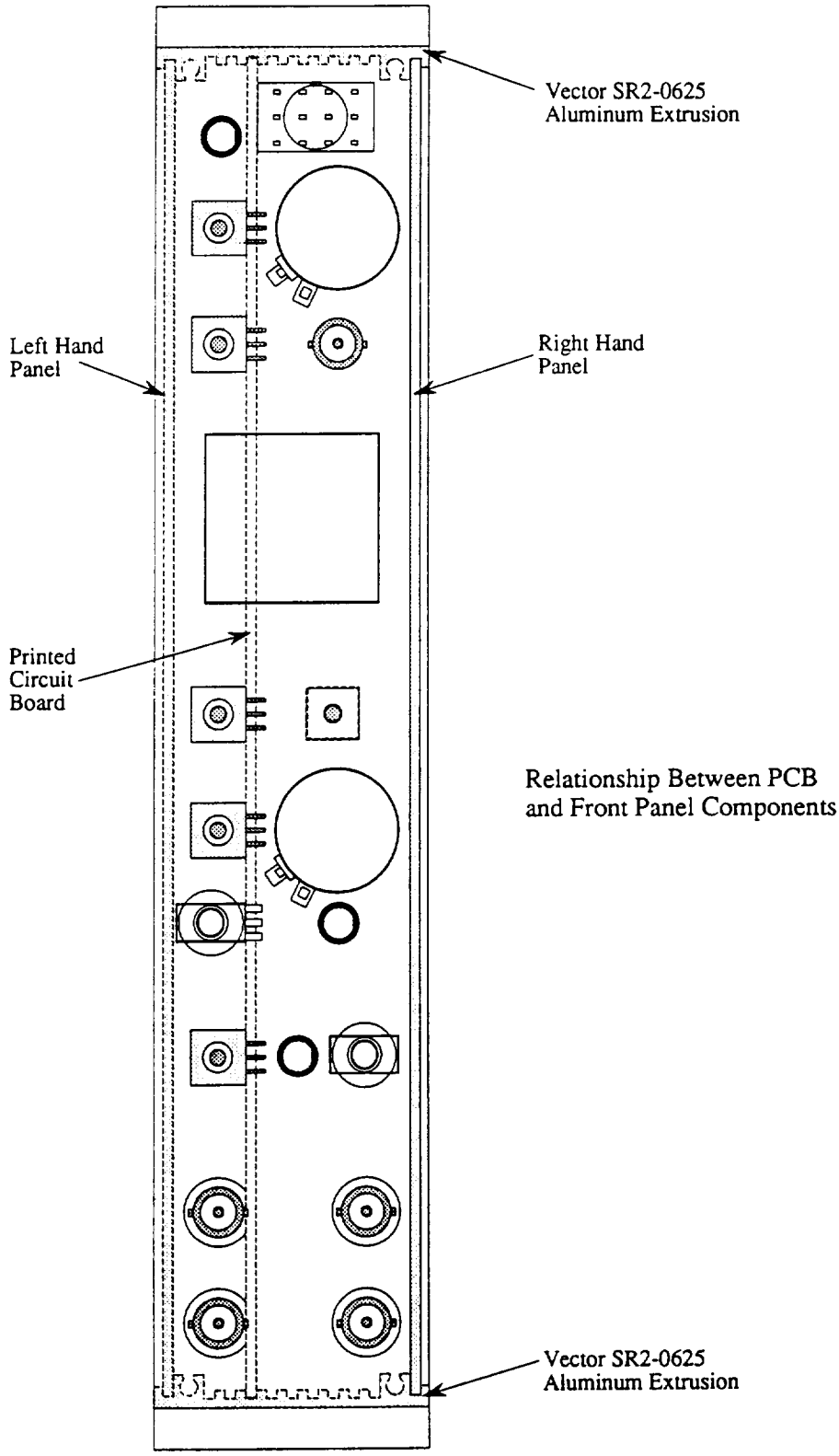

FIGURE 3.2 Relationship between chassis, PCB and front panel components.

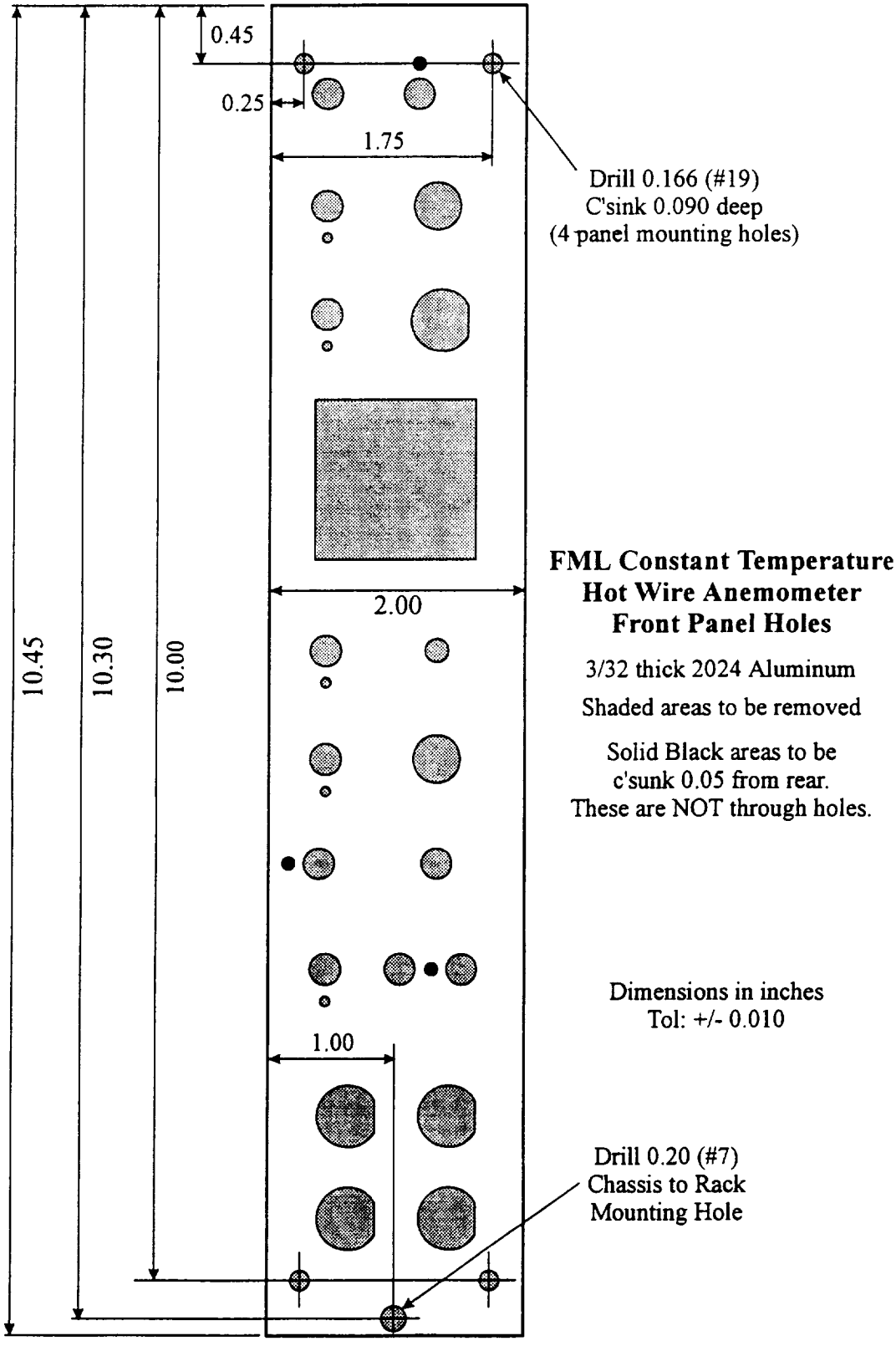

FIGURE 3.3 Drawing of front panel holes. External dimensions of panel and position and size of holes for mounting to chassis and rack specified.

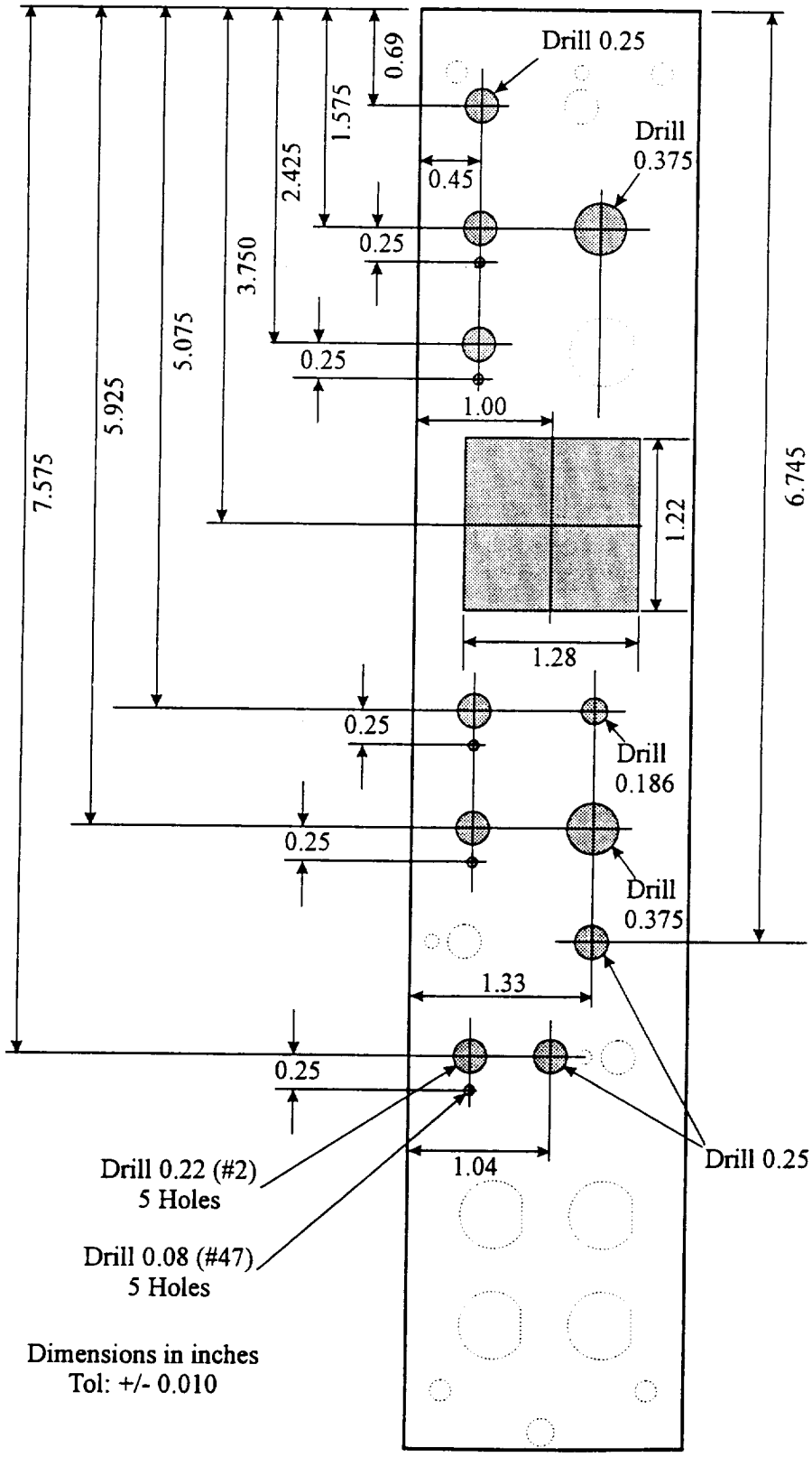

FIGURE 3.4 Position and size of front panel holes for mounting components.

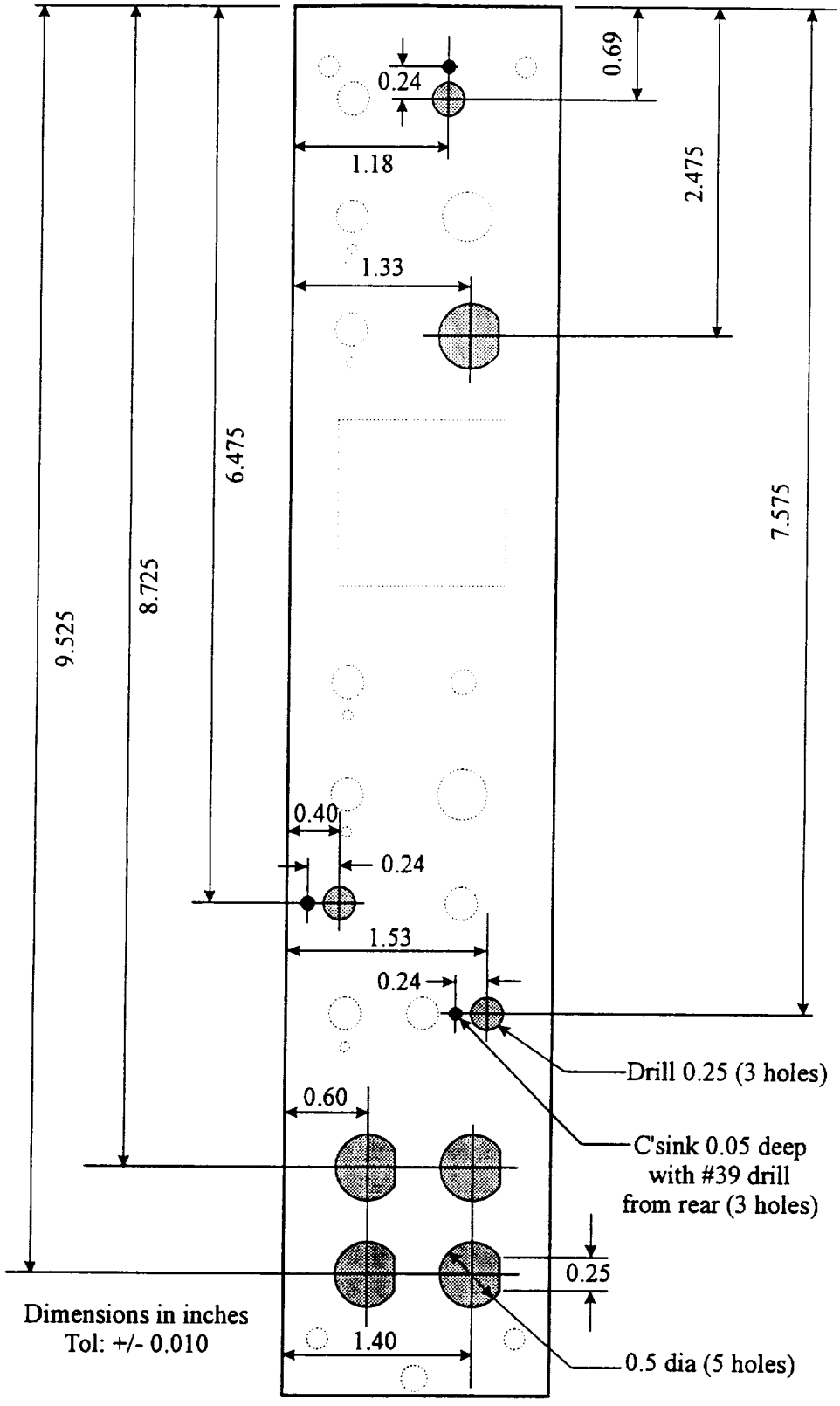

FIGURE 3.4 (Continued) Position and size of front panel holes for mounting components.

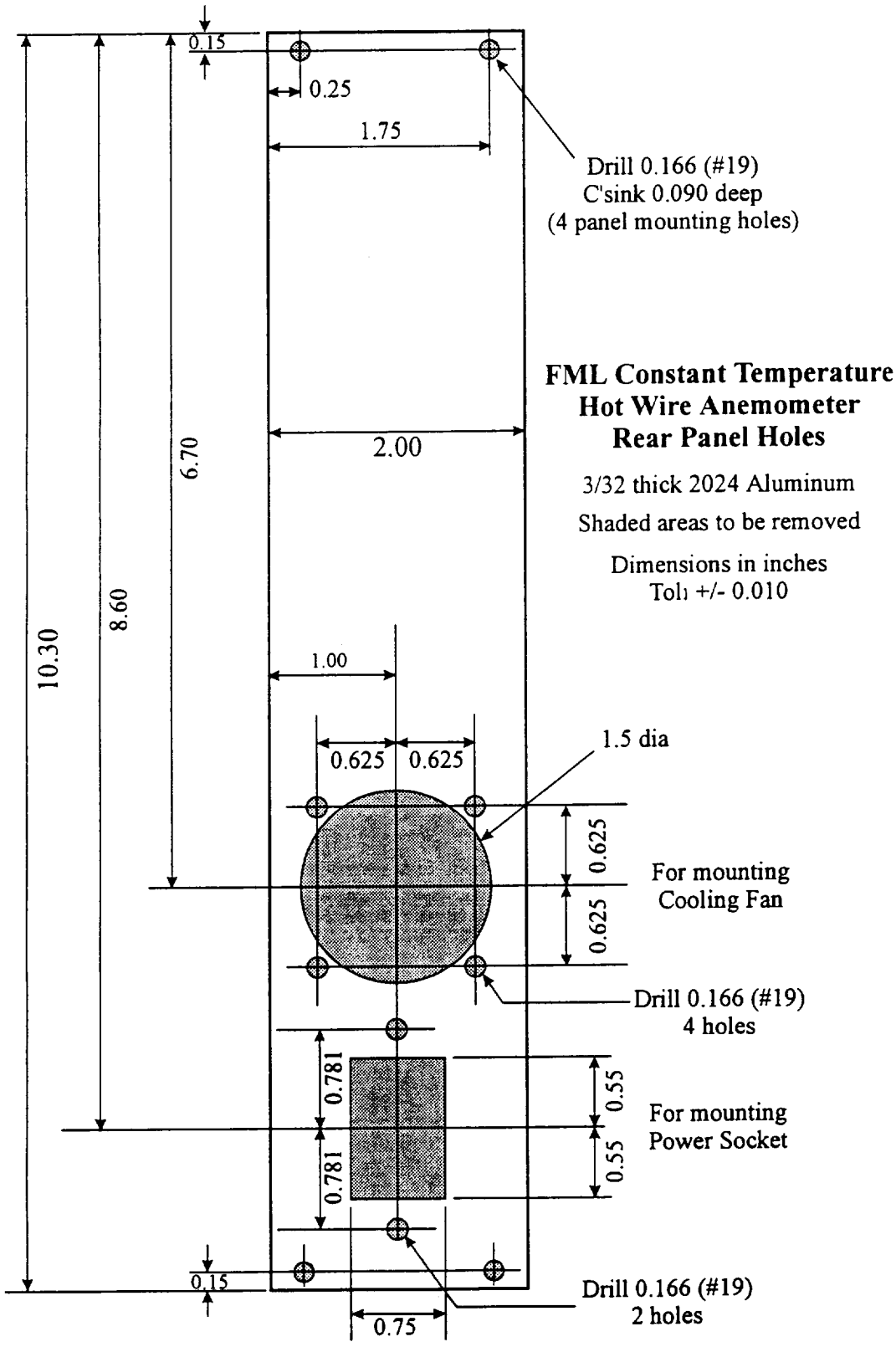

FIGURE 3.5 External dimensions of rear panel and specification for holes.

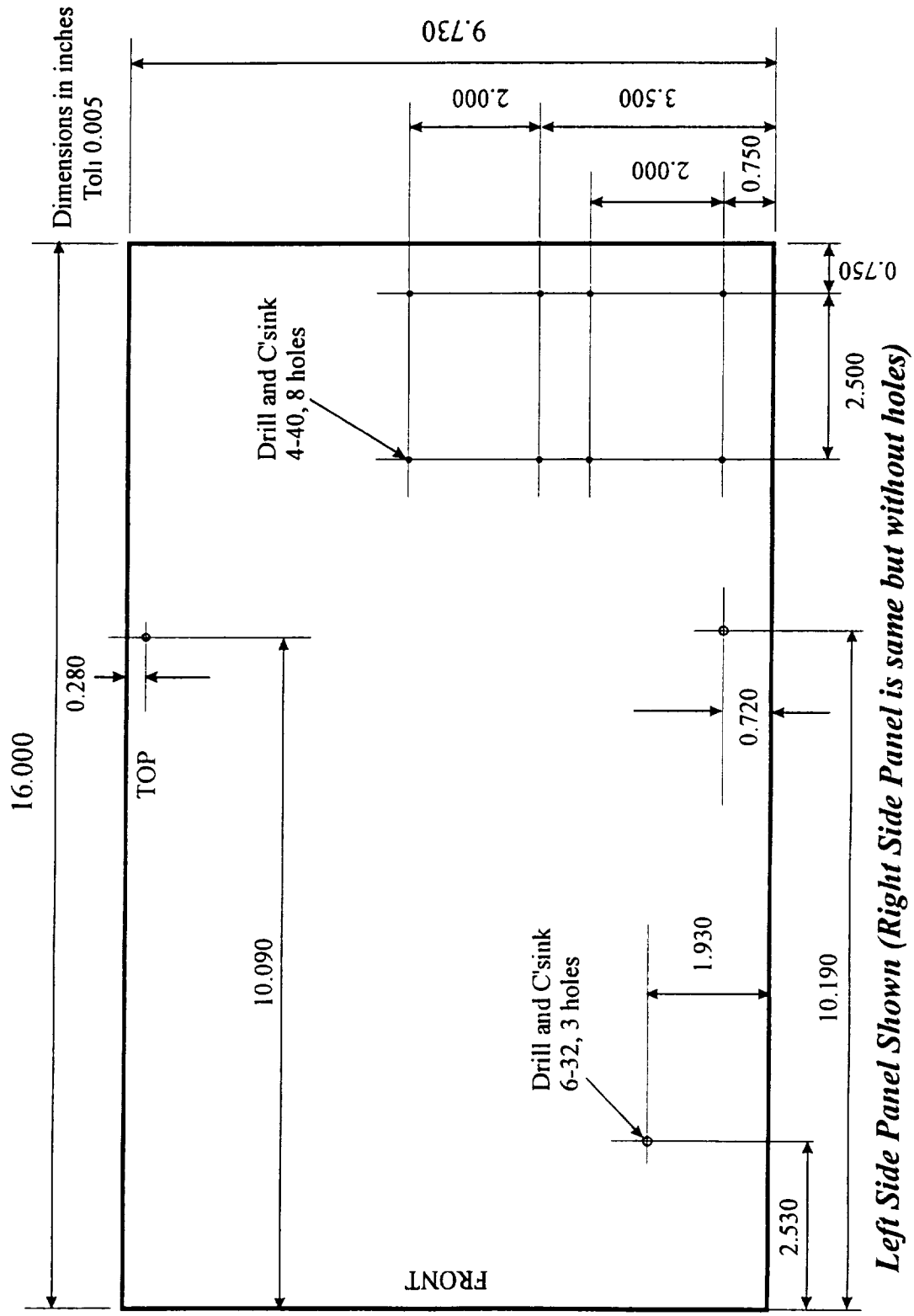

FIGURE 3.6 Specifications for Chassis Side Panels.

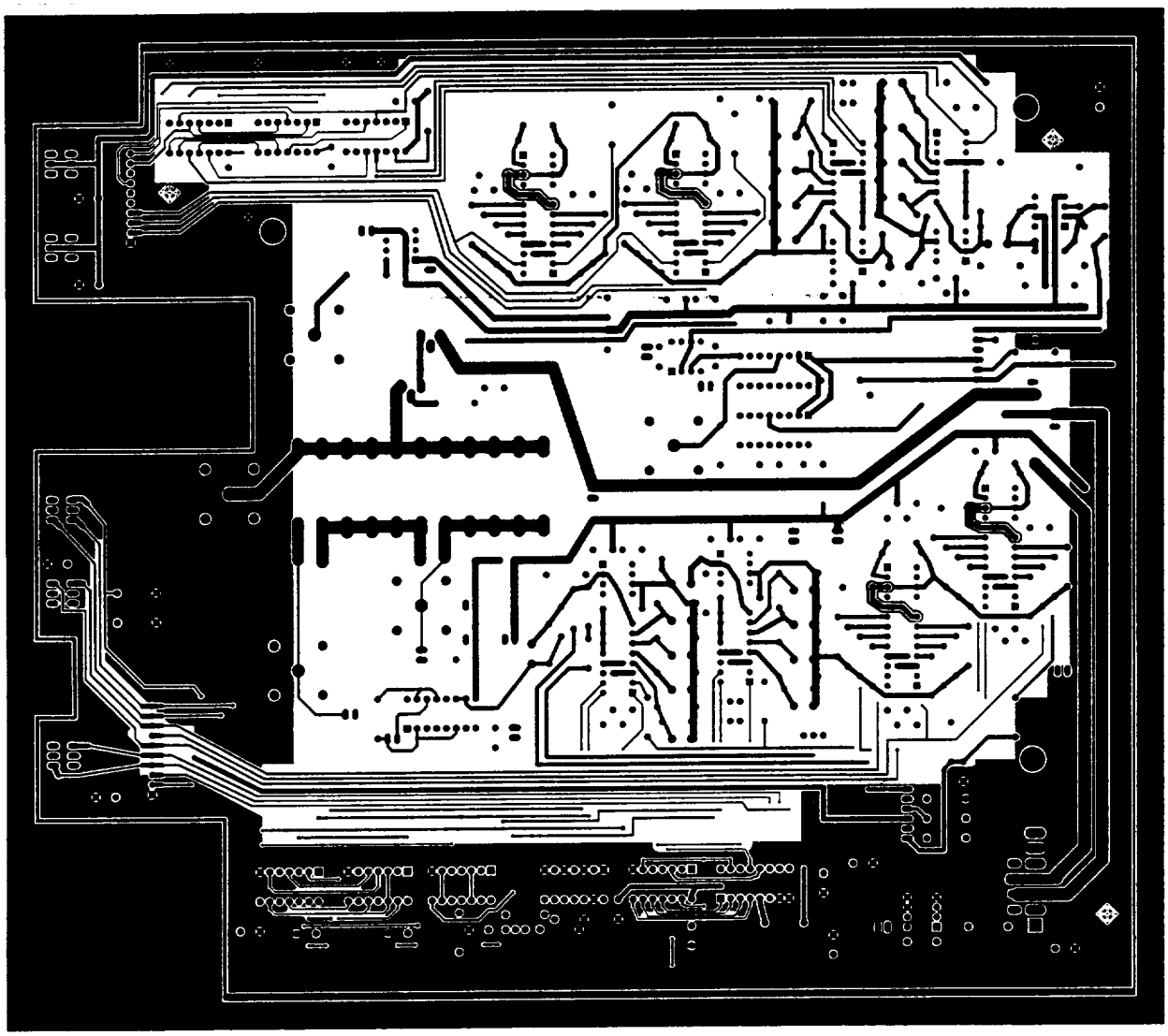

FIGURE 3.7(a) Photocopy (50% reduction) of original photoplot for solder side showing traces, pads, ground plane and ground plane block.

sb_cs.ger	Gerber File	Component Side Ground Block
sldr_msk.ger	Gerber File	Solder Side Ground Block
ss_cs.ger	Gerber File	Component Side Silk Screen

Files for PCB Fabrication

ap_hole.txt	Text File	Aperture for PCB Holes Only
holes.ger	Gerber File	Hole Only

Some manufacturers make photoplots for construction of the PCB's from the Gerber files while others have this work performed by outside organizations. In either case it is cost effective to obtain the photoplots after manufacture so that they can be stored in a safe place. Having the photoplots provides a degree of independence from particular manufacturers and the cost of having extra boards made in the future is reduced.

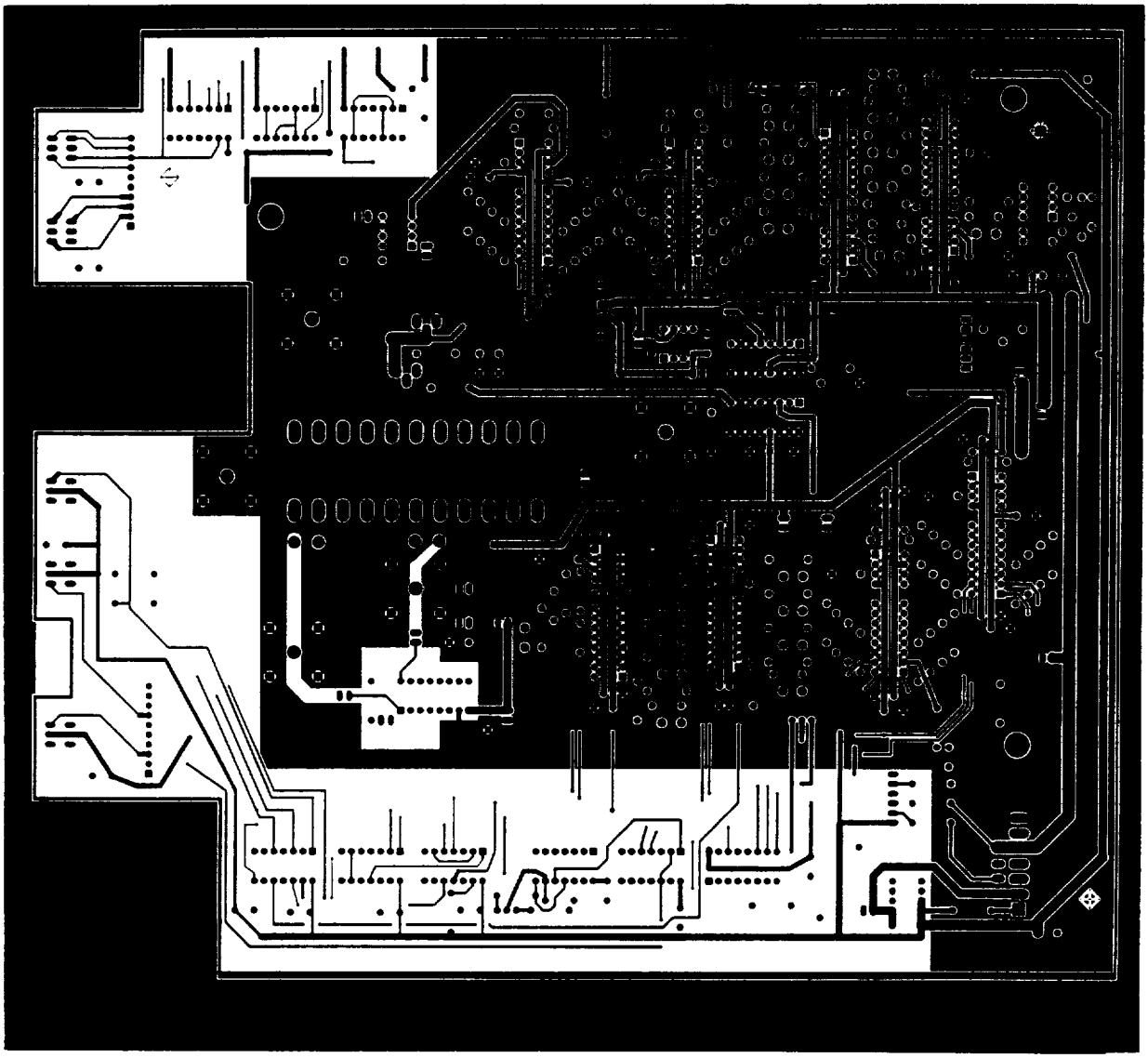

FIGURE 3.7(b) Photocopy (50% reduction) of original photoplot for component side showing traces, pads, ground plane and ground plane block.

The PCB has a silk screen with labels of the components, all pads with holes drilled and deburred, a ground plane and solder mask coatings. The cost of fabricating the boards was around $60 each for quantity 10. The manufacturer delivered finished boards ready for soldering of components. The photoplots for the PCB's in the sets constructed for the FML at NASA Ames Research Center were manufactured independently by Image Technology Incorporated. Two sets of PCB's were manufactured at two different times. A list of manufacturers is supplied at the end of this section.

3.3 Assembly

Fabtronics Systems was used on two occasions to assemble 20 anemometers and at a later date 8 anemometers, chassis and all components and they delivered complete but untested units. This service included plating of the bare chassis and complete preparation of the

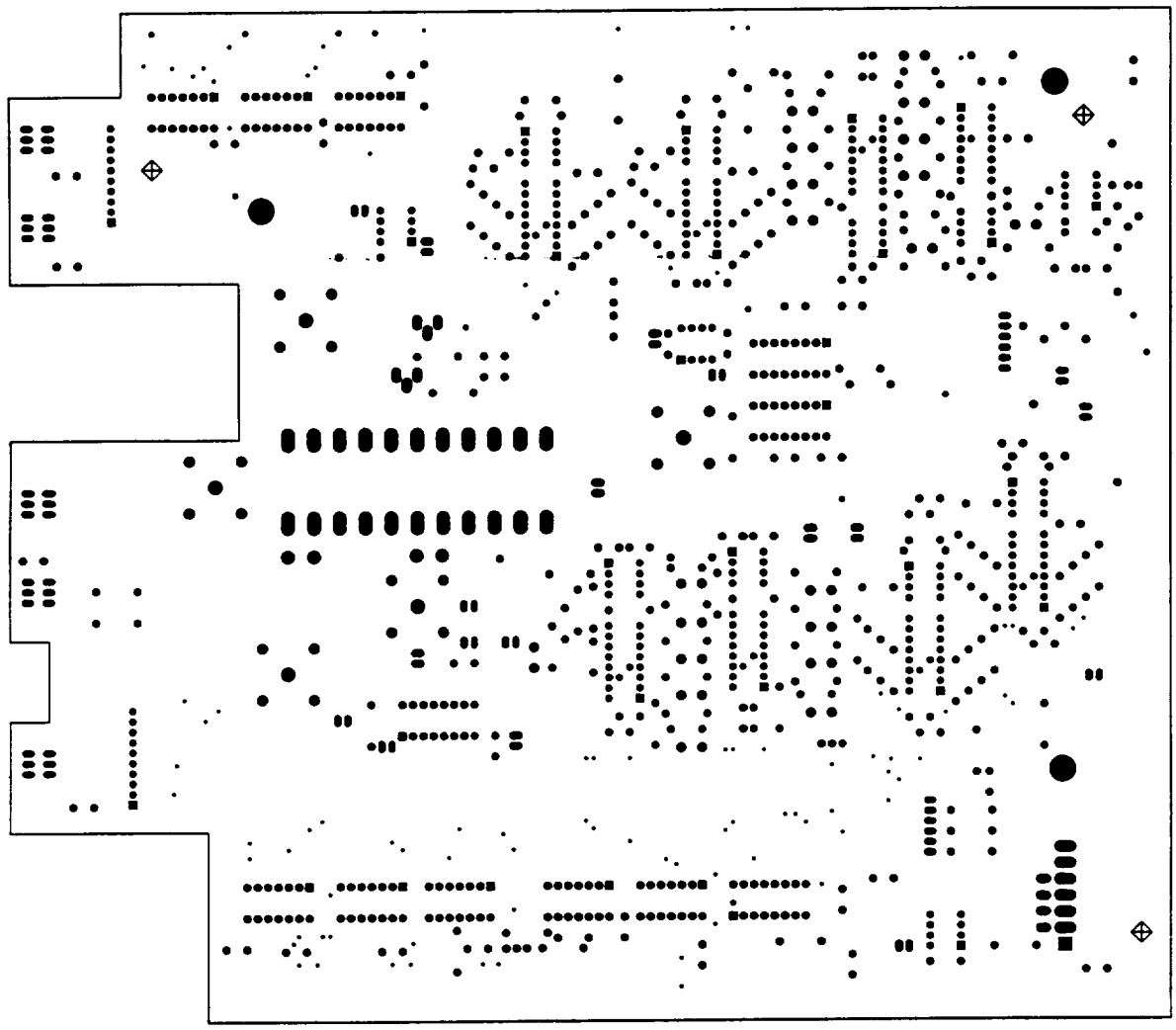

FIGURE 3.7(c) Photocopy (50% reduction) of original photoplot showing solder mask for both sides.

front panel from the blank provided. the front panel holes and silk screening of the multi-colored labels. components were soldered to the PCB and the front panel was attached via the BCD rotary switches. and they were installed on the front panel along with other hardware such as the BNC connectors, toggle switches, LEDs and potentiometers. and power supplies were installed in the chassis and the internal wiring was completed. offered by Fabtronics is not unique and should be available at many other locations. chassis for mounting in an instrument rack, as shown on page (i).

3.4 Preliminary Tests and Tuning

When the sets arrived after fabrication the preliminary test consisted of connecting power without a probe attached. If the fuse blows then an ohmmeter should be used to check for short circuits between the supply rails. A typical cause of short circuits is poor manufacturing techniques in which burrs or other debris cause a short between the power

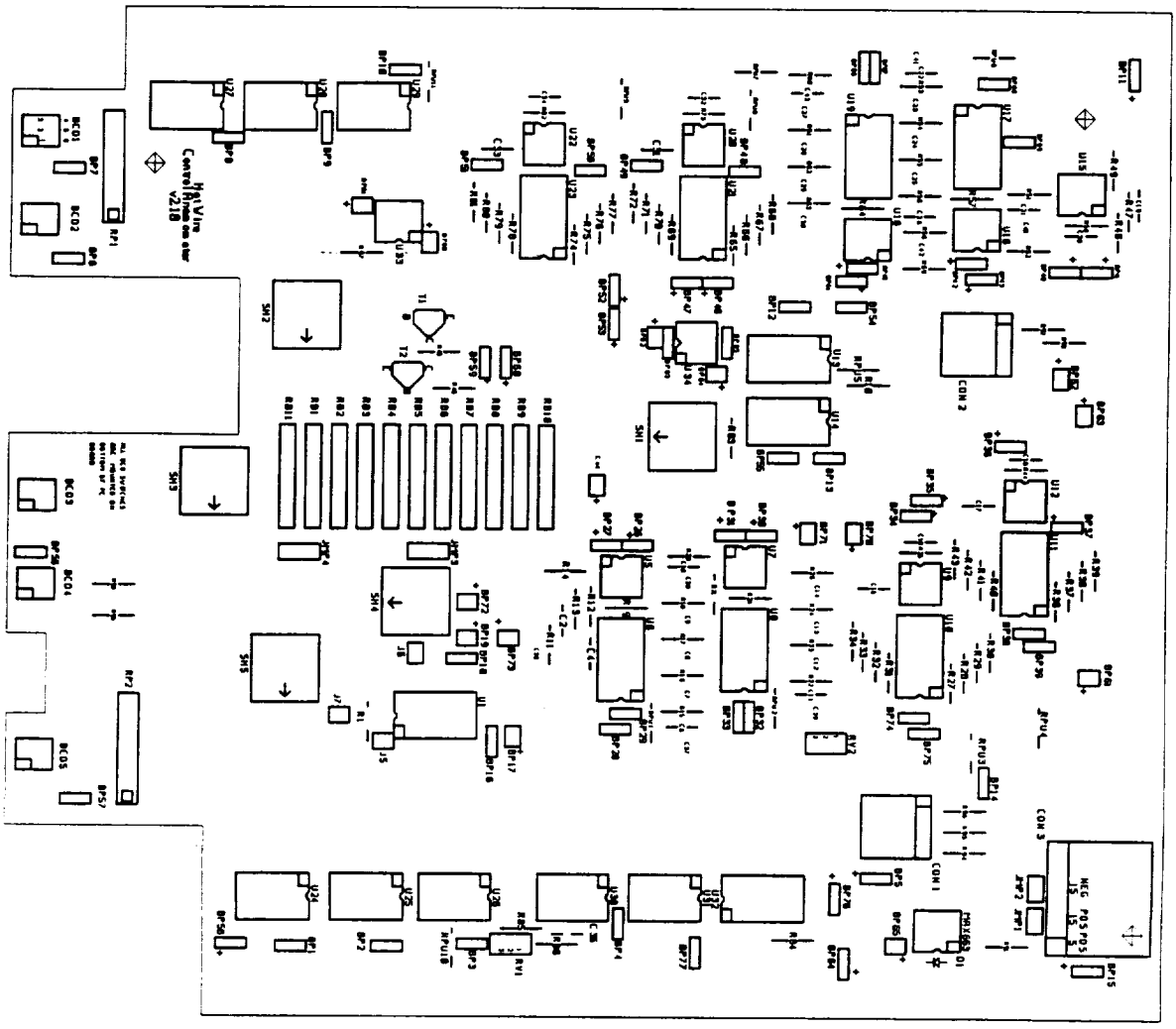

FIGURE 3.7(d) Photocopy (50% reduction) of original photoplot for silk screen labels of components.

supply rails. However this type of error was not found with the 30 PCBs manufactured. The most common cause of short circuit was found to be the reversed installation of a bipolar capacitor or integrated circuit. When all short circuits are removed the next step is to set the magnitude of the square wave to be around ± 100 mV by adjusting the potentiometer labeled $RV2$ located on the PCB.

It is important that the Gain, Filter (frequency response) and Offset voltage of the feedback amplifier are within the range required for stable operation before attempting to operate with a hot-wire connected. If the Offset voltage is not within range then the anemometer will not operate. If the Filter and Gain settings are too high then the system is likely to be unstable. The use of a 1/32 amp fast blow fuse was found to be useful as a substitute for a hot-wire for testing purposes. This fuse has a cold resistance of between 30Ω and 40Ω and was operated with a resistance ratio around 2:1.

Gain setting 3 and filter setting 2 are recommended for this test. Instabilities should

be removed by adjusting the Gain, Filter and Offset of the feedback amplifier. If stable operation cannot be obtained then each stage of the feedback amplifier should be checked. Jumpers $J6$ and $J7$ connect the bridge to the instrumentation amplifier. When these jumpers are removed the feedback is disconnected and the amplifier may be tested by applying a known input and checking the outputs of each amplifier in the cascade. A sinusoidal voltage of 5mV peak-to-peak is recommended because of the high gain of the feedback amplifier.

Similar tests can be performed if problems are experienced with the Output Amplifier. Testing and tuning of the Output Amplifier is simpler since the CAL input can be used to drive the amplifier directly when the anemometer is in standby mode.

3.5 Tuning for Maximum Performance

In order to achieve stable high frequency operation, the feedback amplifier should be tuned so that its frequency response is as high as possible. It is also desirable to have independent control of the gain and frequency response of the feedback amplifier. However the gain and frequency response settings will become related at high frequencies i.e. the system will roll-off at higher gain settings irrespective of the filter setting. The feedback amplifier should be "opened" for tuning purposes by removing jumpers $J6$ and $J7$ which connect the bridge to the instrumentation amplifier. A signal generator capable of supplying a small "clean" signal around, 5mV rms is needed, along with a high frequency rms voltmeter.

Each stage of the amplifier cascade should be tuned in succession by adjusting the capacitors such that the frequency response is maximally flat. An HP3325A Synthesizer/Function Generator generated the signals used to produce figures 3.8, 3.9 and 3.10. An HP3458A Multimeter was used to measure the rms input from the HP3325A and the output of the amplifier. Many general purpose multimeters do not a sufficiently high frequency range for the rms voltage measurements. The HP3325A can measure rms voltages accurately over a frequency range from 1HZ to 10 MHz.

An example of tuning the feedback amplifier is shown in figures 3.8. Testing was conducted at 16 discrete frequencies with approximately uniform logarithmic spacing from 100Hz to 100kHz. The effects of the filters were minimized by using filter setting 8 for these tests. The results for the untuned feedback amplifier are shown in figure 3.8(a) and the roll-off can be detected at frequencies as low as 20kHz although -3db point for the worst case occurs around 80kHz. This type of untuned behavior of the feedback amplifier is acceptable for applications in which the required system frequency response is less than 30kHz. However tuning is recommended for applications requiring a system frequency response in excess of 100kHz. The results of the tuning operation on this particular set are shown in figure 3.8(b). The frequency response is essentially flat up to 100kHz.

The results of tuning another feedback amplifier with filter setting 8 is shown in figure 3.9. The measurements were performed using 40 discrete frequencies over a wider range up to 1MHz. These results indicate that the variable gain stages (the AD744 operational amplifiers) are responsible for the lower roll-off frequencies with increasing gain. Assuming that each variable gain stage has identical behavior and that the roll-off can be treated as a simple pole, then the -3dB point of each variable gain stage can be estimated from

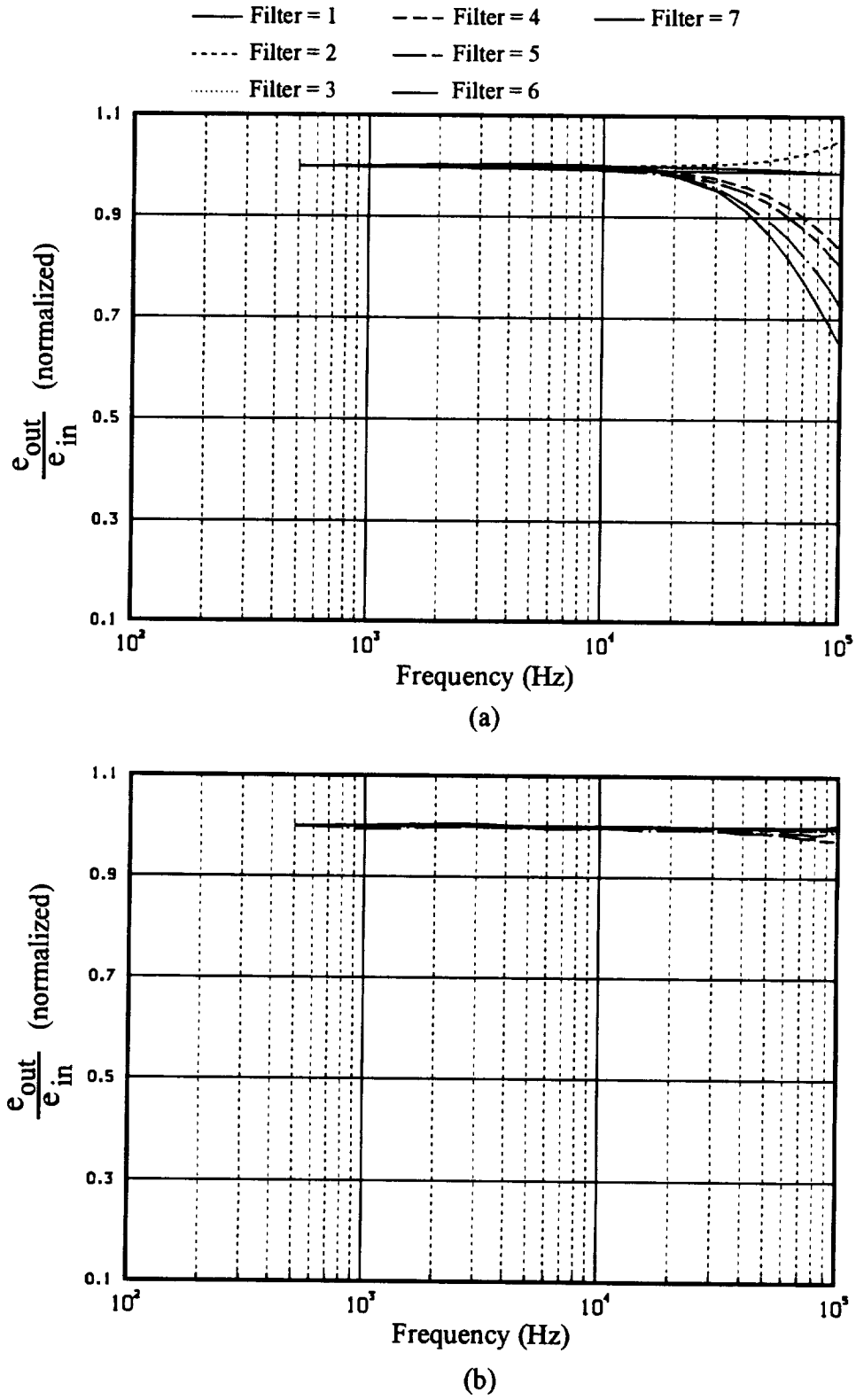

FIGURE 3.8 Typical open-loop frequency response characteristics of the feedback amplifier (a) Before tuning (b) After tuning.

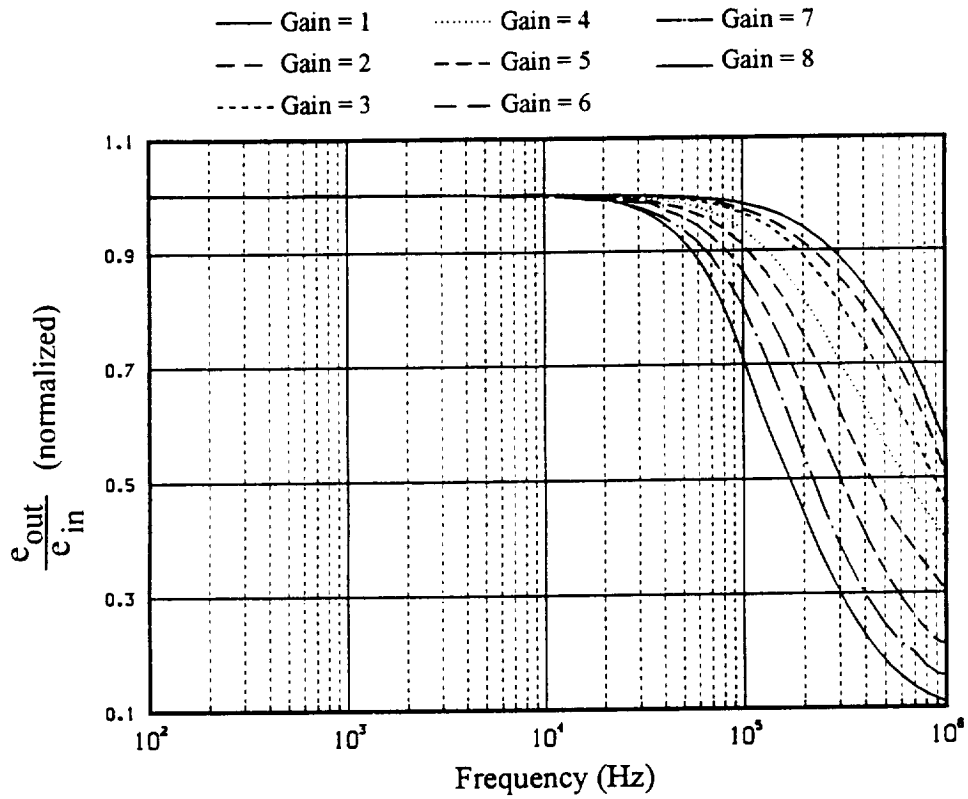

FIGURE 3.9 Results of tuning operation on another unit showing a wider frequency range.

the -6dB point of the plots. The amplitude ratio is plotted using a linear scale and the -6db points correspond to $e_o/e_i \approx 0.5$. With each stage set at unity gain, the -6dB point (i.e. -3dB for each stage) is in excess of 1MHz. For gain setting 7, each stage has a gain $K \approx 8$ and the individual -3dB points occur at a frequency in excess of 200kHz. It should be noted that the overall gain of feedback cascade is 6,400 for these settings leading to a $GBW \approx 1 \times 10^9$Hz. Further, these tests subject the variable gain stages to large signals. Analog Devices specifications for the AD744 amplifier is a small signal unity gain frequency response of 13 MHz and a full power response of 1.2 MHz. Direct testing has not been performed on an isolated stage so the effects of stray capacitance and other influences related to the PCB layout have not been determined. However it appears that these devices are peforming according to the specifications. It should be noted that the fluctuating component of the signal is much smaller when the feedback is enabled by connection to the bridge. Therefore the frequency response of the feedback amplifier will be higher under operating conditions.

The effect of the filter controls is shown for gain setting 1 in figure 3.10(a) and gain setting 7 in figure 3.10(b). The frequency response characteristics of the cascade are essentially identical for filter settings of 4 and lower. This is to be expected since filter setting 4 corresponds to a roll-off frequency of 112kHz which is less than the frequency response of the variable gain stages. Minor differences are observed for filter setting 5 corresponding to a -3dB point of 225kHz which is comparable to the frequency response of the variable

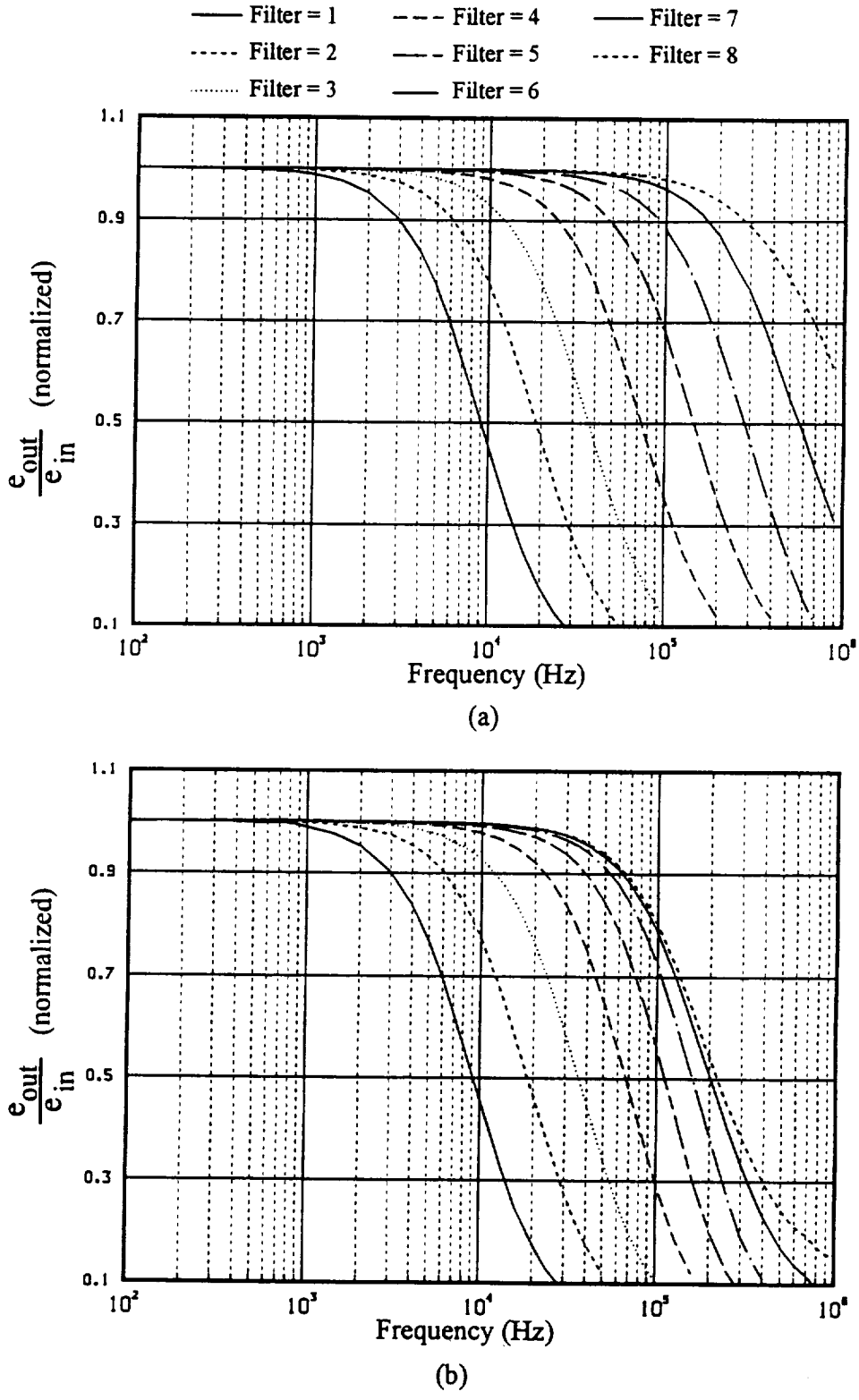

FIGURE 3.10 Effect of filters. (a) Gain setting 1. (b) Gain setting 7.

gain stages at gain setting 7 as shown in figure 3.9. The effect of higher filter settings for gain setting 7 is much reduced compared to the effect for gain setting 1 since the roll-off of the variable gain stages dominate the response.

3.6 Customization

The analysis in section 5 suggests that the only way to nullify both the inductive and capacitive bridge components is to use a symmetrical bridge. The system may be configured with an optional symmetrical bridge as described in section 4. The modifications lead to $R_a = R_c = 200\Omega$ and also require the removal of the Hot-Wire Resistance Thumbwheel switch and balance inductor. The purpose of this configuration is to allow the bridge resistor R_b to be placed at the end of a length of co-axial cable that has been carefully chosen to match the probe cable. This particular option has not been tested.

The gain and filter setting sequence shown in the schematic is approximately logarithmic i.e. each sequence involves a doubling operation. This gain and filter sequence ensures compatibility with a wide range of probes and operating conditions. However for a given probe and operating condition only a small subset of the range of settings can be used and it is not possible to obtain optimum performance by fine tuning. If the anemometer will only be operated with similar probes over the same range of operating conditions then the gain and filter sequence can be modified to suit this range. These modifications are accomplished by replacing the input and feedback components of the variable gain and filter stages. Using a linear sequence for the gain and filter settings would allow the operating point of the anemometer to be more highly optimized.

The tunable Balance Inductor was selected for use with 5μm diameter wires and a co-axial probe cable 5 meters long. The adjustment range is satisfactory for systems with a frequency response of 20kHz to 30kHz, but smaller values of the inductor may be required for optimum frequency response when smaller wires are used since they have a higher frequency response. (Refer to section 5 for suggestions and examples for improving the stability when using miniature wires). For optimum performance it is recommended that the shortest possible co-axial cable be used for the probe. If a shorter cable is used then a smaller Balance Inductor will be required. The scaling for selection of a suitable replacement inductor can be based simply on the ratio of the cable lengths.

The broadband noise level of the TOB output is typically around 2mV to 5mV rms depending on the filter setting of the feedback amplifier. The frequency of the a.c. power and its harmonics show up clearly in spectral measurements. Since the anemometer will function with $\pm$12V d.c. supply voltages, tests were performed using automotive batteries as a substitute for the $\pm$15V modular power supplies. The batteries led to complete disappearance of the spikes at the a.c. frequency and its harmonics and reduced the broadband noise level by about 10% to 20%. The best signal-to-noise ratio is obtained by tuning the frequency response for the required application, and no higher. Unfortunately, an increased high frequency response also means an increased susceptibility to noise.

3.7 Manufacturers, Parts List and Suppliers

The following list of manufacturers were used for the photoplots, manufacture of the PCB's and fabrication of complete but untested assemblies:

Manufacturer of the Photoplots

Image Technology Inc.
821 San Antonio Road
Palo Alto, CA 94303
Tel: (415) 494-3113
Fax: (415) 494-2947

Manufacturer of first set of 20 PCBs

Tel Tec Corporation
3305 Keifer Road
San Jose, CA 95112
Tel: (408) 297-9897
Fax: (408) 297-1540

Manufacturer of second set of 10 PCBs

Hunter Technology
1509 Berger Drive
Santa Clara, CA 95051
Tel: (408) 736-5400
Fax: (408) 736-1908

Assembly of 28 Anemometers

Fabtronics Systems
4749 Bennett Drive G
Livermore, CA 94550
Tel: (510) 447-1316
Fax: (510) 447-1316

The following list of suppliers were used for obtaining the components listed in Table 1. In some cases the components could only be purchased from the manufacturer. These manufacturers are Analog Devices, Burr Brown, Elma Electronics, Modular Power Converters and PD&E Electronics. Components manufactured by Vector Electronic Company were purchased directly from the manufacturer but it may be possible to purchase these items through distributors. The other companies listed are general distributors of electronic components. The total cost of these components is under $700. Neither the author nor NASA Ames Research Center makes a specific recommendation regarding these suppliers. The components are not unique and substitutes are freely available.

List of Suppliers

Analog Devices
One Technology Way
P.O. Box 9106
Norwood, MA 02062-9106
Tel: (617) 329-4700

Arrow Electronics
521 Wedell Drive
Sunnyvale, CA 94086
Tel: (408) 745-6600

Burr Brown
Intl. Airport Industrial Park
Tucson, AZ 85734
Tel: (602) 746-1111

Digi-Key Corporation
701 Brooks Avenue South
P.O. Box 677
Thief River Falls, MN56701-0677
Tel: (800) 344-4539

Elma Electronics
41440 Christy Street
Fremont, CA 94538
Tel: (510) 656-3400

Hamilton Avnet Electronics
1175 Bordeaux Drive
Sunnyvale, CA 94089
Tel: (408) 920-1211

Modular Power Converters Inc.
RFD Box 41
Fremont, NH 03044
Tel: (603) 642-5913

Newark Electronics
1975 Hamilton Avenue
San Jose, CA 95125
Tel: (408) 559-6900

PD&E Electronics
Newington Industrial Park
Newington, NH 03801
Tel: (603) 436-1211

Vector Electronic Company
12460 Gladstone Avenue
P.O. Box 4336
Sylmar, CA 91342-4336
Tel: (818) 365-9661

Semiconductors, Modular Electronic Components
(Note that IC numbers U2, U3 and U4 are not used).

Description	Specification	PCB/Drawing Reference	Supplier	Supplier Part No.	Price/Qty	Qty per Set	Price/Set
Instrumentation Amp.	GBW=100MHz	U1	Burr Brown	INA103KP	$12.70 Each	1	$12.70
Op. Amp.	GBW=13MHz, 4uV Noise 0.1 -10Hz	U5, U7, U16, U18, U34	Analog Devices	AD744JN	$225.00/100	5	$11.25
Op. Amp.	GBW=5MHz, JFET, High Speed	U9, U12, U15, U20, U22	Arrow Electronics	LF356N A+	$0.96 Each	5	$4.80
Buffer Amp.	For driving long cables	U33	Burr Brown	OPA633KP	$7.05 Each	1	$7.05
8 Chan Analog MUX	LF13508	U6, U8, U10, U11, U13, U14, U17, U19, U21, U23	Arrow Electronics	LF13508CN	$5.00 Each	10	$50.00
Quad 2 Input NAND Gate	CMOS Digital I.C.	U25, U26, U28, U29	Digi-Key Corporation	MM74HC00N	$0.25 Each	4	$0.25
Hex Schmit Trigger	CMOS Digital I.C.	U24, U27, U30	Digi-Key Corporation	MM74HC14N	$0.35 Each	3	$0.35
8 Chan Digital MUX	CMOS Digital I.C.	U32	Digi-Key Corporation	MM74HC151N	$0.48 Each	1	$0.48
4 Bit Counter	CMOS Digital I.C.	U31	Digi-Key Corporation	MM74HC393N	$0.60 Each	1	$0.60
Transistor	NPN Power Transistor	T1	Newark Electronics	D44H10	$14.30/10	1	$1.43
Transistor	PNP Power Transistor	T2	Newark Electronics	2N2905	$5.63/10	1	$0.56
Diode	2 amp	D1	Newark Electronics	1N914	$0.55 Each	1	$0.55
High Efficiency LED	Red	LED1, LED2, LED3	Digi-Key Corporation	HLMP3316	$80.00/100	3	$2.40
5V Voltage Ref	3 pin IC	MAX633	Digi-Key Corporation	MAX633CPA	$88.00/40	1	$0.22
+/- 15 Volt Power Supply	200ma, 2mv rms Noise	PS1, PS2	Mod. Power Conv.	MCP15D200CM	$52.00 Each	2	$104.00
						Total	$196.64

TABLE 3.1 List of Semiconductors and modular electronic components and suppliers.

Switches

Description	Specification	PCB/Drawing Reference	Supplier	Supplier Part No.	Price/Qty	Qty per Set	Price/Set
Rotary Switch	BCD, Make before Break	BCD1, BCD2, BCD3, BCD4, BCD5	Elma Electronics	07-1133	$692.00/100	5	$34.60
Knob	For Rotary Switch	Front Panel	Elma Electronics	020-2120	$90.00/100	5	$4.50
Red Cap	For Rotary Switch	Front Panel	Elma Electronics	040-1030	$14.00/100	2	$0.28
Blue Cap	For Rotary Switch	Front Panel	Elma Electronics	040-1040	$14.00/100	2	$0.28
Green Cap	For Rotary Switch	Front Panel	Elma Electronics	040-1050	$14.00/100	1	$0.14
Numbered Dial	For Rotary Switch	Front Panel	Elma Electronics	042-2400	$43.00/100	5	$2.15
Stator	For Rotary Switch	Front Panel	Elma Electronics	043-2220	$48.00/100	5	$2.40
Thwheel Switch	C & K 1-2-2-2-2 Type	Front Panel	Newark Electronics	21F510	$6.36 Each	3	$19.08
Thwheel Ends	For Thwheel	Front Panel	Newark Electronics	21F589	$1.08 Each	2	$2.16
Thwheel Screw	For Thwheel	Front Panel	Newark Electronics	21F592	$0.29 Each	2	$0.58
Thwheel Nut	For Thwheel	Front Panel	Newark Electronics	21F591	$0.05 Each	2	$0.10
Toggle Switch	4PDT	S1, Front Panel	Digi-Key Corporation	CNK1038-ND	$13.20 Each	1	$13.20
Toggle Switch	SPST	S2 and S3, Front Panel	Digi-Key Corporation	CNK1023-ND	$3.92 Each	2	$7.84
						Total	$87.31

Connectors, Misc. Hardware

Description	Specification	PCB/Drawing Reference	Supplier	Supplier Part No.	Price/Qty	Qty per Set	Price/Set
6 Pin Male Cnctr.	Molex	Con 1, Con 2	Digi-Key Corporation	WM4304	$50.13/100	2	$1.00
6 Pin Female Cnctr.	Molex	N/A	Digi-Key Corporation	WM2004	$26.17/100	2	$0.52
Terminals	Molex	N/A	Digi-Key Corporation	WM2200	$5.29/100 pack	1/10 Pk	$0.53
7 Pin Male Cnctr.	Molex	Con 3	Digi-Key Corporation	WM4705	$4.79/100	2	$0.96
7 Pin Female Cnctr.	Molex	N/A	Digi-Key Corporation	WM2105	$4.19/100	2	$0.84
Terminals	Molex	N/A	Digi-Key Corporation	WM2300	$5.14/100 pack	1/10 Pk	$0.51
8 Pin DIP Sockets	For 8 pin I.C.'s	N/A	Newark Electronics	81N9132	$0.83 Each	15	$12.45
14 Pin DIP Sockets	For 14 pin I.C.'s	N/A	Newark Electronics	81N9133	$1.15 Each	11	$12.65
16 Pin DIP Sockets	For 16 pin I.C.'s	N/A	Newark Electronics	81N9134	$1.25 Each	8	$10.00
Isol. BNC Bulkhead	Front Panel	BNC1, BNC2, BNC3, BNC4, BNC5	Digi-Key Corporation	ARF1073-ND	$376.68/100	5	$18.85
BNC cable connector	To suit miniature internal cables	connecting PCB BNC to F.P. BNC	Digi-Key Corporation	A1803-ND	$4.30 Each	8	$34.40
PCB Mount BNC	Solder connect, Right angle	SH1, SH2, SH3, SH4, SH5	Newark Electronics	46F2206	$13.85 Each	5	$69.25
Variable Inductor	10 microH	Front Panel	PD&E Electronics	Type 1000-F Coil	$24.96 Each	1	$24.95
Power Cord	110v AC	Rear Panel	Newark Electronics	C102-ND	$53.20/10	1	$5.32
Power Socket	With EMI filter included	Rear Panel	Newark Electronics	15F2456	$6.45 Each	1	$6.45
Fuse	1/8 Amp, slow blow	Rear Panel	Digi-Key Corporation	F305-ND	$6.62/5	1	$1.32
Fuse Holder	For fuse above	Rear Panel	Digi-Key Corporation	3536K-ND	$0.67 Each	1	$0.67
Chassis Components	Grooved Upper/Lower Strips	See Front panel Drawing	Vector Electronic Co.	SR2-062S-41	$48.00/4	2	$24.00
Heat Sink	For Transistor T1	For T1	Digi-Key Corporation	HS-111	$0.34 Each	1	$0.34
						Total	$225.01

TABLE 3.1 (continued) List of switches, connectors and miscellaneous hardware and suppliers.

Capacitors

Description	Specification	PCB/Drawing Reference	Supplier	Supplier Part No.	Price/Qty	Qty per Set	Price/Set
Ceramic Capacitor	0.1 uF +/- 20%	BP1, BP2, BP3, BP4, BP6, BP7, BP8, BP9, BP10, BP12, BP13, BP14, BP16, BP18, BP28, BP29, BP32, BP33, BP38, BP39, BP48, BP49, BP50, BP51, BP54, BP55, BP56, BP57, BP59, BP66, BP67, BP68, BP69, BP74, BP75, BP77, BP83, BP85, C4	Digi-Key Corporation	P4430	$117.30/100	39	$43.57
Tantalum Capacitor	2.2 uF +/- 20%	BP5, BP11, BP15, BP17, BP19, BP26, BP27, BP30, BP31, BP34, BP35, BP36, BP37, BP40, BP41, BP42, BP43, BP44, BP45, BP46, BP47, BP52, BP53, BP58, BP60, BP64, BP76, BP80, BP81, BP82, BP84	Digi-Key Corporation	P2045	$184.90/100	31	$57.32
Mica Capacitor	7.5 pF +/- 10%	C16, C18, C19, C20, C32, C34	Digi-Key Corporation	SE101	$43.80/100	6	$2.62
Mica Capacitor	30 pF +/- 10%	C10, C21, C22, C26, C36, C37, C39, C43	Newark Electronics	15F1347	$0.22 Each	8	$1.76
Ceramic Capacitor	47 pF +/- 10%	C15, C17, C31, C33	Digi-Key Corporation	P4020	$4.50/100	4	$0.18
Ceramic Capacitor	1000 pF +/- 10%	C35	Digi-Key Corporation	P4141	$7.80/100	1	$0.08
Electrolytic Capacitor	47 uF +/- 20%	BP61, BP62, BP63, BP65, BP70, BP71, BP72, BP73, C44	Digi-Key Corporation	P6053	$22.55/100	9	$2.03
Variable Capacitor	1.4-10 pF +/- 10%	C9, C14, C25, C30	Digi-Key Corporation	SG1029	$5.25/100	4	$2.09
Variable Capacitor	2-15 pF +/- 10%	C8, C13, C24, C29	Digi-Key Corporation	SG1030	$5.25/100	4	$2.09
Variable Capacitor	3-32 pF +/- 10%	C2, C6, C7, C11, C12, C23, C27, C28, C38, C40, C41, C42	Digi-Key Corporation	SG1032	$5.25/100	12	$6.27
						Total	$118.01

TABLE 3.1 (continued) List of capacitors and suppliers.

Resistors

Description	Specification	PCB/Drawing Reference	Supplier	Supplier Part No.	Price/Qty	Qty per Set	Price/Set
Metal Film Resistor	100 Ohm 1/4W +/- 1%	R87, R88, R89, R90, R97	Digi-Key Corporation	100X	$7.98/200	1	$0.04
Carbon Resistor	1.2K Ohm 1/4W +/- 5%	R91, R92, R94, R95, R96	Digi-Key Corporation	1.2KQ		5	$0.09
Metal Film Resistor	1.54K Ohm 1/4W +/- 1%	R34, R43, R72, R81	Digi-Key Corporation	1.54KQ	$7.98/200	4	$0.16
Metal Film Resistor	1K Ohm 1/4W +/- 1%	R84	Digi-Key Corporation	1.00KX	$7.98/200	1	$0.04
Metal Film Resistor	2.21K Ohm 1/4W +/- 1%	R14, R21, R45, R49, R52, R59	Digi-Key Corporation	2.21KX	$7.98/200	6	$0.24
Metal Film Resistor	3.4K Ohm 1/4W +/- 1%	R33, R42, R71, R80	Digi-Key Corporation	3.40KX	$7.98/200	4	$0.16
Metal Film Resistor	4.99K Ohm 1/4W +/- 1%	R11, R12, R13, R15, R20, R22, R47, R48, R50, R93	Digi-Key Corporation	4.99KX	$7.98/200	10	$0.40
Metal Film Resistor	7.5K Ohm 1/4W +/- 1%	R32, R41, R70, R79	Digi-Key Corporation	7.50KX	$7.98/200	4	$0.16
Metal Film Resistor	1K Ohm 1W +/- 1%	RB1, RB2, RB3, RB4, RB5, RB6, RB7, RB8, RB9, RB10, RB11	Hamilton-Avnet	CPF-1	$0.18 Each	11	$1.98
Metal Film Resistor	10K Ohm 1/4W +/- 1%	R10, R16, R23, R35, R44, R46, R51, R53, R58, R60, R73, R82, R83, R98, R99, RPU1, RPU2, RPU3, RPU4, RPU5, RPU6, RPU7, RPU8, RPU9, RPU10, RPU11	Digi-Key Corporation		$20.63/100	26	$5.36
Metal Film Resistor	15K Ohm 1/4W +/- 1%	R31, R40, R69, R78, R85	Digi-Key Corporation	15KX	$7.98/200	5	$0.20
Metal Film Resistor	20K Ohm 1/4W +/- 1%	R17, R24, R54, R61	Digi-Key Corporation	20KX	$7.98/200	4	$0.16
Metal Film Resistor	30K Ohm 1/4W +/- 1%	R30, R39, R68, R77	Digi-Key Corporation	30.1KX	$7.98/200	4	$0.16
Metal Film Resistor	40.2K Ohm 1/4W +/- 1%	R18, R25, R55, R62	Digi-Key Corporation	40.2KX	$7.98/200	4	$0.16
Metal Film Resistor	50K Ohm 1/4W +/- 1%	R86	Digi-Key Corporation	49.9KX	$7.98/200	1	$0.04
Metal Film Resistor	60K Ohm 1/4W +/- 1%	R29, R38, R67, R76	Digi-Key Corporation	60.4KX	$7.98/200	4	$0.16
Metal Film Resistor	80.6K Ohm 1/4W +/- 1%	R19, R26, R56, R63	Digi-Key Corporation	80.6KX	$7.98/200	4	$0.16
Metal Film Resistor	120K Ohm 1/4W +/- 1%	R28, R37, R66, R75	Digi-Key Corporation	121KX	$7.98/200	4	$0.16
Metal Film Resistor	162K Ohm 1/4W +/- 1%	R57, R64	Digi-Key Corporation	162KX	$7.98/200	2	$0.08
Metal Film Resistor	249K Ohm 1/4W +/- 1%	R27, R36, R65, R74	Digi-Key Corporation	249KX	$7.98/200	4	$0.16
Metal Film Resistor	1.0 Ohm 150ppm	For Thumbwheel Switches	Hamilton-Avnet	CMK-550010DT-0	$0.45 Each	1	$0.45
Metal Film Resistor	2.0 Ohm 150ppm	For Thumbwheel Switches	Hamilton-Avnet	CMK-550020DT-0	$0.40 Each	4	$1.60
Metal Film Resistor	10.0 Ohm 150ppm	For Thumbwheel Switches	Hamilton-Avnet	CMK-550100DT-0	$0.40 Each	1	$0.40
Metal Film Resistor	20.0 Ohm 150ppm	For Thumbwheel Switches	Hamilton-Avnet	CMK-550200DT-0	$0.40 Each	4	$1.60
Metal Film Resistor	100.0 Ohm 150ppm	For Thumbwheel Switches	Hamilton-Avnet	CMK-551000DT-0	$0.40 Each	1	$0.40
Metal Film Resistor	200.0 Ohm 150ppm	For Thumbwheel Switches	Hamilton-Avnet	CMK-552000DT-0	$0.40 Each	4	$1.60
Series Resistor Pack	10K Ohm	RP1, RP2	Digi-Key Corporation	770-101-R10K	$32.00/100	2	$0.68
10 Turn Potentiometer	10K Ohm	RV1, RV2	Digi-Key Corporation	73JA103-ND	$92.60/10	2	$18.52
10 Turn Potentiometer	10K Ohm, Front Panel	RV3, RV4	Digi-Key Corporation	CEG14	$18.40/10	2	$3.68
						Total	$39.00

TABLE 3.1 (continued) List of resistors and suppliers.

4. OPERATOR GUIDE

4.1 Overview of Controls

Figure 3.1 is a schematic of the front panel where labels are used to define the controls and LED indicators. The five rotary switches on the left-hand side of the panel have BNC coded digital outputs corresponding to ten positions. The digital outputs are used to control analog switches on the PCB which connect different resistors across the devices which form the adjustable gain and filter blocks. It is important to realize that only the first three BCD outputs are used for the filter setting. This means that *only the first eight positions* correspond with the sequential operations described below. (Switch positions 9 and 10 have the same effect as positions 1 and 2 respectively).

The uppermost on/off toggle switch and LED indicator for the power refer to the connection of $\pm$15V power to the PCB. The 110V 60Hz AC power is not switchable and it is connected to the power supplies via the rear panel connector and internal fuse. The power supplies are responsible for a large proportion of the internal heating so it is preferable to leave them on continuously, even when the anemometer is in standby mode, since this will maintain the enclosure close to the thermal equilibrium point to be experienced under operating conditions.

The horizontal lines which are inscribed on the panel serve to divide it into five sections. The central section contains the controls for the gain, frequency response and offset voltage of the feedback amplifier as well as the tunable cable compensation inductor which is located in the balance arm of the Wheatstone bridge. The labels on the front panel and the buttons for the rotary switches are color-coded red in this region. These controls are used to adjust the stability and frequency response of the anemometer as discussed in section 2.3. Also located in this section is the Standby/Operate switch and indicator LED. When the switch is in the Standby position the input to the power transistor pair is connected to ground. These transistors are responsible for providing current to the bridge for heating the wire so that grounding the inputs disables the anemometer. The switch must be in the standby position when the probe is connected or disconnected from the anemometer otherwise transient currents may cause the probe to burn out. Additionally, when the Standby/Operate switch is in the standby position, any signal that is applied to the Calibration Input BNC Connector is connected to the input of the output amplifier. The Calibration Input BNC connector (labeled CAL) is located in the output amplifier section. When the Standby/Operate switch is in the Operate position the output of the feedback amplifier is connected to the power transistors and the LED indicator is turned on. This connection completes the feedback circuit thereby making the anemometer operational. Simultaneously, the Calibration Input connection to the output amplifier is replaced with the output voltage of the anemometer. Note that the anemometer output voltage is defined to be the voltage at the Top of the Bridge (TOB). The anemometer output voltage is available at the BNC connector labeled TOB which is located within the group of four BNC connectors on the lower portion of the panel. The connection of the TOB voltage to the output amplifier is performed internally on the PCB using an analog switch.

Immediately below the power switch and LED indicator are the controls for the output amplifier section. The labels on the front panel and the buttons for the rotary switches are color-coded blue in this region. Typically, the output voltage of a constant-temperature hot-wire anemometer consists of a relatively large d.c. component upon which are superimposed the small fluctuations which are of interest. As mentioned in section 2.4, it is common practice to utilize a separate "buck and gain" amplifier to subtract a d.c. voltage from the anemometer output and to amplify the resultant signal so that the range of voltages fills the voltage window of a digitizer. For example, the numerical resolution of analog-to-digital converters are limited and the output amplifier can be used to maximise the numerical resolution of the fluctuations.

For convenience, an output amplifier has been incorporated into the instrument for this purpose. The amplifier is essentially an analog computer circuit which is hardwired to perform the linear transformation given by equation (2.1). The output amplifier is configured as an inverting amplifier because the sensitivity of the anemometer (TOB) output voltage is negative. With this arrangement the sensitivity of the output voltage is positive with respect to velocity. The gain G is adjusted using the rotary switch labeled GAIN and the gain follows the logarithmic sequence 1, 2, 4, 8 ... 256 which correspond to switch positions 1 to 9. Gain setting 10 also has a gain of 256. The offset voltage E_{off} is adjusted using the locking counting dial labeled OFFSET on the panel. As mentioned above, when the system is switched to Standby mode the input voltage E_i consists of the signal applied to the Calibration Input BNC connector. This allows the constants G and E_{off} in equation (2.1) to be determined by direct calibration. One reason for wanting these constants with high precision is to enable the recalculation in software of the TOB voltages from the digitized values of the output amplifier signals. This is necessary for hot-wire calibration schemes that are based on King's Law for example. The output amplifier is configured with a low-pass filter consisting of two simple poles in series which are controlled by the rotary switch labeled FILTER. The -3dB points follow the logarithmic sequence shown on the schematic in figure 2.2. It should be emphasized that these filter values are nominal and that tuning capacitors are provided for adjustment of the roll-off frequency and to ensure that the Bode diagram is flat. The Bode diagram cannot be guaranteed to be flat out to these -3dB points unless the tuning capacitors have been tuned manually. The one exception corresponds to switch position 8 since the tuning capacitors have the smallest effect in this position. However tuning capacitors are provided for setting the maximum frequency response and these should be adjusted if the signal content exceeds around 25kHz. It is highly recommended that the Filter switch be used in position 8 unless the circuit has been manually tuned for the other filter settings.

No provision has been included for measuring the cold resistance of wires because this function should only need to be performed occasionally. Inclusion of the extra electronics for such an infrequently used function was considered to be of the lowest priority early in the design stage. Finally, it became apparent that there would be insufficient space for the extra controls despite the rather large size of the front panel. Therefore some other device must be used for measuring the cold resistance. This device should be selected with care. Some Ohm meters will pass a small but significant current through the wire and of course this will change the resistance of the wire. A Kelvin bridge or other null current

device is best for this purpose. The operating resistance of the hot-wire is set using the Hot-Wire Resistance Thumbwheel Switch labeled RESISTANCE in figure 3.1. The switch is configured such that the setting corresponds to the balance resistor setting in ohms i.e. the setting shown in figure 3.1 corresponds to R_b=123.0Ω. In the standard configuration the cross-bridge ratio is 10:1 so that this thumbwheel switch setting corresponds to a hot operating resistance of R_w=12.3Ω for the hot-wire.

A square-wave test is required for tuning the anemometer and this capability is provided via the Square Wave toggle switch. The LED indicates when the square-wave circuit is turned on. In order to minimize noise, all the digital circuitry used for the square-wave is powered down when the switch is the off position. The amplitude of the square-wave signal must be adjusted on the PCB using the trimming potentiometer $RV2$. The amplitude should be small enough to avoid nonlinear behavior i.e. the response to postive and negative fluctuations should be approximately symmetrical. The square-wave frequency is not a critical parameter and the rotary control switch is provided merely for convenience.

4.2 Operation

The hot-wire should be connected to the BNC connector labeled PROBE which is located among the group of four connectors on the lower portion of the front panel as shown in figure 3.1. As mentioned previously, the anemometer output voltage TOB and the output amplifier voltage are also available in this region. If the anemometer appears to be inoperable then the use of 1/32 amp fuse is recommended for testing purposes. Use of the fuse may avoid burning out a good hot-wire. Section 3.4 "Preliminary Tests and Tuning" describes some of the procedures used to set the Offset Voltage and Gain and Filter settings. Experience has shown that the most common cause of problems is associated with an inappropriate Offset Voltage setting for the feedback amplifier.

After the anemometer is operational the next step involves setting the stability and frequency response. The toggle switch in the region labeled SQUARE WAVE on the front panel introduces a square wave perturbation to the Offset Voltage of the feedback amplifier. Tuning of the anemometer should be performed by observing the square wave response at the TOB output on an oscilloscope as the controls are adjusted. Using the output amplifier for tuning purposes is not recommended because of the extra time constants associated with this amplifier. Optimal setting of the square-wave response is discussed in section 6. It is emphasized here again that the electronic square-wave test is an indirect method for setting the stability and frequency response. Proper interpretation of the square-wave response often requires subtle insights into the system behavior. It is easy for an inexperienced operator to be deluded and infer a frequency response that is much higher than the actual system response. Examples are provided in Section 6 which demonstrate how this can occur. Additional cases are considered that should provide a useful guide for relating the influence of the anemometer controls on the square-wave response. The advice contained in this section should also prove useful to experienced operators.

The BNC connector labeled EXT RB is required for the optional configuration in which the cross-bridge ratio is altered from 10:1 to a 1:1 symmetrical bridge by setting jumpers on the PCB. With this optional symmetrical bridge configuration the Hot-Wire Resistance Thumbwheel switch is removed from the bridge and the balance resistor R_b must be located

at the end of a length of co-axial cable that has been carefully chosen to match the probe cable. This configuration offers superior compensation to the simple lumped inductor (by using actual cable instead). Once again, it is emphasized that the bridge must be symmetrical for this option to work properly.

The Cable Compensation Inductor was selected for use with 5μm diameter wires and a 5 meter long probe cable. The adjustment range is satisfactory for systems with a frequency response of 20kHz to 30kHz, but smaller values of the inductor may be required for optimum frequency response when smaller wires are used since they have a higher frequency response (see section 6.5). One simple solution in this situation is to use a longer cable rather than substitute a smaller inductor. However the overall performance of the system will be improved if a smaller inductor is used. In this case the benefits of reducing the cable length to a practical minimum should be considered in conjunction with the substitution of the inductor since performance is improved when the total inductance is reduced. The scaling for selection of a suitable replacement inductor can be based on the ratio of the cable lengths.

5. ANALYSIS

5.1 Introduction

In the constant-temperature mode of operation the hot-wire filament is located in a Wheatstone bridge and a feedback amplifier is used to maintain the wire at very nearly constant resistance. It will be shown by example in section 6 that the feedback amplifier must have the potential for both a high gain and a high frequency response in order for the system as a whole to achieve stable high frequency operation. Practical constant temperature hot-wire anemometer designs should use a cascade of amplifiers rather than a single feedback amplifier because of the gain-bandwidth product (GBW) limitations of physical devices. Therefore a cascade of n amplifiers is used in the model shown in figure 5.1. The device labeled I is a current booster stage which usually consists of a pair of power transistors. It will be assumed that the current booster has unity gain and zero offset exactly. The assumption of a perfect voltage follower means that the current booster need not be considered in the analysis. The behavior of each amplifier will be assumed to be linear with zero offset voltage. The net offset voltage of the amplifier cascade is controlled by introducing a d.c. voltage E_{qi} and a perturbation voltage e_S into the m^{th} amplifier. The d.c. voltage is used to adjust the frequency response and stability of the system while the perturbation voltage is used for estimating the system frequency response. The perturbation voltage usually consists of a square-wave although sinusoidal inputs are sometimes used. In general, upper case letters refer to d.c. quantities while the lower case letters refer to small perturbations. $Z_a(s)$, $Z_b(s)$, $Z_c(s)$ and $Z_w(s)$ represent the electrical impedances of each arm of the bridge and s is the Laplace variable.

5.2 The static operating point

Only the resistive components of the Wheatstone Bridge need to be considered for the static analysis below i.e. $Z_a(s) = R_a$, $Z_b(s) = R_b$, $Z_c(s) = R_c$ and $Z_w(s) = R_w$. The voltage at the top of the bridge i.e. the output of the n^{th} amplifier is given by

$$E_{o_n} = K_b\left[K_a(I_1 R_a - I_2 R_c) + E_{qi}\right] \tag{5.1}$$

where $K_a = K_1 ... K_{m-1}$ is the total gain of the cascade up to (but not including) the m^{th} amplifier where the offset voltage is injected and $K_b = K_m ... K_n$ is the total gain of the cascade from the m^{th} to the n^{th} amplifier. The bridge voltage can also be expressed in terms of the currents I_1 and I_2,

$$E_{o_n} = I_1(R_a + R_w) \tag{5.2}$$

and

$$E_{o_n} = I_2(R_b + R_c) \tag{5.3}$$

Substituting E_{o_n} from equation (5.2) and I_2 from equation (5.3) into equation (5.1) leads to the following expression for the wire current

$$I_1 = \frac{K_b E_{qi}(R_b + R_c)}{(R_a + R_w)(R_b + R_c) + K\mathring{R}} \tag{5.4}$$

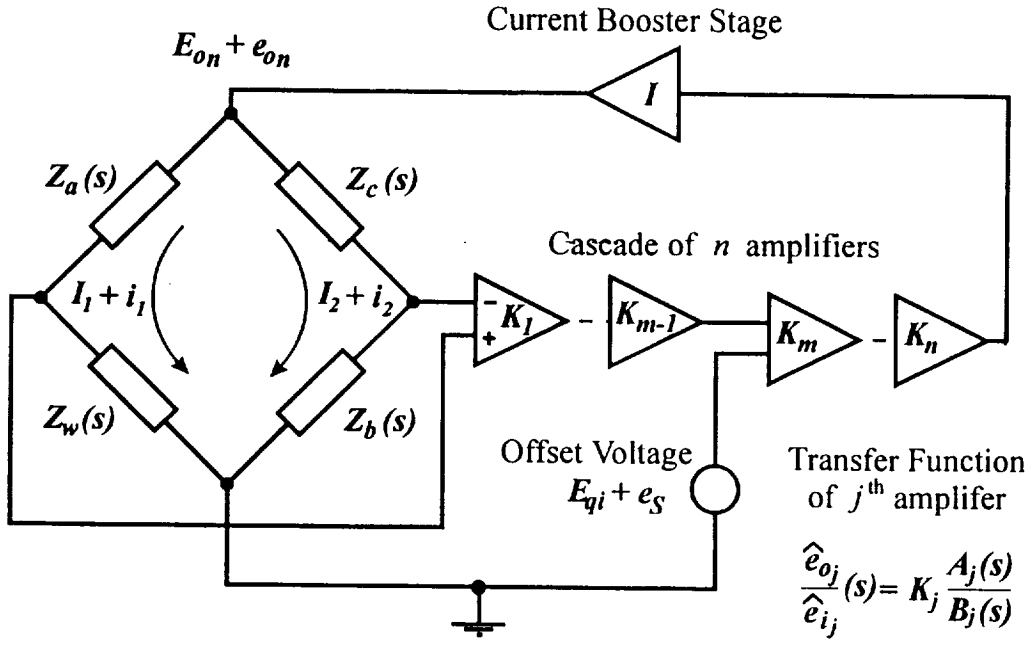

FIGURE 5.1 Model of Constant-Temperature Hot-wire Anemometer.

where $\mathring{R} = R_w R_c - R_a R_b$ represents the bridge imbalance and $K = K_a K_b$ is the overall gain of the cascade. Equation (5.4) represents the behavior of the circuit. Following Smits, Perry and Hoffman (1978), an equation which represents the balance between the heat transfer and the Joule heating of the filament is given by

$$I_1{}^2 = \left(\frac{1}{R_g} - \frac{1}{R_w}\right)\frac{\pi l K_g \,\mathrm{Nu}}{c} \tag{5.5}$$

where R_g is the wire resistance at fluid temperature, l is the length of the wire, K_g is the thermal conductivity of the fluid, Nu is the Nusselt number and c is the temperature coefficient of resistivity of the wire material. The operating point is defined by the intersection of equations (5.4) with (5.5) which must be solved by iteration.

A number of important asymptotes and limits exist with respect to the circuit equation. For example, the r.h.s. of equation (5.4) must be indeterminate if I_1 is to remain finite as $E_{qi} \to 0$ i.e.

$$(R_a + R_{wa})(R_b + R_c) + K\mathring{R}_a = 0 \tag{5.6}$$

where $\mathring{R}_a = R_{wa} R_c - R_a R_b$ is the value of $\mathring{R}$ corresponding to the asymptotic value of the wire resistance

$$R_{wa} = \frac{K R_a R_b - R_a(R_b + R_c)}{K R_c + (R_b + R_c)} \tag{5.7}$$

It is important to realize that perfect bridge balance can be achieved only in the limit as the offset voltage $E_{qi} \to 0$ and as the overall gain of the amplifier cascade $K \to \infty$. However the quantity $K\mathring{R}$ always remains finite, even as the limits mentioned above are

approached. The quantity $K\mathring{R}$ has a strong effect on the system stability and frequency response and it is controlled by adjusting the offset voltage.

Wood (1975) performed an analysis of the type of system in which the gain of the feedback amplifier is frequency dependent. For systems with a frequency dependent gain the term $K\mathring{R}$ is multiplied by the ratio of the a.c. gain to the d.c. gain which can be as small as 0.003. This minimizes the effect of offset voltage and the system stability and frequency response are adjusted by varying the a.c. gain in conjunction with the balance inductance and roll-off frequency of the amplifier. This is typical of some commercially available systems and is thought to offer several advantages over the type of system considered in this report. Firstly, tuning the system frequency response by adjusting the a.c. gain does not alter the hot-wire calibration as does offset voltage adjustment in the system described here. However if the frequency response and stability of the system are properly tuned then there should be no need for further adjustments after calibration. Secondly, as mentioned above, a constant-temperature hot-wire anemometer cannot maintain the bridge in perfect balance. The wire resistance varies slightly with mean velocity so that the calibration curve deviates from the ideal constant temperature behavior. Systems with high d.c. gain amplifiers are designed to minimize the bridge imbalance so that the hot-wire system can be thought to more closely follow some idealized heat transfer law, such as King's law. Smits and Perry (1980) studied the influence of the overall gain by assuming King's law and solving equations (5.4) and (5.5) for the operating point as the velocity is varied. They found that the deviations from ideal behavior were of order 1% for a gain of 500 and that increasing the gain beyond 1000 brings only a diminishing return. These small deviations from ideal behavior would be accounted for in practice by the curve fit used for the calibration. In any case, a hot-wire filament cannot be regarded as a straight infinitely long cylinder of uniform circumferential and spanwise temperature (see Perry 1982) so it seems unlikely that there exists a single universal heat-transfer law for hot-wire calibrations. When these practical considerations are taken into account the advantage of frequency dependent gain systems should be considered idealistic and of minor significance.

Of more concern is that a negative step in the Bode diagram occurs when the feedback amplifier has a frequency dependent gain. One shortcoming of the analysis of Wood (1975) is that it applies only for frequencies below which the a.c. gain is flat. Although he could not calculate the response from his analysis in the frequency range where the amplifier gain is falling from its d.c. level to its a.c. plateau, Wood realized that a significant step in the frequency response could occur. He argued, by worst case example, that the effect is only important (7%) at low resistance ratios and for low a.c. gains. However Smits and Perry (1980) found that the step size can be significant for resistance ratios greater than 1.1. Even for resistance ratios of order 1.5 they showed that the size of the step can be as large as 3% of the static response. For these reasons, the feedback amplifier of the anemometer described in this report was designed to have a flat frequency response.

5.3 Transfer functions for dynamic response

The circuit shown in figure 5.1 will be analyzed using Laplace transform methods since transient phenomena can be examined (such as the square-wave response) in addition to the usual steady-state sinusoidal response. It will be assumed that the dynamic behavior

of any j^{th} amplifier in the cascade can be adequately described by

$$\frac{\hat{e}_{o_j}}{\hat{e}_{i_j}}(s) = K_j \frac{A_j(s)}{B_j(s)} \tag{5.8}$$

which is the transfer function for output voltage fluctuations in terms of the input voltage fluctuations. The circumflex denotes the Laplace transform i.e.

$$\hat{e}_{i_j}(s) = \mathbf{L}\{e_{i_j}(t)\} = \int_0^\infty e_{i_j}(t)e^{-st}dt \tag{5.9}$$

K_j is the amplifier gain and the roots of the polynomials $A_j(s)$ and $B_j(s)$ are the zeros and poles of the amplifier. An overview of the application of Laplace transform methods to systems of differential equations is given in Appendix A along with definitions of a transfer function and its poles and zeros. From now on the circumflex will be dropped but the Laplace transform is still implied.

In a physical circuit the current booster stage usually has a frequency response well in excess of the amplifiers. For the purpose of modeling it will be assumed that the frequency response is infinite in addition to the assumptions of exact unity gain and zero offset voltage. As mentioned previously, the assumption of an "ideal" current booster stage means that it need not be considered in the following analysis.

The small perturbation output voltage of the first amplifier in the cascade is given by

$$e_{o_1} = K_1 \frac{A_1(s)}{B_1(s)} \Big[i_1 Z_a(s) - i_2 Z_c(s) \Big] \tag{5.10}$$

where i_1 and i_2 are the small perturbation bridge currents and $Z_a(s)$ and $Z_c(s)$ represent the electrical impedances of the upper half of the bridge (see figure 5.1). The small perturbation bridge currents i_1 and i_2 are dependent on both offset voltage and velocity perturbations. The system transfer functions will be derived for the two cases of offset voltage perturbations (with no velocity fluctuations) and velocity fluctuations (with no offset voltage perturbations).

5.3.1 System Transfer Function for Offset Voltage Perturbations

In the absence of velocity fluctuations, the small perturbation currents i_1 and i_2 can be expressed in terms of the voltage fluctuation at the top of the bridge i.e. the output e_{o_n} of the last (n^{th}) amplifier

$$i_1 = \frac{e_{o_n}}{Z_a(s) + Z_w(s)} \tag{5.11a}$$

and

$$i_2 = \frac{e_{o_n}}{Z_b(s) + Z_c(s)} \tag{5.11b}$$

The electrical impedance of each arm of the bridge can be expressed as transfer functions i.e.

$$\begin{aligned} Z_a(s) &= \frac{Z_{a_N}(s)}{Z_{a_D}(s)}, & Z_b(s) &= \frac{Z_{b_N}(s)}{Z_{b_D}(s)}, \\ Z_c(s) &= \frac{Z_{c_N}(s)}{Z_{c_D}(s)}, \quad \text{and} & Z_w(s) &= \frac{Z_{w_N}(s)}{Z_{w_D}(s)}. \end{aligned} \tag{5.12}$$

This representation is completely general and an arbitrarily large number of elements can be used. The only restriction is that the elements must consist of lumped components. Using equations (5.11a) and (5.11b) to substitute for i_1 and i_2 in equation (5.10) and then applying equation (5.8) along the amplifier cascade leads to the expression for the output of the last (n^{th}) amplifier e_{o_n}, i.e.

$$e_{o_n} = K_m \cdots K_n \frac{A_m(s) \cdots A_n(s)}{B_m(s) \cdots B_n(s)} \left[K_1 \cdots K_{m-1} \frac{A_1(s) \cdots A_{m-1}(s)}{B_1(s) \cdots B_{m-1}(s)} \right.$$
$$\left. \times \left(\frac{e_{o_n} Z_a(s)}{Z_a(s) + Z_w(s)} - \frac{e_{o_n} Z_c(s)}{Z_c(s) + Z_b(s)} \right) + e_S \right] \tag{5.13}$$

Equation (5.13) implies that a minimum of two equivalent amplifier stages are needed to properly account for the introduction of offset voltage perturbations. The first of these two equivalent amplifiers, a, has a transfer function equal to the amplifier cascade up to (but not including) the m^{th} amplifier where the offset voltage is injected, i.e.

$$\frac{e_{o_a}}{e_{i_a}} = K_1 \cdots K_{m-1} \frac{A_1(s) \cdots A_{m-1}(s)}{B_1(s) \cdots B_{m-1}(s)} \tag{5.14}$$
$$= K_a \frac{A_a(s)}{B_a(s)} \tag{5.15}$$

The second equivalent amplifier, b, has a transfer function equivalent to the amplifier cascade from the m^{th} to the n^{th} amplifier, i.e.

$$\frac{e_{o_b}}{e_{i_b}}(s) = K_m \cdots K_n \frac{A_m(s) \cdots A_n(s)}{B_m(s) \cdots B_n(s)} \tag{5.16}$$
$$= K_b \frac{A_b(s)}{B_b(s)} \tag{5.17}$$

The transfer function of the system response to offset voltage fluctuations using the equivalent amplifiers a and b is obtained from equation (5.13) as,

$$\frac{e_{o_n}}{e_S}(s) = K_e \frac{Q_e(s)}{P(s)} \tag{5.18}$$

where $K_e = K_b$ and the polynomial expression for the system zeros is given by

$$Q_e(s) = A_b(s) B_a(s) Z_1(s) \tag{5.19}$$

and the polynomial expression for the system poles is given by

$$P(s) = B_a(s) B_b(s) Z_1(s) + K_a K_b A_a(s) A_b(s) Z_2(s) \tag{5.20}$$

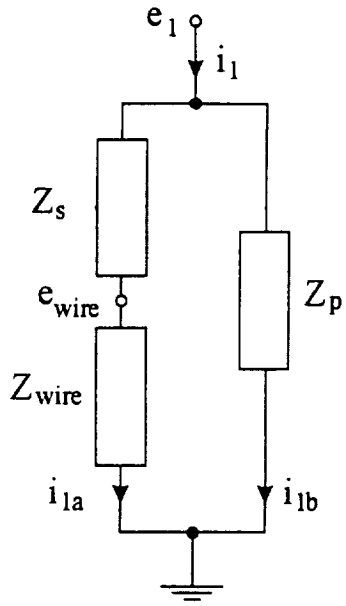

FIGURE 5.2 General representation of Bridge Impedance Z_w required used to derive the System Transfer Function for Velocity Fluctuations.

where,

$$Z_1(s) = \left[Z_{a_N}(s)Z_{w_D}(s) + Z_{a_D}(s)Z_{w_N}(s)\right]\left[Z_{b_N}(s)Z_{c_D}(s) + Z_{b_D}(s)Z_{c_N}(s)\right] \qquad (5.21)$$

and

$$Z_2(s) = Z_{a_D}(s)Z_{b_D}(s)Z_{c_N}(s)Z_{w_N}(s) - Z_{a_N}(s)Z_{b_N}(s)Z_{c_D}(s)Z_{w_D}(s) \qquad (5.22)$$

Note that the poles of the amplifiers which precede the offset voltage injection stage appear as zeros in the overall system transfer for offset voltage fluctuations in equation (5.19).

5.3.2 System Transfer Function for Velocity Fluctuations

Voltage fluctuations across the hot-wire filament originate from both velocity fluctuations and perturbations in wire current. In the previous case, the fluctuations in wire current were the result of offset voltage perturbations and the current perturbations in each arm of the bridge could be simply expressed in terms of the bridge impedances in equations (5.11). The voltage fluctuations at the top of the bridge could then be calculated directly using equation (5.13). In the case of velocity fluctuations the wire acts as the source of the voltage fluctuations and the current perturbations depend on the nature of the impedances forming the wire arm of the bridge $Z_w(s)$. The representation of $Z_w(s)$ required for the derivation of the transfer functions for velocity fluctuations is shown in figure 5.2. The operational impedance $Z_s(s)$ is in series with the wire and $Z_p(s)$ is the impedance in

parallel with the wire and $Z_s(s)$. This representation is also completely general and an arbitrarily large number of elements can be used to form the impedances $Z_s(s)$, $Z_{\text{wire}}(s)$ and $Z_p(s)$.

Let the transfer functions representing the impedances be given by,

$$Z_{\text{wire}}(s) = \frac{Z_{\text{wire}_N}(s)}{Z_{\text{wire}_D}(s)}, \qquad Z_s(s) = \frac{Z_{s_N}(s)}{Z_{s_D}(s)} \quad \text{and} \quad Z_p(s) = \frac{Z_{p_N}(s)}{Z_{p_D}(s)}. \tag{5.23}$$

The voltage perturbation across the wire is given by

$$e_{\text{wire}} = Z_{\text{wire}}(s)\ i_{1a} + S_u\ F_u(s)\ u \tag{5.24}$$

where i_{1a} is the wire current, S_u is the sensitivity to velocity perturbations (i.e. $\partial E_{\text{wire}}/\partial U$) at zero frequency, u is the velocity perturbation and $F_u(s)$ represents the normalized frequency response characteristics of the wire i.e. $F_u(0) = 1$. S_u is a constant at fixed velocity. The voltage across the wire arm of the bridge is given by

$$e_1 = \Big[Z_s(s) + Z_{\text{wire}}(s)\Big]\ i_{1a} + S_u\ F_u(s)\ u \tag{5.25}$$

which is also equal to the voltage across the parallel impedance i.e.

$$e_1 = Z_p(s)\ i_{1b}. \tag{5.26}$$

The total perturbation current ($i_1 = i_{1a} + i_{ib}$) can be found from equations (5.25) and (5.26) so that the voltage perturbation at the top of the bridge can be determined i.e.

$$e_{o_n} = \Big[Z_a(s) + Z_w(s)\Big]\ i_1 + \ S_u\ F_u(s)F_z(s)\ u \tag{5.27}$$

where

$$F_z(s) = \frac{Z_p(s)}{Z_p(s) + Z_s(s) + Z_{\text{wire}}(s)} \tag{5.28}$$

and the impedance of the wire arm of the bridge is given by

$$Z_w(s) = \frac{Z_p(s)\big[Z_s(s) + Z_{\text{wire}}(s)\big]}{Z_p(s) + Z_s(s) + Z_{\text{wire}}(s)} \tag{5.29}$$

Substituting for i_1 from equation (5.27) and i_2 from equation (5.11b) into equation (5.10) and using the two amplifier model for the cascade, the system transfer function for velocity fluctuations is given by

$$\frac{e_{o_n}}{u}(s) = K_u \frac{Q_u(s)}{P(s)} \tag{5.30}$$

where

$$K_u = S_u K_a K_b \tag{5.31}$$

and

$$Q_u(s) = A_a(s)A_b(s)Z_3(s)F_u(s)Z_{\text{wire}_D}(s) \tag{5.32}$$

where

$$Z_3(s) = Z_{a_N}(s)Z_{p_N}(s)Z_{s_D}(s)\Big[Z_{b_N}(s)Z_{c_D}(s) + Z_{b_D}(s)Z_{c_N}(s)\Big] \tag{5.33}$$

The behavior of a hot-wire filament is very complex. For example, Perry (1982) discusses aeroelastic effects and perturbations in the symmetry of the temperature distribution along the wire. Even relatively simple models which allow for a non-uniform temperature distribution along the wire must use a partial differential equation in space and time. In order to keep the analysis tractable a simple lumped model will be used for the hot-wire filament i.e.

$$F_u(s) = \frac{1}{T_w s + 1} \tag{5.34}$$

and

$$\frac{Z_{\text{wire}_N}(s)}{Z_{\text{wire}_D}(s)} = \frac{R_w T_w s + R_w + \alpha}{T_w s + 1} \tag{5.35}$$

T_w is the lumped time constant of the wire arising from its thermal inertia, R_w is the d.c. wire resistance and $\alpha = R_w(R_w - R_g)/R_g$ where R_g is the wire resistance at fluid temperature. The simple lumped model for the filament possesses the same time constant for the simple poles of the sensitivity to velocity and current fluctuations and this leads to a simplified expression for the system zeros

$$Q_u(s) = A_a(s)A_b(s)Z_3(s) \tag{5.36}$$

In the limit $Z_p(s) \to \infty$ (i.e. when there are no elements in parallel with the wire) the expression for $Z_3(s)$ given by equation (5.33) should not be used since it implies that $Q_u(s) \to \infty$. The expressions for $Z_1(s)$ and $Z_2(s)$ given by equations (5.21) and (5.22) can be factored by $Z_{p_N}(s)$ and when $Z_p(s) = \infty$ the expression for $Z_3(s)$ is given by

$$Z_3(s) = Z_{a_N}(s)Z_{s_D}(s)\Big[Z_{b_N}(s)Z_{c_D}(s) + Z_{b_D}(s)Z_{c_N}(s)\Big] \tag{5.37}$$

Equations (5.21) and (5.22) can still be used to evaluate $Z_1(s)$ and $Z_2(s)$ when $Z_p(s) = \infty$.

It is important to note that the poles of the transfer functions for both offset and velocity fluctuations are identical (provided that $F_u(s)Z_{\text{wire}_D}(s) = 1$). This result is completely general in the sense that the system poles are identical, independent of the number of amplifiers in the cascade, the complexity of the overall transfer function for the feedback amplifier and the number of lumped components used to model the bridge impedances.

5.4 Some illustrative examples of transfer functions

Unlike the poles, the zeros of the transfer function for offset and velocity fluctuations are quite different. It has already been noted that the poles of amplifiers preceding the offset voltage control stage appear as zeros in the transfer function for offset voltage perturbations

but not for the velocity fluctuations. Other differences between the zeros of the two system transfer functions depend on the nature of the bridge impedances and these will be considered in the examples below. It should be emphasized that the derivation of the polynomial expressions for the system poles and zeros in equations (5.19), (5.20) and (5.36) can be quite involved, even for relatively simple configurations. It is instructive to consider some particular cases.

5.4.1 The Simplest Possible Configuration

For the simplest possible configuration only resistive elements appear in the bridge i.e.

$$Z_{a_N}(s) = R_a, \qquad Z_{a_D}(s) = 1 \tag{5.38}$$

$$Z_{b_N}(s) = R_b, \qquad Z_{b_D}(s) = 1 \tag{5.39}$$

$$Z_{c_N}(s) = R_c, \qquad Z_{c_D}(s) = 1 \tag{5.40}$$

and from equations (5.35) and (5.12) the impedance of the wire arm of the bridge is given by

$$\begin{aligned} Z_{w_N}(s) &= R_w T_w s + R_w + \alpha \\ Z_{w_D}(s) &= T_w s + 1 \end{aligned} \tag{5.41}$$

Substituting equations (5.38) ... (5.41) into (5.21), (5.22) and (5.37) leads to the expressions

$$Z_1(s) = (R_b + R_c)\left[(R_a + R_w)T_w s + (R_a + R_w + \alpha)\right] \tag{5.42}$$

$$Z_2(s) = \mathring{R}(T_w s + 1) + R_c \alpha \tag{5.43}$$

$$Z_3(s) = R_a(R_b + R_c) \tag{5.44}$$

Assuming an ideal amplifier i.e. one with infinite frequency response, then

$$A_a(s) = B_a(s) = A_b(s) = B_b(s) = 1 \tag{5.45}$$

Let the feedback amplifier consist of a single stage such that $K_a = 1$ and $K_b = K$. Substitution of equations (5.42) ... (5.45) into (5.19), (5.20) and (5.36) leads to

$$Q_e(s) = (R_a + R_w)(R_b + R_c)T_w s + (R_a + R_w + \alpha)(R_b + R_c) \tag{5.46}$$

$$Q_u(s) = R_b + R_c \tag{5.47}$$

$$\begin{aligned} P(s) = {} & \left[(R_b + R_c)(R_a + R_w) + K\mathring{R}\right]T_w s \\ & + (R_b + R_c)(R_a + R_w + \alpha) + K(\mathring{R} + R_c + \alpha) \end{aligned} \tag{5.48}$$

The time constant of the simple zero in equation (5.46) is approximately the same as the time constant T_w of the wire filament. It is this zero which causes the system response to a step input of offset voltage to appear like the response expected from a delta-function impulse of velocity. Note that this system possesses only one simple pole so that the step

response can only exhibit an exponential decay i.e. the system response cannot exhibit ringing. The static response and the dynamic response are coupled through the quantity $\mathring{R}$ which is controlled by adjusting the offset voltage. Consideration of equations (5.6) and (5.48) indicates that the time constant of the simple pole approaches zero (i.e. the frequency response of the system becomes infinite) as the offset voltage approaches zero. In practice the frequency response is limited by other higher order effects. It was once believed that the frequency response characteristics of the feedback amplifier were the dominant factor in the determination of overall system performance and stability. However Davis and Davies (1968) demonstrated the importance of the inductance of the probe cable and the offset voltage. Perry and Morrison (1971) extended this work and the results for an inductive system are given in the next section.

5.4.2 Hot-wire System with Inductance

Perry and Morrison modeled the hot-wire cable as a simple lumped inductive element L_w in series with the wire. Equations (5.35) and (5.12) give the components of impedance of the wire arm of the bridge as,

$$\begin{aligned} Z_{w_N}(s) &= L_w T_w s^2 + (R_w T_w + L_w)s + (R_w + \alpha) \\ Z_{w_D}(s) &= T_w s + 1 \end{aligned} \tag{5.49}$$

They demonstrated that the system stability and frequency response could be improved by incorporating a tunable balance inductor L_b in series with the bridge resistor R_b. From equation (5.12), the components of the impedance of this arm of the bridge are,

$$\begin{aligned} Z_{b_N}(s) &= L_b s + R_b \\ Z_{b_D}(s) &= 1 \end{aligned} \tag{5.50}$$

The upper bridge elements are purely resistive and substitution of equations (5.38), (5.40), (5.49) and (5.50) into equations (5.21), (5.22) and (5.37) leads to the expressions

$$\begin{aligned} Z_1(s) = {} & L_b L_w T_w s^3 \\ & + \left\{ \left[(R_b + R_c)L_w + (R_a + R_w)L_b \right] T_w + L_b L_w \right\} s^2 \\ & + \left\{ (R_b + R_c)\left[(R_a + R_w)T_w + L_w \right] + (R_a + R_w + \alpha)L_b \right\} s \\ & + (R_b + R_c)(R_a + R_w + \alpha) \end{aligned} \tag{5.51}$$

$$Z_2(s) = (R_c L_w - R_a L_b)T_w s^2 + (\mathring{R} T_w + R_c L_w - R_a L_b)s + (\mathring{R} + R_c \alpha) \tag{5.52}$$

$$Z_3(s) = R_a \left[L_b s + (R_b + R_c) \right] \tag{5.53}$$

Perry and Morrison did not consider the frequency response characteristics of the feedback amplifier so that the poles and zeros are given by equation (5.45). Substitution of these expressions into equation (5.20) for $P(s)$ leads to a 3rd-order polynomial for the system poles

$$P(s) = P_3 s^3 + P_2 s^2 + P_1 s + P_0 \tag{5.54}$$

where the constants $P_0 ... P_3$ are given by

$$\begin{pmatrix} P_0 \\ P_1 \\ P_2 \\ P_3 \end{pmatrix} = \begin{pmatrix} 1 & 0 & 0 & 0 \\ 0 & 1 & 0 & 0 \\ 0 & 0 & 1 & 0 \\ 0 & 0 & 0 & 1 \end{pmatrix} \begin{pmatrix} C_0 \\ C_1 \\ C_2 \\ C_3 \end{pmatrix} + K \begin{pmatrix} 1 & 0 & 0 \\ 0 & 1 & 0 \\ 0 & 0 & 1 \\ 0 & 0 & 0 \end{pmatrix} \begin{pmatrix} C_{K0} \\ C_{K1} \\ C_{K2} \end{pmatrix} \tag{5.55}$$

$C_0 \cdots C_3$ and $C_{K0} \cdots C_{K2}$ are constants that depend on the system parameters i.e.

$$\begin{aligned} C_0 &= (R_b + R_c)(R_a + R_w + \alpha) \\ C_1 &= (R_b + R_c)\big[(R_a + R_w)T_w + L_w\big] + (R_a + R_w + \alpha)L_b \\ C_2 &= \big[(R_b + R_c)L_w + (R_a + R_w)L_b\big]T_w + L_b L_w \\ C_3 &= L_b L_w T_w \\ C_{K0} &= \mathring{R} + R_c\alpha \\ C_{K1} &= \mathring{R}T_w + R_c L_w - R_a L_b \\ C_{K2} &= (R_c L_w - R_a L_b)T_w \end{aligned} \tag{5.56}$$

The presentation of equation (5.55) using matrix notation has the advantage of being compact while retaining the overall appearance of equation (5.20) and allows the important features of the coefficients to be examined in equation (5.56).

A single zero occurs in the transfer function for velocity fluctuations i.e.

$$Q_u(s) = R_a(L_b s + R_b + R_c). \tag{5.57}$$

In most configurations this zero is located well beyond the frequency range of interest so that it is not of great significance. The expression for the zeros of the transfer function for offset voltage fluctuations is 3^{rd}-order

$$Q_e(s) = C_3 s^3 + C_2 s^2 + C_1 s + C_0. \tag{5.58}$$

The simple zero given by equation (5.46) for the simple system with only resistive bridge elements has a time constant that is approximately the same as the wire filament. It turns out there is always a simple zero in equation (5.58) with a time constant of similar value. Therefore the response to a step input will also appear like the response expected from a delta-function impulse of velocity. However the expression for the poles is now 3^{rd}-order so that a pair of complex conjugate poles are possible. In this case the step response may exhibit ringing i.e. the decaying sinusoidal response which users of hot-wire anemometers are familiar with.

5.4.3 Effect of the Frequency Response of the Feedback Amplifier

The positions of the system poles on the s-plane are independent of how the poles and zero are distributed among the first and second equivalent amplifiers. However extra zeros will appear in the transfer function for offset voltage fluctuations if the poles are located

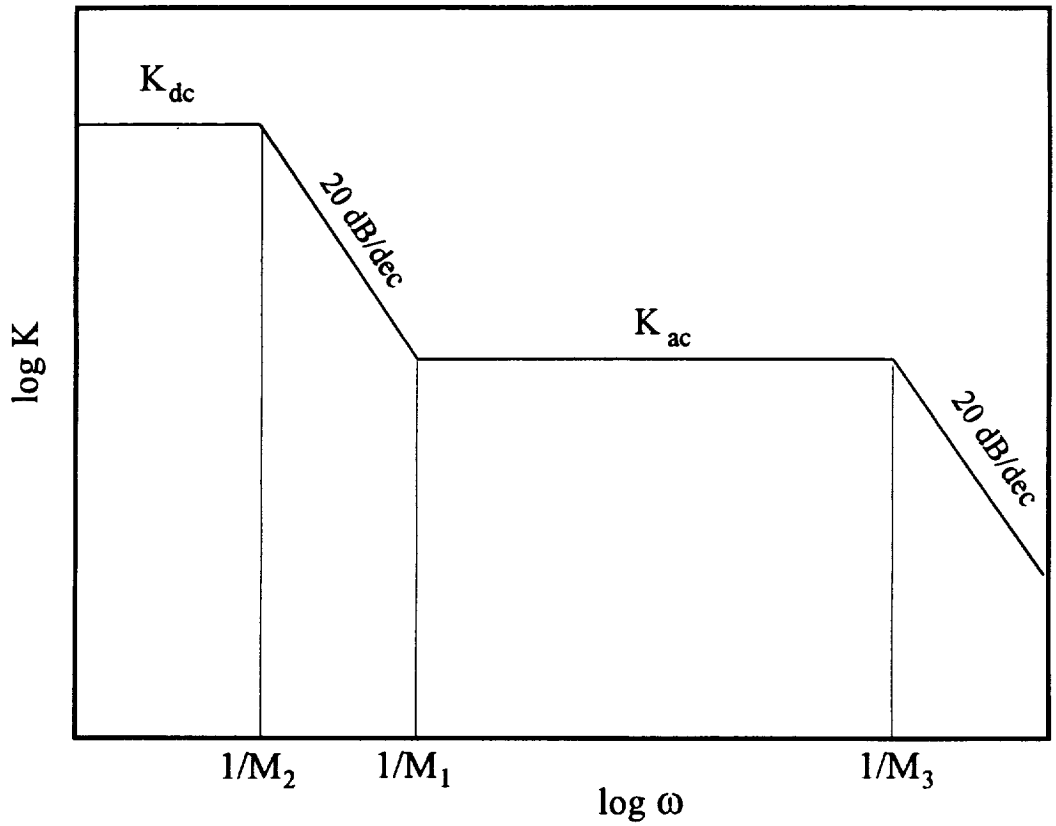

FIGURE 5.3 Sketch of Bode diagram for amplitude of a feedback amplifier with a simple zero with time constant M_1 and two simple poles with time constants M_2 and M_3

before the offset voltage control stage i.e. $B_a(s)$, see equation (5.19). The number of zeros in the transfer function for velocity fluctuations remains unaltered in this situation, see equation (5.36). Further, a zero that is incorporated into the feedback amplifier will only appear in both system transfer functions if it is added to the second equivalent amplifier. If any poles and/or zeros are deliberately added to the feedback amplifier for control purposes then it is highly recommended that they be added only to the second equivalent amplifier i.e. after the offset voltage injection stage. This will avoid introducing any further differences between the system transfer functions for velocity and offset voltage fluctuations. The inherent differences between the transfer functions already make it difficult enough to correctly infer the system frequency response from square-wave tests.

The addition of a simple zero with time constant M_1 and two simple poles with time constants M_2 and M_3 to the second equivalent amplifier (equation 5.17) leads to a system in which the polynomial for the poles is 5^{th}-order i.e.

$$P(s) = P_5 s^5 + P_4 s^4 + P_3 s^3 + P_2 s^2 + P_1 s + P_0 \tag{5.59}$$

where the constants $P_0 ... P_5$ are given by

$$\begin{pmatrix} P_0 \\ P_1 \\ P_2 \\ P_3 \\ P_4 \\ P_5 \end{pmatrix} = \begin{pmatrix} 1 & 0 & 0 & 0 \\ M_2 + M_3 & 1 & 0 & 0 \\ M_2 M_3 & M_2 + M_3 & 1 & 0 \\ 0 & M_2 M_3 & M_2 + M_3 & 1 \\ 0 & 0 & M_2 M_3 & M_2 + M_3 \\ 0 & 0 & 0 & M_2 M_3 \end{pmatrix} \begin{pmatrix} C_0 \\ C_1 \\ C_2 \\ C_3 \end{pmatrix}$$

$$+K \begin{pmatrix} 1 & 0 & 0 \\ M_1 & 1 & 0 \\ 0 & M_1 & 1 \\ 0 & 0 & M_1 \\ 0 & 0 & 0 \\ 0 & 0 & 0 \end{pmatrix} \begin{pmatrix} C_{K0} \\ C_{K1} \\ C_{K2} \end{pmatrix} \qquad (5.60)$$

The matrix notation in equation (5.60) illustrates the coupling between the gain and the poles and zeros of the feedback amplifier. The expressions for the zeros can be obtained by multiplying the polynomials in equations (5.57) and (5.58) by $(M_1 s + 1)$. As a matter of interest this configuration could be used for examination of systems in which the gain of the feedback amplifier is frequency dependent by putting $M_2 > M_1 > M_3$. The Bode diagram of a feedback amplifier with this particular frequency dependent gain distribution is sketched in figure 5.3. Smits and Perry (1980) considered the behavior of systems with a feedback amplifier with a frequency dependent gain but did not account for the high frequency roll-off i.e. $M_3 = 0$. For the reasons mentioned previously this type of system has not been used for the anemometer design described in this memorandum.

5.4.4 Effect of additional reactive bridge components

Including the frequency response characteristics of the feedback amplifier introduces a relatively small increase in the effort required to expand the transfer function polynmials. However the addition of a small number of reactive bridge elements leads to a much higher level of complexity. Using a single lumped inductor is a rather simplistic representation of a co-axial hot-wire cable with its distributed inductance, capacitance, resistance and leakage conductance. A slightly more sophisticated model for the cable could include a lumped capacitor C_w in parallel with lumped inductor L_w and the wire. A balance capacitor C_b could be introduced in parallel with the balance resistor and balance inductor. This configuration was studied by Watmuff (1987) and leads to a system in which the polynomial for the poles is 7^{th}-order i.e.

$$P(s) = P_7 s^7 + P_6 s^6 + P_5 s^5 + P_4 s^4 + P_3 s^3 + P_2 s^2 + P_1 s + P_0 \qquad (5.61)$$

where the constants $P_0 ... P_7$ are given by

$$\begin{pmatrix} P_0 \\ P_1 \\ P_2 \\ P_3 \\ P_4 \\ P_5 \\ P_6 \\ P_7 \end{pmatrix} = \begin{pmatrix} 1 & 0 & 0 & 0 & 0 & 0 \\ M_2+M_3 & 1 & 0 & 0 & 0 & 0 \\ M_2M_3 & M_2+M_3 & 1 & 0 & 0 & 0 \\ 0 & M_2M_3 & M_2+M_3 & 1 & 0 & 0 \\ 0 & 0 & M_2M_3 & M_2+M_3 & 1 & 0 \\ 0 & 0 & 0 & M_2M_3 & M_2+M_3 & 1 \\ 0 & 0 & 0 & 0 & M_2M_3 & M_2+M_3 \\ 0 & 0 & 0 & 0 & 0 & M_2M_3 \end{pmatrix} \begin{pmatrix} C_0 \\ C_1+C_1{}' \\ C_2+C_2{}' \\ C_3+C_3{}' \\ C_4{}' \\ C_5{}' \end{pmatrix}$$

$$+K \begin{pmatrix} 1 & 0 & 0 & 0 & 0 \\ M_1 & 1 & 0 & 0 & 0 \\ 0 & M_1 & 1 & 0 & 0 \\ 0 & 0 & M_1 & 0 & 0 \\ 0 & 0 & 0 & M_1 & 0 \\ 0 & 0 & 0 & 0 & M_1 \\ 0 & 0 & 0 & 0 & 0 \\ 0 & 0 & 0 & 0 & 0 \end{pmatrix} \begin{pmatrix} C_{K0} \\ C_{K1}+C_{K1}{}' \\ C_{K2}+C_{K2}{}' \\ C_{K3}{}' \\ C_{K4}{}' \end{pmatrix} \tag{5.62}$$

The constants C_0, C_1, C_2, C_3, C_{K0}, C_{K1} and C_{K2} are given in equation (5.56) and

$$\begin{aligned}
C_1{}' &= R_bR_c(R_a+R_w+\alpha)C_b \\
&\quad + R_a(R_b+R_c)(R_w+\alpha)C_w \\
C_2{}' &= R_a(R_b+R_c)(R_wT_w+L_w)C_w \\
&\quad + R_a(R_w+\alpha)L_bC_w \\
&\quad + R_bR_c\big[(R_a+R_w)T_w+L_w\big]C_b \\
&\quad + R_c(R_a+R_w+\alpha)L_bC_b \\
&\quad + R_aR_bR_c(R_w+\alpha)C_bC_w \\
C_3{}' &= R_a(R_b+R_c)L_wT_wC_w \\
&\quad + R_a(R_wT_w+L_w)L_bC_w \\
&\quad + R_c\big[(R_a+R_w)T_w+L_w\big]L_bC_b \\
&\quad + R_bR_cL_wT_wC_b \\
&\quad + R_aR_bR_c(R_wT_w+L_w)C_bC_w \\
&\quad + R_aR_c(R_w+\alpha)L_bC_bC_w \\
C_4{}' &= R_aR_c\big[(R_wL_b+R_bL_w)T_w+L_bL_w\big]C_bC_w \\
&\quad + (R_cC_b+R_aC_w)L_bL_wT_w \\
C_5{}' &= R_aR_cL_bL_wT_wC_bC_w \\
C_{K1}{}' &= R_b(R_w+\alpha)(R_cC_b-R_aC_w) \\
C_{K2}{}' &= \big[L_b(R_w+\alpha)+R_b(R_wT_w+L_w)\big](R_cC_b-R_aC_w) \\
C_{K3}{}' &= \big[(R_wL_b+R_bL_w)T_w+L_bL_w\big](R_cC_b-R_aC_w) \\
C_{K4}{}' &= L_bL_wT_w(R_cC_b-R_aC_w)
\end{aligned} \tag{5.63}$$

The zeros for offset voltage perturbations are given by

$$Q_e(s) = (M_1 s + 1)\left[C_5' s^5 + C_4' s^4 + (C_3 + C_3')s^3 + (C_2 + C_2')s^2 + (C_1 + C_1')s + C_0\right] \quad (5.64)$$

and the zeros for velocity fluctuations are given by

$$Q_u(s) = R_a(M_1 s + 1)\left[L_b C_b s^2 + (R_b R_c C_b + L_b)s + R_b + R_c\right]. \quad (5.65)$$

It is significant that the terms $(R_c L_w - R_a L_b)$ and $(R_c C_b - R_a C_w)$ appear in the expressions for the transfer function coefficients given by equations (5.56) and (5.63) since the influence of the reactive bridge elements can be minimized if these terms approach zero. For both of these terms to be zero requires that $L_b/L_w = R_c/R_a =$ (cross-bridge ratio) and that $C_b/C_w = R_a/R_c = 1/$(cross-bridge ratio). This means that the only way to nullify both of these terms is to make the cross-bridge ratio unity. This may be the reason why a symmetrical bridge is offered as an option for high frequency operation with one commercially available system. The anemometer described in this memorandum can be configured with a symmetrical bridge as an option.

5.5 Discussion

The expansions given above illustrate that the derivation of transfer functions for even high order systems would be extremely tedious, particularly for systems with large numbers of reactive bridge elements. One way to avoid the tedious algebra is to derive the transfer functions numerically. In essence, the numerical expressions for the system transfer functions can be built up in stages from the bridge impedances and amplifier transfer functions using routines for adding and multiplying the polynomials in s. The roots of the transfer function polynomials can then be solved numerically. One disadvantage of the numerical approach is that the relationships between the parameters forming the coefficients of the transfer function polynomials are hidden. However the analytical expressions for the polynomial coefficients for higher-order systems approach such a complexity that little can be inferred by direct examination anyway.

It has been the authors experience that the bare minimum configuration capable of reproducing the behavior observed in real systems is that defined in section 5.4.3 which includes the frequency response characteristics of the feedback amplifier and the lumped inductor representing the probe cable and the balance inductor. Examples of system behavior are given in section 6.

6. EXAMPLES OF SYSTEM BEHAVIOR

6.1 Interpretation of Electronic Square-Wave Tests

It has been proved (see equation 5.21) that the poles appearing in the transfer functions for both offset and velocity fluctuations are identical, independent of the number of amplifiers in the cascade, the complexity of the overall transfer function for the feedback amplifier and the number of lumped components used to model the bridge impedances. This is extremely fortunate since the frequency response of the system to velocity fluctuations can be estimated using electronic tests.

It is emphasized here again that one of the additional zeros in the system transfer function for offset voltage perturbations is always a simple zero with a time constant close to that of the wire filament e.g. see equation (5.37). The time constants of the system poles are usually at least an order of magnitude smaller than this zero. Consequently the *d.c.* component of the system response to a step input of offset voltage is greatly diminished with respect to the higher frequency components. Therefore this simple zero is responsible for causing the electronic square wave response to have an appearance resembling that expected from a delta-function impulse of velocity.

The most commonly used method for tuning anemometers is to adjust the square wave response such that it exhibits optimally damped second-order behavior and then to estimate the frequency response from the ringing frequency. However it is important to note that the ringing frequency is always less than the system frequency response. The time constant of the system is given by $\tau_o = 2\pi/|\sigma + j\omega|$ while the time constant for the ringing is $\tau_r = 2\pi/\omega$. The step (square-wave) response of a system possessing optimally damped complex conjugate dominant poles is shown in figure 6.1(a). Optimum damping for complex conjugate poles given by $T^2s^2 + \zeta Ts + 1$ occurs for $\zeta = 0.6$. For the case of optimum damping $\tau_o \ / \ \tau_r = 0.8$. When the system is slightly underdamped, as shown in figure 6.1(b), the ringing frequency provides a more accurate estimation of the system frequency response. In this case, $\zeta = 0.42$, and $\tau_o/\tau_r = 0.91$.

While the square-wave test is an invaluable aid for tuning anemometers it is easy to misinterpret the actual frequency response since the system can be strongly affected by the higher-poles in addition to the lower-order poles appearing in the transfer function. The characteristic frequency of a pole is equal to the scalar distance of the pole from the origin of the s-plane. When there is more than one pole in the system the frequency response or "roll-off" frequency of the system will be defined to be equal to the lowest characteristic frequency of all the system poles. The pole(s) possessing this characteristic frequency will be referred to here as the dominant pole(s). Although the system will respond to higher frequency inputs it is strictly unusable beyond this point since the system sensitivity varies with frequency. Of particular concern is whenever a simple pole possesses a characteristic frequency that is lower than the complex conjugate poles. Under these conditions the square-wave response may still exhibit a high frequency ring but this will be at a higher frequency than the system response which is dominated by the simple pole.

The results of computer simulations are used below to demonstrate the danger of blindly

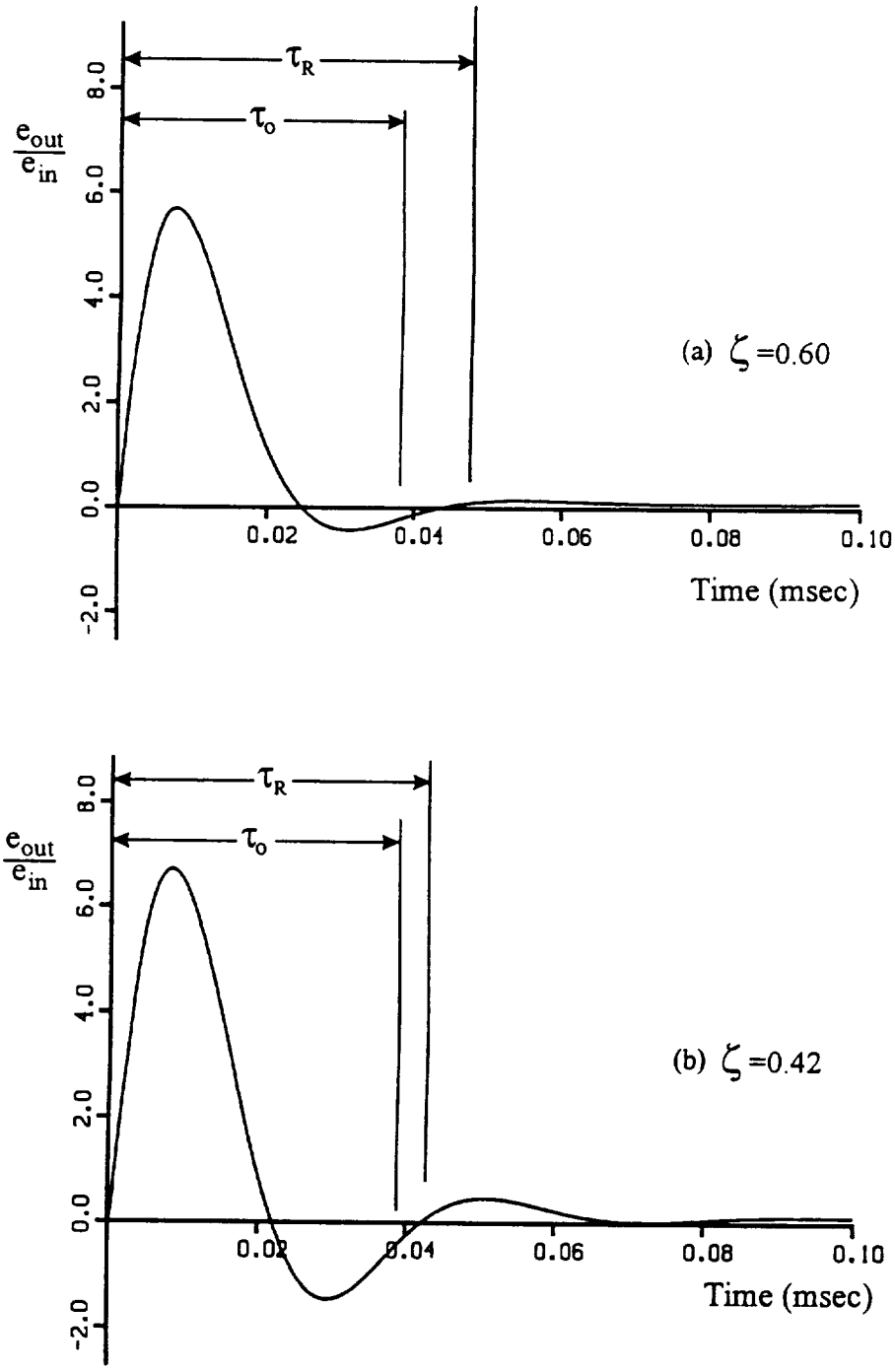

FIGURE 6.1 Response of system with complex cojugate dominant poles. τ_o and τ_r are the time constants of the system and for the ringing. (a) Optimally damped ($\zeta = 0.6$). (b) Underdamped ($\zeta = 0.42$).

following the simplistic recipe described above. Computer simulations are a convenient tool for exploring the behavior of hot-wire systems since the trajectories of the poles and zeros on the s-plane, the Bode diagrams and the square-wave response can all be calculated for each operating point as the anemometer controls are adjusted. In a real system the operator can only view the square-wave response. A computer simulation allows operating conditions to be examined that are beyond current technology and extreme operating conditions can be explored without the penalty of wire breakage. In addition to illustrating these undesirable modes of operation, instructions are given on how to avoid them by appropriate adjustment of the anemometer controls.

An interactive program has been written by the author for examining the stability and frequency response of constant temperature hot-wire systems. All the parameters are menu selectable including the number and type of components forming the impedance of each arm of the bridge and the fluid and wire properties. The poles and zeros of the two equivalent amplifiers for the feedback can be specified and the transfer functions are calculated using equations (5.16) and (5.18). For a given set of parameters, the static operating point is obtained by iteration using equations (5.4) and (5.5) allowing the lumped time constant of the wire T_w to be evaluated. The impedance of each arm of the bridge is calculated as the ratio of two polynomials as expressed in equations 5.13(a)...(d). The coefficients of $Z_1(s)$, $Z_2(s)$ and $Z_3(s)$ given by equations (5.22), (5.23) and (5.28) are calculated using general purpose routines for multiplying and adding polynomials. These routines are then used to calculate the coefficients of the polynomial expressions for the transfer function zeros $Q_e(s)$ and $Q_u(s)$ using equations (5.20) and (5.27) and the poles $P(s)$ using equation (5.21). The roots of the transfer function polynomials (i.e. the poles and zeros) are found numerically using the Lin-Bairstow method of successive quadratic factorization. If the system input (i.e. u or e_s) is sinusoidal then the output will also be sinusoidal after a sufficient time has elapsed for the transients to have decayed. This corresponds to putting $s = j\omega$ in the transfer function which gives a complex number for e_o/e_s and e_o/u. The absolute values $|e_o/e_s|$ and $|e_o/u|$ give the Bode diagrams for amplitude. The response to a more general class of inputs is given in Appendix A. The square-wave response is calculated using equation (A1.16).

6.2 Offset Voltage of the Feedback Amplifier

The results of a systematic parametric study suggest that only two types of dominant pole s-plane trajectories are observed as the amplifier offset voltage E_{qi} is varied. The type of dominant pole trajectory depends on the nature of these poles as the frequency response of the feedback amplifier $f_A \to \infty$. The effect of varying E_{qi} on the higher-order poles is usually very small.

Two examples that are representative of each type of behavior have been calculated using the 5^{th}-order system model derived in section 5.4.3. The frequency response of the feedback amplifier is assumed to be flat through to a simple second-order roll-off i.e. $M_1 = 0$ and $M_2 = M_3 = M$ in equation (5.51). In each example the gain K and frequency response f_A of the feedback amplifier are fixed at $K = 1000$ and $f_A \approx 79.6$ kHz (i.e. $M = 2 \times 10^{-6}$ sec) and the trajectories of the system poles on the s-plane are traced out as the offset voltage E_{qi} is varied. Only quadrant 2 of the s-plane is shown since quadrant 3 is the mirror image of 2 being reflected about the real axis.

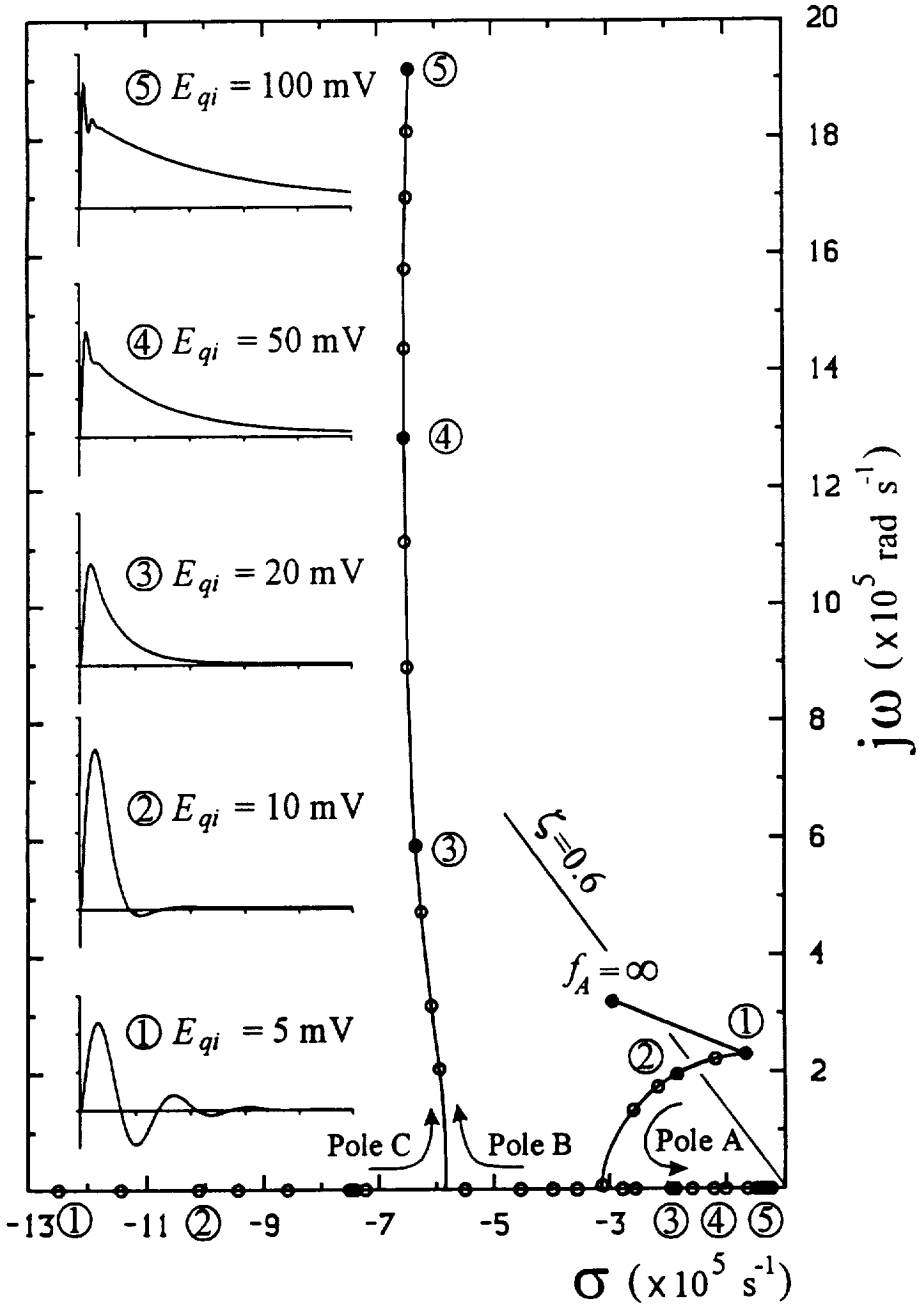

FIGURE 6.2 Calculated s-plane trajectories (2^{nd}-quadrant only) of dominant poles for 5^{th}-order system with increasing offset voltage E_{qi}. Inductor values $L_b = 8\mu$H, $L_w = 1\mu$H, amplifier frequency response $f_A \approx 79.6$kHz and gain K=1000 are constant. Flow velocity U=20 m/s. Point $f_A = \infty$ corresponds to model of Perry and Morrison (i.e. $M = 0$) for conditions at point 1. Square-wave response for operating points 1 to 5 also shown. Line ζ=0.6 shows optimum damping for complex poles.

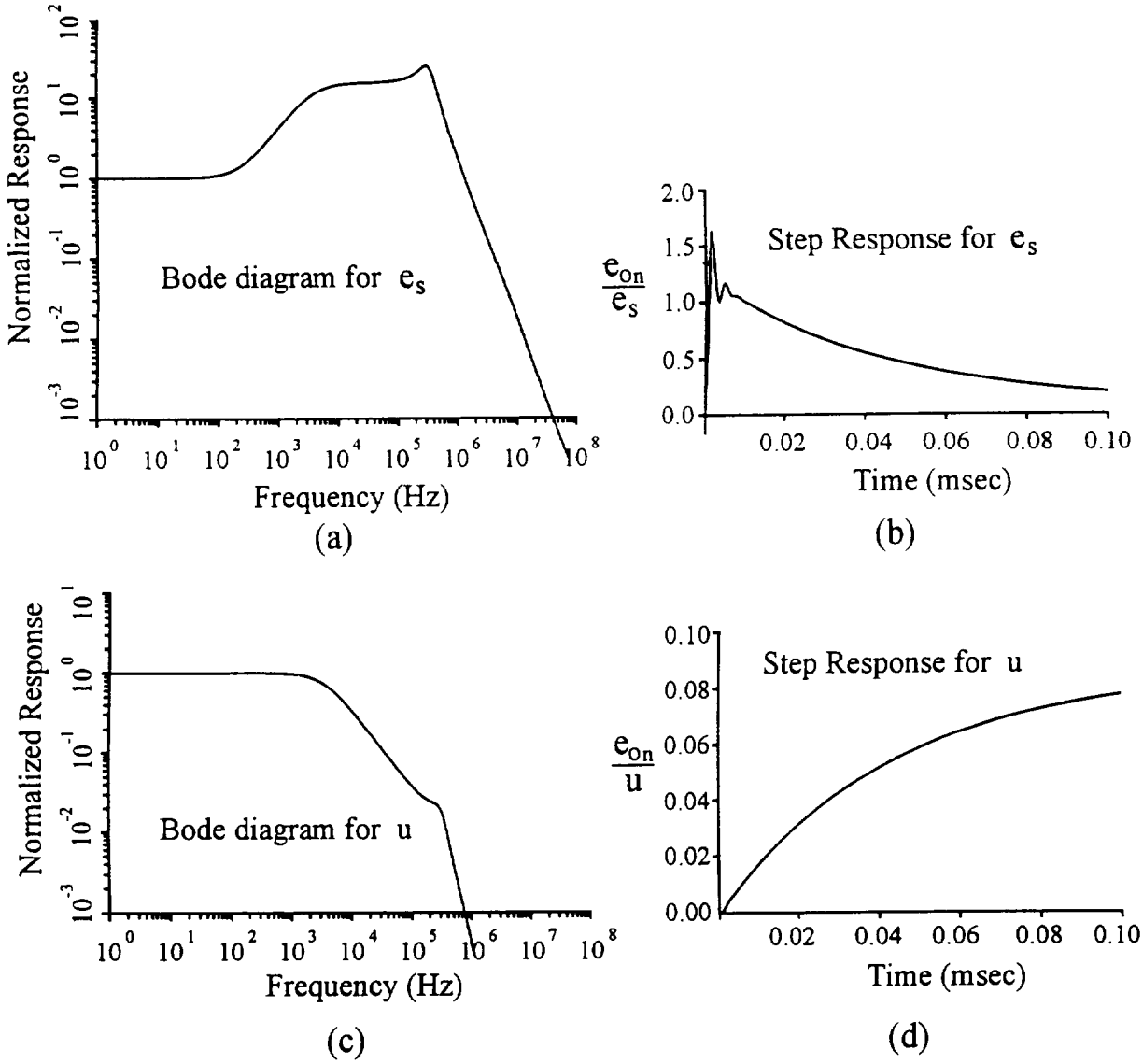

FIGURE 6.3 Bode diagrams and step-response for point 5 in figure 6.2 where E_{qi} =100mV, (a) and (b) offset voltage perturbations e_s, (c) and (d) for velocity fluctuations u.

Initially, in the first example, at the point labeled 1 in figure 6.2, the system is dominated by a pair of complex conjugate poles labeled A (with image B). There is also a simple pole labeled C and another two higher-order simple poles D and E which remain well beyond the frequency range of interest and their trajectories are not shown. Note that if the frequency response of the feedback amplifier were increased to infinity while the other parameters were held fixed the system would still be dominated by a pair of complex conjugate poles but they would be more damped as illustrated by point labeled $f_A = \infty$ in figure 6.2. Increased damping of the dominant poles with increased f_A appears to be a general property of constant temperature hot-wire systems. This rather surprising property will be discussed in more detail in section 6.4. Returning to conditions at point

1, as E_{qi} is increased, the complex conjugate poles A and B move towards the real axis where they eventually meet and split to form two simple poles. These points are known as breakaway points in the system theory literature. As E_{qi} is further increased the simple pole C, which has been moving towards the origin, now merges with the simple pole B to form a new complex conjugate pair. However pole A has continued to move closer to the origin and therefore it dominates the system frequency response. This behavior is typical of systems in which the dominant poles remain complex as $f_A \rightarrow \infty$.

The square-wave response corresponding to the points labeled 1 to 5 are also shown in the figure. The square-wave response can be very misleading under these conditions. For example, for conditions corresponding to point 5 in figure 6.2, where $E_{qi} = 100mV$, the ringing frequency is around 320 kHz, but the simple pole A limits the system frequency response to about 3.6 kHz. The Bode diagrams and the step-response for both offset voltage perturbations and velocity fluctuations corresponding to this situation are shown in figure 6.3 and they clearly demonstrate why this type of system behavior is undesirable.

An example of the second type of trajectory is shown in figure 6.4. For conditions corresponding to point 1 the dominant poles are also complex conjugates. However in the limit $f_A \rightarrow \infty$ this system possesses ALL simple poles and different s-plane trajectories are observed as the offset voltage E_{qi} is varied. With increasing E_{qi} poles A and B remain complex conjugate while simple pole C moves towards to the origin and eventually dominates the system. This behavior is typical of systems which possess only simple poles when $f_A \rightarrow \infty$. Despite the different trajectories of the dominant poles the end result is much the same as in the first example and the system possesses similar undesirable Bode diagrams and step-response characteristics.

It turns out that for the 3rd-order system considered by Perry and Morrison (1971) (i.e. $f_A = \infty$, see section 5.4.2), the type of behavior observed in the above examples can only be produced when the balance inductor L_b is set to be very close to the value required for *a.c.* bridge balance i.e. $L_{b0} = (R_c/R_a)L_w$. For values of L_b slightly less than this, the system is dominated by the usual complex conjugate pole pair. For values of L_b slightly greater than L_{b0} the poles rapidly cross over to the RHS of the s-plane and the system becomes unstable. However in a real system the phenomena described above can be produced over a wide range of balance inductor settings by increasing the offset voltage E_{qi}. The only way to simulate these observations is to include the frequency response characteristics of the feedback amplifier.

6.3 Balance Inductor

As mentioned above, the analysis of Perry and Morrison predicts instability when the balance inductor L_b is in excess of the value required for *a.c.* bridge balance L_{b0}. However systems with finite frequency response amplifiers are capable of maintaining system stability when the balance inductor exceeds the *a.c.* balance value L_{b0}. For a fixed amplifier frequency response f_A it is possible to obtain significant improvements in the system frequency response f_o by suitably adjusting the offset voltage as L_b is increased to values in excess of L_{b0}. In fact having control of only E_{qi} and L_b requires that $L_b > L_{b0}$ to obtain the optimum system response. However if L_b is too large it may be impossible to obtain a satisfactory response by adjusting the offset voltage.

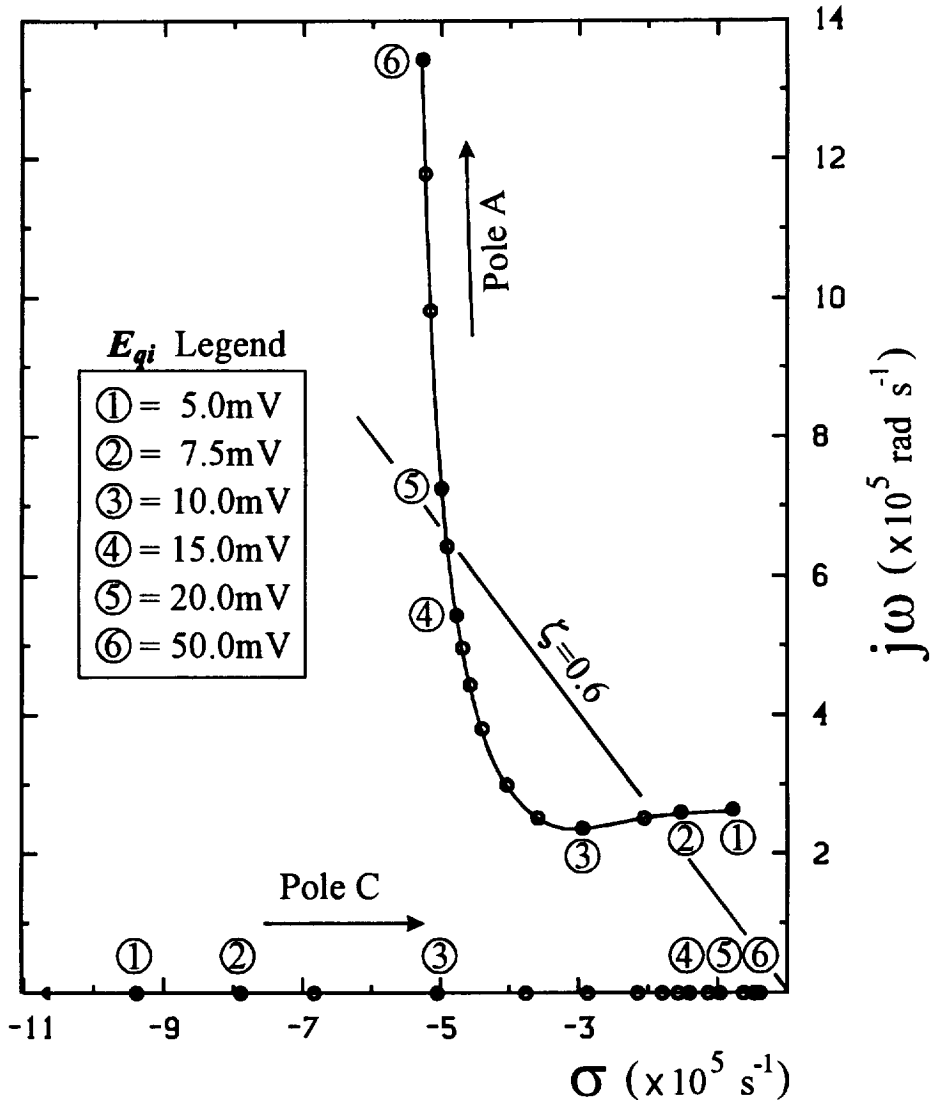

FIGURE 6.4. Same as figure 6.2 but with $L_b = 0.5\mu$H and $L_w = 0.1\mu$H. Despite the different s-plane trajectories the end result is much the same as in figure 6.2 for large E_{qi}.

L_b/L_{b0} =0.5 in the example shown in figure 6.4 and this configuration will serve as a baseline from which to illustrate these effects. The s-plane trajectories for this configuration are reproduced in figure 6.5 along with those of five other configurations in which the values of L_b/L_{b0} are held fixed at 1, 2, 3, 4, and 5 respectively. For small values of the offset voltage (e.g. $E_{qi} < 2mV$) nearly all the configurations are unstable since the poles A (and B) are located on the right-half-plane. As E_{qi} is increased these poles cross to the left-half-plane and the simple pole C of each system moves along the real axis towards the origin. For a given offset voltage, the initial position of pole C is further from the origin for smaller values of L_b. However this effect is pronounced only when E_{qi} is small. As E_{qi} is increased the location of the simple poles C become more and more independent of L_b. For each L_b, the best response will be defined to be when the characteristic frequency

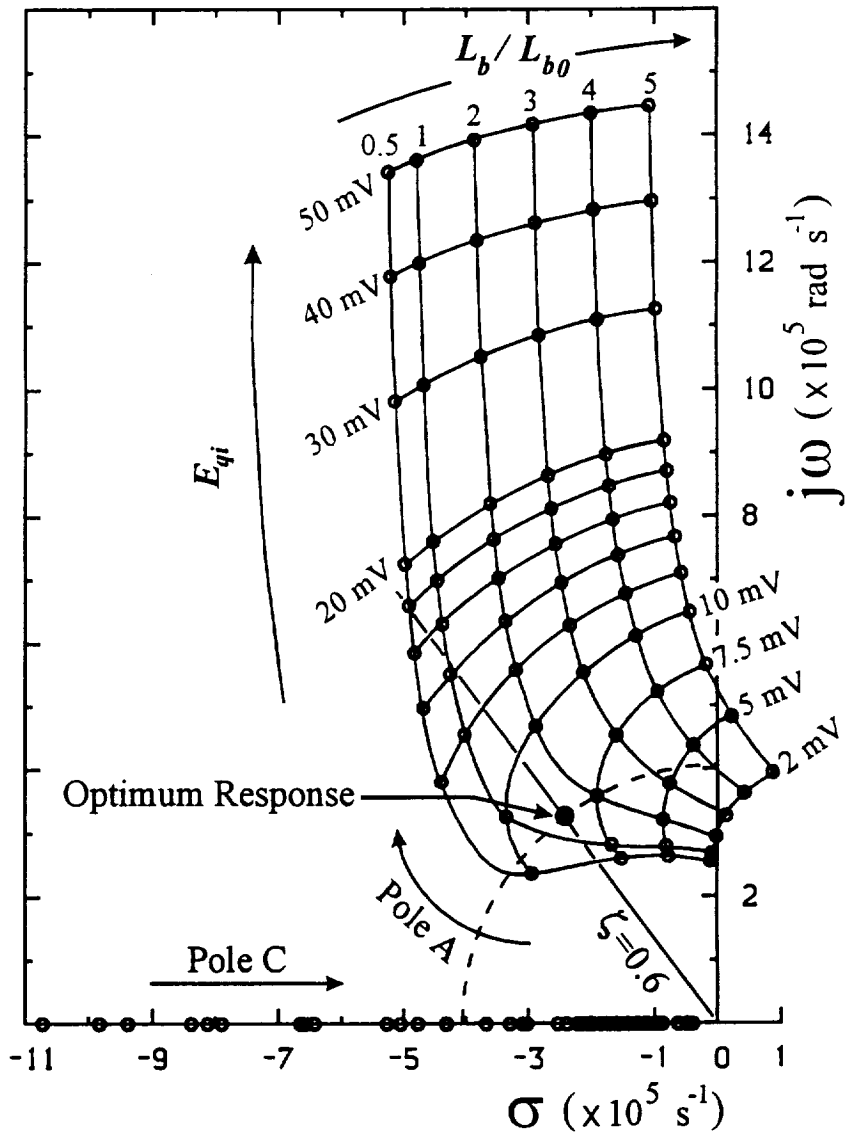

FIGURE 6.5. Same as figure 6.4 where $L_w = 0.1\mu$H and $L_{b0} = (R_c/R_a)L_w = 1\mu$H. Trajectories for L_b/L_{b0}= 0.5, 1, 2, 3, 4 and 5 also shown. Dashed line shows locus of points where poles A, (B) and C have equal characteristic frequencies. Having E_{qi} and L_b as the only tunable parameters leads to an optimum response when $L_b \approx 1.5L_{b0}$.

(i.e. $|\sigma + j\omega|/2\pi$) of poles A and B and simple pole C are equal. For $L_b \leq L_{b0}$ the best response occurs when the poles A (and B) are overdamped. When $L_b > L_{b0}$ the poles A (and B) never reach the optimum damping condition so that the best response occurs when they are underdamped. The locus of the operating point with best response that can be obtained by adjusting both the offset voltage E_{qi} and the balance inductor L_b is shown as a dashed curve. Optimum damping (ζ=0.6) occurs when $L_b \approx 1.5L_{b0}$. The square-wave response corresponding to various operating points are shown in figure 6.6 and these may help users interpret anemometer behavior. In particular note how there is no adjustment

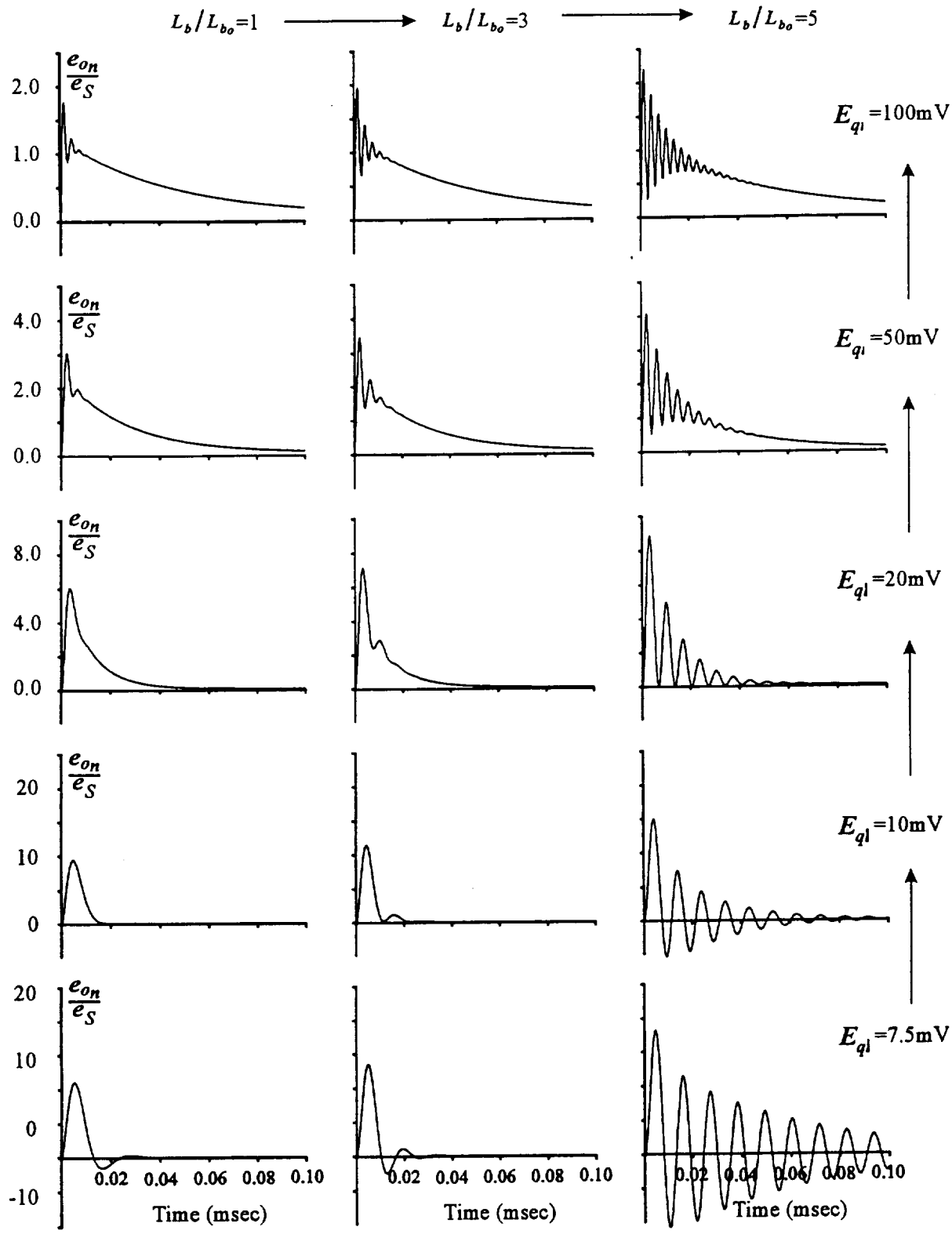

FIGURE 6.6. Square-wave response corresponding to a spread of points in Figure 6.5. It is impossible to obtain a satisfactory response by adjusting E_{qi} when L_b/L_{b0} is excessive.

of E_{qi} that will increase the damping of system to a satisfactory level when L_b is very large. An operator observing this type of square-wave response is advised to reduce the size of the balance inductor.

6.4 Frequency Response and Gain of the Feedback Amplifier

Intuitively it might be expected that the roll-off frequency of the feedback amplifier would play a dominant role in determining the overall system frequency response. Analysis predicts that the frequency response of hot-wire systems $f_o \rightarrow \infty$ in the limits of $f_A \rightarrow \infty$, $K \rightarrow \infty$, $E_{qi} \rightarrow 0$ and $L_b \rightarrow L_{b0}$. However, attempts to approach these limits in practice are invariably frustrated by the appearance of instabilities. For example, Smits and Perry (1980) observed that hot-wire systems are prone to instabilities as $L_b \rightarrow L_{b0}$ since there is an extreme sensitivity to very small variations in L_b. However this observation was made for 3rd-order systems where $f_A = \infty$. Systems with finite frequency response amplifiers have an optimum frequency response when $L_b > L_{b0}$ and stability can be maintained even when L_b is excessively large. Nevertheless one might suspect that the form of dominant pole instability described by Smits and Perry would eventually occur as f_A is increased. However the results of a systematic parametric study suggests that other higher-order instabilities are more likely to arise beforehand. While there are still significant improvements to be found by increasing the frequency response and gain of the amplifier, its role is often more critical in determining the system stability by influencing the higher-order poles. Two examples are given in figures 6.7 and 6.8.

Calculated s-plane trajectories of a typical 5th-order system are shown in figure 6.7. Two cases are considered i.e. increasing amplifier frequency response and increasing gain. The behavior of the dominant poles labeled A and B and the higher-order poles labeled C, D and E are shown separately in figures 6.7 (a) and (b) because of the wide range of values observed. In the first case, the amplifier gain K=1000, the offset voltage E_{qi}=12.5 mV and the inductors $L_b = 40\mu$H and $L_w = 5\mu$H are held constant. Note that the damping of the dominant poles A and B increases with increasing amplifier frequency response. As a matter of interest the system frequency response ($f_o \approx$17.8 kHz) is higher than the amplifier frequency response ($f_A \approx$15.9 kHz i.e. $M = 1.0 \times 10^{-5} s$) for conditions corresponding to point 1A labeled in figure 6.7. The system response increases rapidly with increasing amplifier frequency response but only to $f_o \approx$27 kHz for $f_A \approx$106 kHz (i.e. $M = 1.5 \times 10^{-6}$ sec). Further increases in the amplifier frequency response only have a small effect on the dominant poles e.g. $f_o \rightarrow$31 kHz for $f_A \rightarrow \infty$ (i.e. $M \rightarrow 0$). As the amplifier frequency response is increased two of the higher-order simple poles C and D move towards each other and merge to become complex conjugates for $f_A \approx$ 106 kHz. This point is labeled 2A in figure 6.7(b). The third simple pole labeled E moves further away from the origin and exerts negligible influence on the system. With further increases in the amplifier frequency response the two higher-order conjugate poles C and D move towards the imaginary axis and ultimately cross over to the RHS of the s-plane resulting in instability.

Similar behavior is observed if the amplifier gain K is increased while the other parameters are held constant as shown in figure 6.7(b). Although the dominant poles move along slightly different trajectories the endpoints $K = \infty$ and $f_A = \infty$ are very closely the

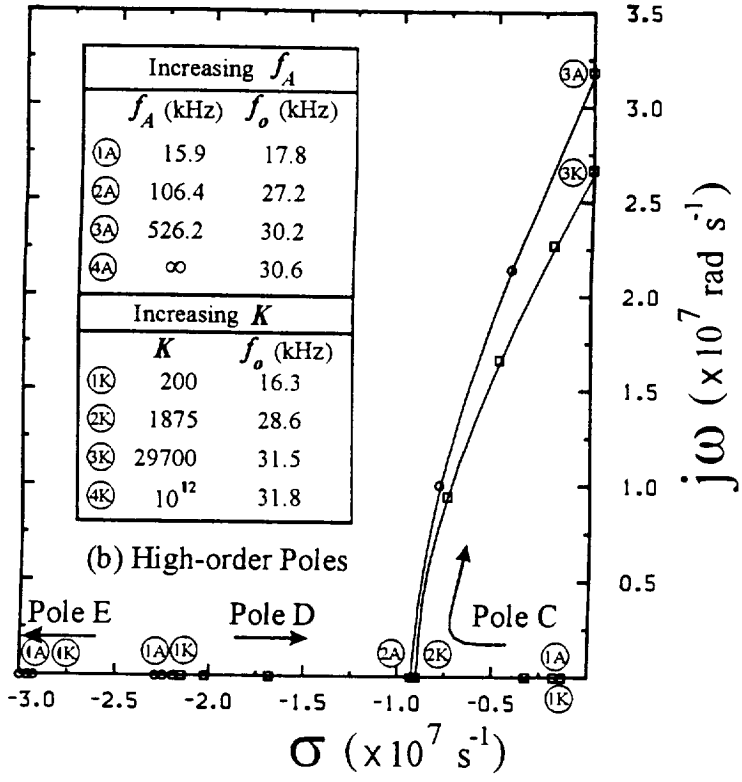

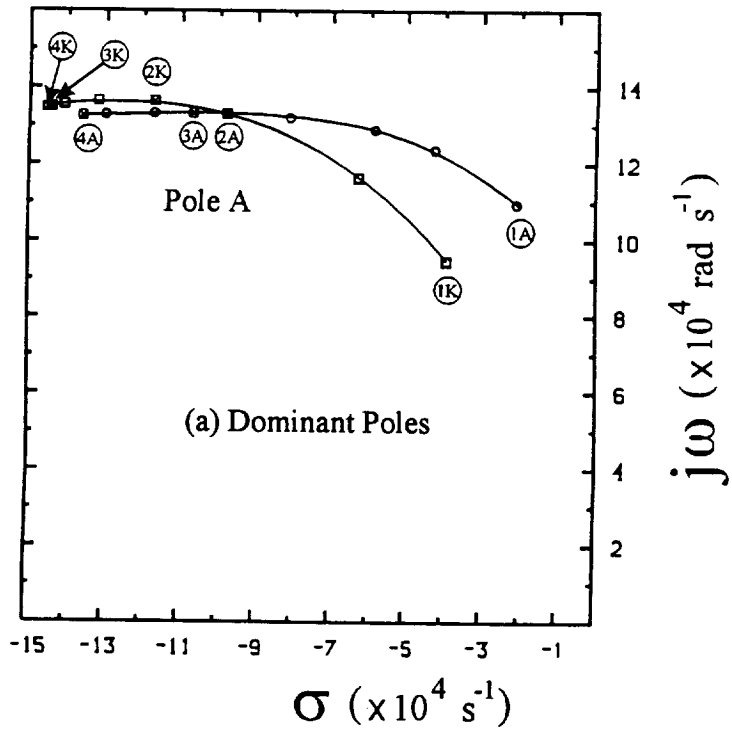

FIGURE 6.7. Calculated s-plane trajectories of system poles for increasing f_A (with constant K=1000) and for increasing K (with constant $f_A \approx 79.6$ kHz). $E_{qi} = 12.5$mV, $L_w = 5\mu$H and $L_b = 40\mu$H. (a) Dominant poles (b) Higher order poles.

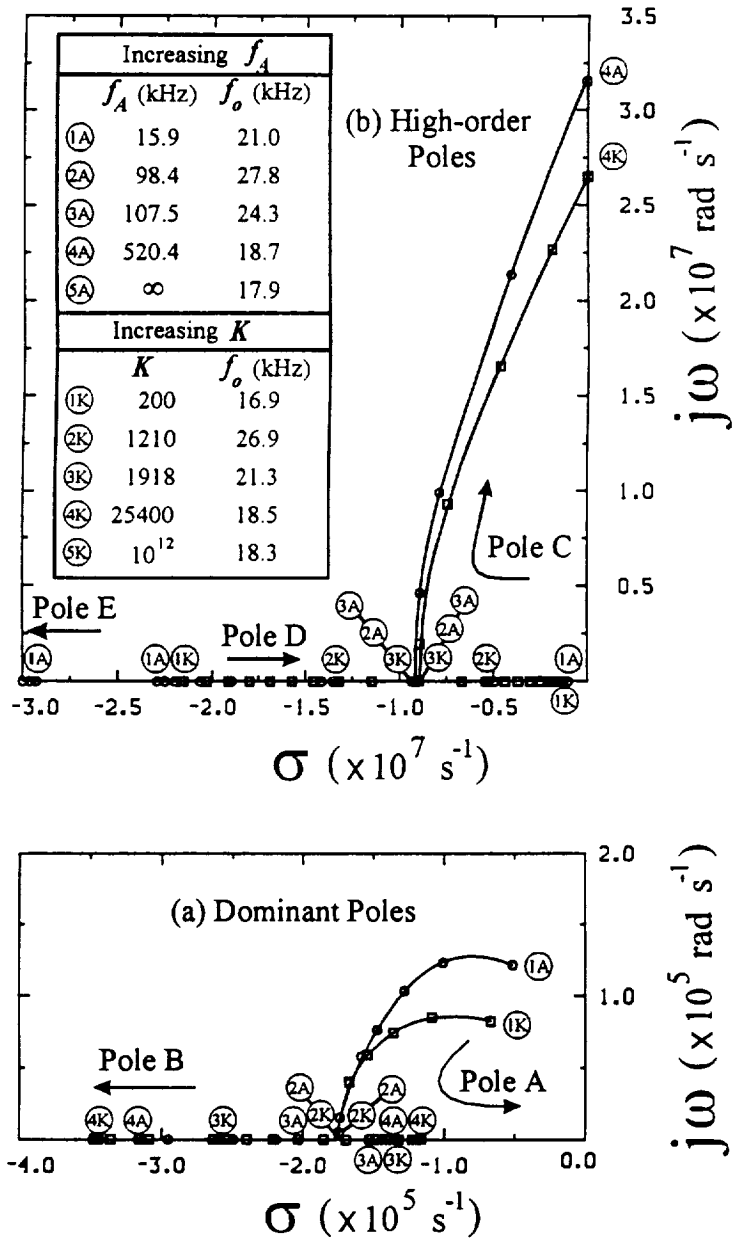

FIGURE 6.8. Same system as figure 6.6 but E_{qi} increased to 20mV. Calculated s-plane trajectories of system poles for increasing f_A (with constant K=1000) and for increasing K (with constant $f_A \approx 79.6$ kHz). (a) Dominant poles (b) Higher order poles.

same. The s-plane trajectories of the higher-order system poles C and D are very similar as $K \rightarrow \infty$ and $f_A \rightarrow \infty$.

In the previous example the dominant poles approach the complex conjugate 3rd-order system values asymptotically as $K \rightarrow \infty$ and as $f_A \rightarrow \infty$. In the second example shown in figure 6.8(a), a different type of trajectory is observed i.e. the dominant poles A and B move towards the real axis where they meet and split to form two simple poles. These poles also approach the 3rd-order system values asymptotically as $K \rightarrow \infty$ and as $f_A \rightarrow \infty$.

This type of behavior is also consistent with the observation mentioned previously that relates the increased damping of the dominant poles with increased frequency response and gain of the feedback amplifier. Note that increasing f_A or K beyond the point where the dominant complex poles are transformed into two simple poles actually reduces the overall system frequency response since pole A moves closer to the origin. The effects of increasing K and f_A on the higher-order poles are very similar to those in the previous example, despite the different trajectories for the dominant poles, i.e. the poles C and D merge to become complex conjugate and move towards the imaginary axis. The higher-order poles ultimately cross over to the RHS of the s-plane resulting in system instability as shown in figure 6.8(b).

These examples demonstrate several important properties of constant temperature hot-wire systems. The effects of increasing K and f_A are quite similar and have the unexpected effect of increasing the stability of the dominant poles. This appears to be true for all systems i.e. the author has not found one contrary example to this observation out of a large number of cases studied. It is the higher-order poles that are responsible for the system instability under these conditions. It is often difficult to determine the damping of the higher-order poles during a square-wave test, even when they are grossly underdamped, since the oscillations can still decay rapidly when compared to the response of the dominant poles. However a small change in either K or f_A from this point could result in instability. This type of higher-order instability can occur suddenly and without warning to the anemometer operator who can only observe the square-wave response.

6.5 Instabilities with Subminiature Wires

Some workers (e.g. Miller, Shah and Antonia 1987) have reported frustration with instabilities when using subminiature hot-wires. One way of comparing system behavior with different diameter wires is to non-dimensionalize the poles and zeros with the lumped time constant of the wire T_w. Alternatively, the coefficients of s^n in the system transfer functions can be made non-dimensional by division with ${R_w}^2{T_w}^n$. The relative positions of the non-dimensional poles and zeros will be the same for systems in which R_a/R_w, R_b/R_w, R_c/R_w, $\mathring{R}/R_w$, $L_b/(R_wT_w)$, $L_w/(R_wT_w)$ and M/T_w are equivalent.

For a given l/d ratio, $R_g \propto 1/\mathrm{d}$, so that R_g for a typical subminiature wire (e.g. d=0.5 μm) is about an order of magnitude greater than a more conventional wire (e.g. d=5 μm). T_w is reduced for smaller diameter wires, but by a smaller factor than the length-scale ratio since the Reynolds number is also reduced. Consequently the product R_wT_w becomes larger as the wire is made smaller. This leads to a beneficial reduction in the size of the non-dimensional bridge inductance $L_b/(R_wT_w)$ and $L_w/(R_wT_w)$. Values of R_a/R_w, R_b/R_w, R_c/R_w and $\mathring{R}/R_w$ can be altered by adjusting the bridge resistors and the offset voltage. Finally, the frequency response of the feedback amplifier must be increased to obtain the same value of M/T_w.

If f_A is fixed then M/T_w can be considerably larger with subminiature wires. This is especially significant since it has been demonstrated that the dominant poles become less damped as f_A is reduced. If f_A is too small then the dominant poles may be unstable. Figure 6.9 shows the effect of reducing the wire diameter while maintaining the same length-to-diameter ratio (1:200) and the same resistance ratio $R \approx 2$ (by increasing R_b).

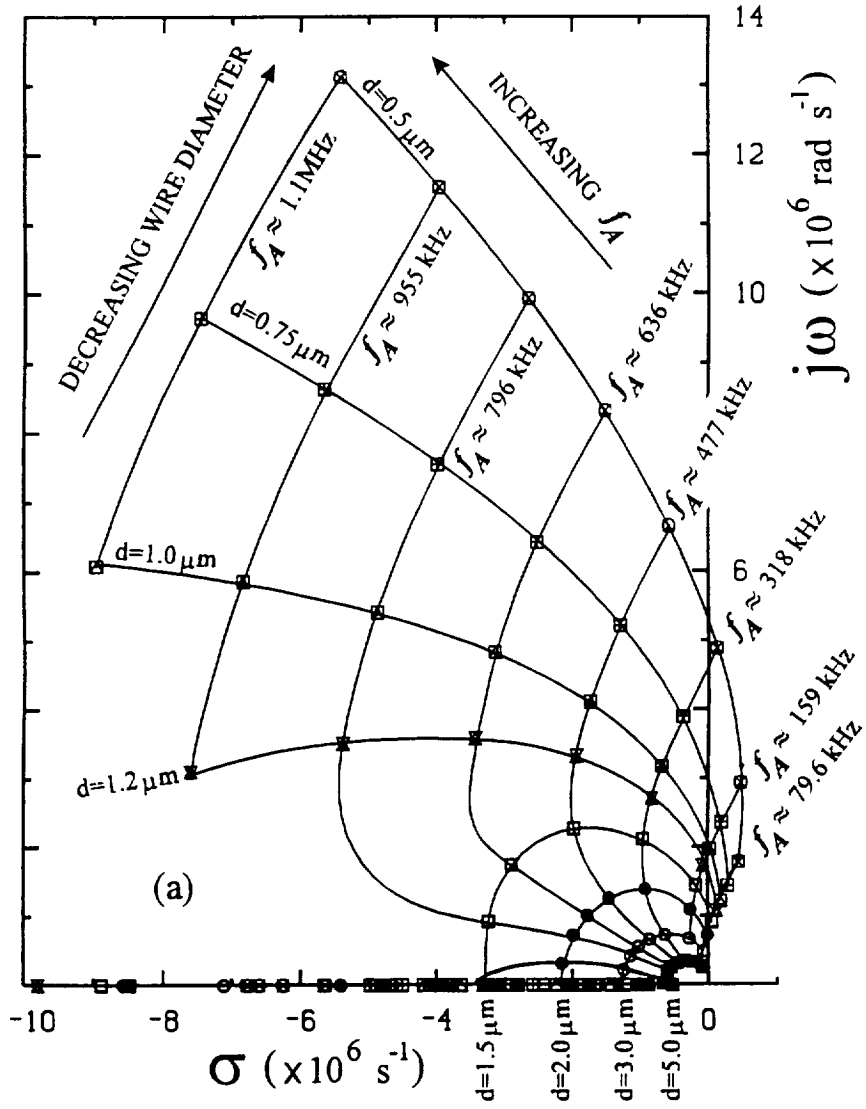

FIGURE 6.9. Calculated s-plane trajectories of the dominant poles for a range of wire diameters with the same length to diameter ratio. R_b has been adjusted to closely give the same resistance ratio i.e. $R \approx 2$. E_{qi} = 5mV, L_b=0.5 μH and L_w=0.1 μH. Higher values of K and f_A are required for stability as the wire diameter is reduced. (a) Increasing f_A (with constant gain K=1000).

At the lowest values of f_A and K the dominant poles are unstable for small wire diameters. As either f_A or K is increased these poles move to the LHS of the s-plane and the systems become stable. The effect on the higher-order poles is similar to the examples shown in figures 6.7 and 6.8.

The wire current required for a given resistance ratio is smaller for subminiature wires so that the static output voltage at the top of the bridge is considerably less than that obtained with conventional wires. Therefore increasing R_a and R_c to obtain the same values of R_a/R_w and R_c/R_w, as suggested above, would also help restore the size of the

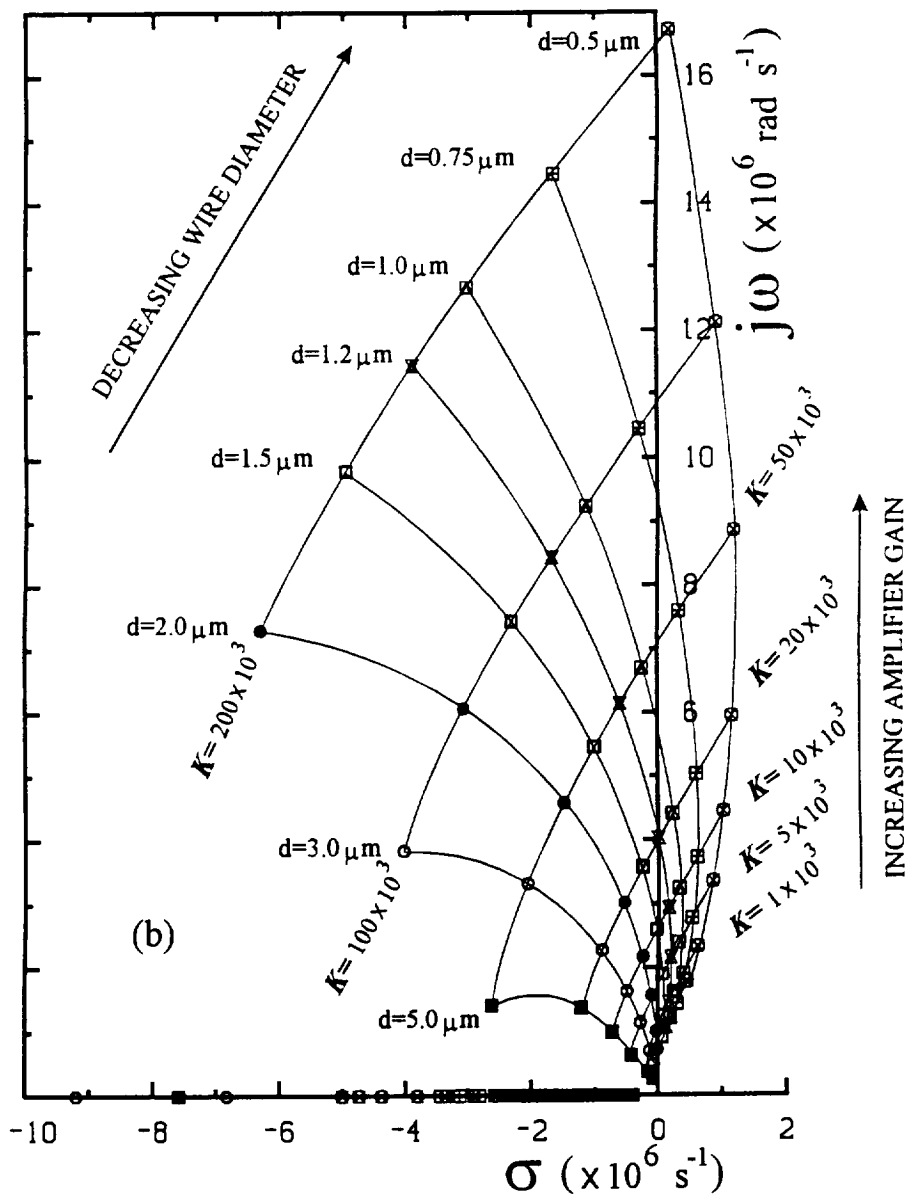

FIGURE 6.9. Continued, (b) Increasing K (with constant $f_A \approx 79.6$ kHz).

output signal. However this is not recommended since increasing R_a and R_c tends to reduce the damping of the dominant poles as shown in figure 6.10. The largest values of R_a/R_w and R_c/R_w correspond to the values used for the d=5.0μm wires in earlier sections. An even higher frequency response amplifier would be required to obtain a satisfactory system response under these conditions.

The author suggests that insufficient frequency response of the feedback amplifier is the most likely cause of system instability when using subminiature wires.

6.6 Effects of Bridge Capacitance

The previous examples used a 5^{th}-order system in which the frequency response of the

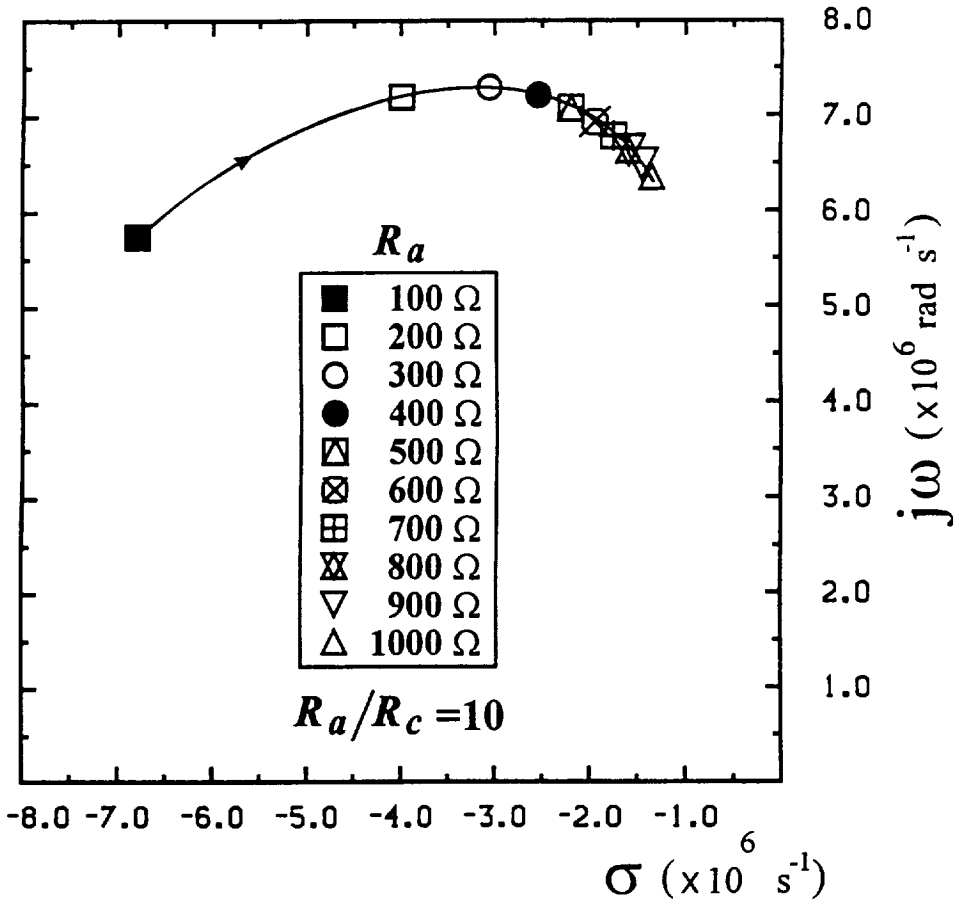

FIGURE 6.10. Increasing upper bridge resistors R_a and R_c causes dominant poles to become less damped. Subminiature platinum filament of length 0.1mm and diameter d=0.5μm ($R_g \approx 80\Omega$). Largest values of R_a/R_w and R_c/R_w are approximately the same as for the d=5μm wires in figures 6.2 to 6.8. $L_b = 8\mu$H, $L_w = 1\mu$H, $R_b = 1.6k\Omega$ and the amplifier frequency response $f_A \approx 1.6$MHz, gain K=1000 and offset voltage $E_{qi} = 5$mV are constant. Air velocity is 20 m/s.

feedback amplifier is assumed to be flat through to a simple second-order roll-off i.e. $M_1 = 0$ and $M_2 = M_3 = M$ in equation (44). In this section an example of the effect of bridge capacitance will be presented. The transfer functions for a system with capacitance in the active and balance arms of the bridge was expanded in section 5.4.4.

Figure 6.11(a) shows the step response and Bode diagram for offset voltage perturbations corresponding to the 5th-order system defined in figure 6.7 (i.e. $C_b = C_w = 0$), where the gain and the frequency response of the feedback amplifier are K=1000 and f_A =477 kHz (i.e. $M = 3.33 \times 10^{-7}$ sec). The spike appearing in the Bode diagram at around 5 MHz is the result of the higher-order complex conjugate poles which are close to the imaginary axis. Although these poles are very much underdamped, the oscillations caused by exciting the system with a square-wave decay rapidly when compared to the response of the dominant poles. When a small capacitor (C_w =5pF) is placed in the active arm of the

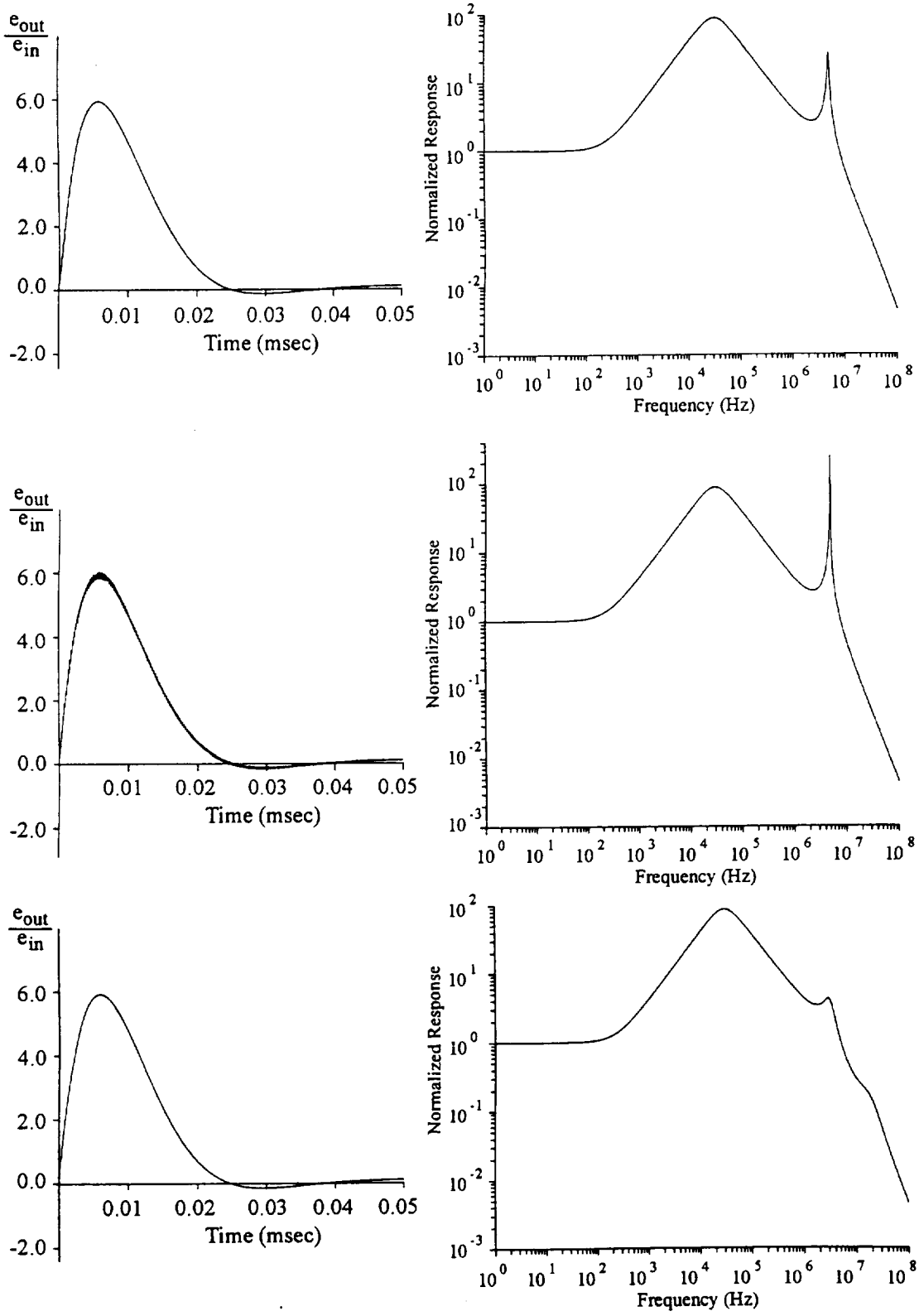

FIGURE 6.11. Effect of bridge capacitance on step response and Bode diagrams for offset voltage perturbations. (a) Same as figure 6.7 but with K=1000 and f_A =477 kHz. (b) Effect of addition of C_w =5pF. (c) Effect of addition of C_b =10pF.

bridge these poles move even closer to the imaginary axis while the effect on the dominant poles is barely detectable. An additional simple pole is introduced since the system transfer function is now 6^{th}-order but it is located well away from the region of interest and exerts very little influence on the system. As a result of the movement of the higher-order poles, the spike in the Bode diagram is much sharper as shown in figure 6.11(b). The envelope for the exponential decay of the oscillations is now much slower than the dominant poles so that high frequency oscillations are clearly visible in the step-response as shown in figure 6.11(b). If a small capacitor is added to the balance arm of the bridge (C_b =10pF) the system transfer function becomes 7^{th}-order. The higher-order simple pole originally present in the 5^{th}-order system forms a complex conjugate with the additional pole but this pair is close to optimum damping and they are located far away from the region of interest. The simple pole resulting from the addition of C_w=5pF is unaffected by the addition of C_b and once again the effect on the dominant poles is negligible. However the complex conjugate poles which were moved closer to the imaginary axis are now moved away towards the optimum damping condition resulting in almost complete removal of the high frequency spike in the Bode diagram as shown in figure 6.11(c). This example serves to demonstrate that even small quantities of bridge capacitance can have a dramatic effect on the system stability but very little influence on the dominant poles which determine the overall frequency response of the system.

APPENDIX A. LAPLACE TRANSFORM METHODS

A1.1 Introduction

The hot-wire anemometer is a difficult instrument to understand properly. Subtle insights into the system behavior are often required to detect an erroneous mode of operation. A major source of difficulty is that the electronic square-wave test is an indirect method for estimating the frequency response. While the poles of the transfer function for velocity and offset voltage fluctuations are identical, the zeros are quite different and this is often the source of considerable confusion.

Once the transfer function is known, the behavior of complicated systems of differential equations can be analyzed in the so called frequency domain by using simple algebra. By taking inverse transforms, the complete time domain solutions can be obtained by applying the simple algorithms that are described below. These techniques have been adapted into a computer simulation which is used to examine how models of the Constant Temperature Hot-wire Anemometer respond to various forcing conditions. The advantage of a computer simulation is that the trajectories of the poles and zeros on the s-plane, the Bode diagrams and the square-wave response, can all be calculated for both velocity and offset voltage fluctuations as the anemometer controls are adjusted. With a real system the operator can only observe the electronic square-wave response which is open to misinterpretation.

A1.2 Definitions

Given a function of time $f(t)$, then the Laplace Transform $\mathbf{L}\{f(t)\}$ is defined as

$$\mathbf{L}\{f(t)\} = \int_0^\infty f(t)e^{-st}dt = \hat{f}(s) \tag{A.1}$$

The Laplace variable s is in general a complex quantity i.e. $s = \sigma + j\omega$. The Laplace transform of a derivative has the extremely useful property that

$$\mathbf{L}\left\{\frac{d^n f(t)}{dt^n}\right\} = s^n \hat{f}(s) - \left\{s^{n-1}f(0) + s^{n-2}\frac{df(t)}{dt}\bigg|_{t=0} + \cdots + \frac{d^{n-1}f(t)}{dt^{n-1}}\bigg|_{t=0}\right\} \tag{A.2}$$

For systems in which all initial conditions are zero, the transfer function can be derived by expressing the differential equation in terms of the input and output variables and simply replacing the differential operator $d^n f(t)/dt^n$ with s^n. The equation can then be manipulated by treating s as an ordinary algebraic quantity. The following differential equation is used to provide some definitions.

$$A_n\frac{d^n e_o}{dt^n} + A_{n-1}\frac{d^{n-1}e_o}{dt^{n-1}} + \cdots + e_o = K\left\{B_m\frac{d^m e_i}{dt^m} + B_{m-1}\frac{d^{m-1}e_i}{dt^{m-1}} + \cdots + e_i\right\} \tag{A.3}$$

The input e_i and its derivatives on the r.h.s side of (A.3) are known as the forcing function. Assuming that all initial conditions are zero, then applying equation (A.2) gives

$$\frac{\hat{e_o}}{\hat{e_i}}(s) = K\,\frac{B_m s^m + B_{m-1}s^{m-1} + \cdots + 1}{A_n s^n + A_{n-1}s^{n-1} + \cdots + 1} \tag{A.4}$$

When dealing with electrical circuits the concept of operational impedance allows the transfer function to be constructed without having to write down the differential equations. The operational impedance of a capacitor is $1/Cs$. The operational impedance of an inductor Ls. The transfer function for a circuit $(\hat{\epsilon}/\hat{i})$ can then be evaluated by using Kirchoff's Laws.

Some alternative forms of the transfer function are given below:

$$\frac{\hat{\epsilon_o}}{\hat{\epsilon_i}}(s) = K\,\frac{B_m}{A_n}\,\frac{s^m + \frac{B_{m-1}}{B_m}s^{m-1} + \cdots + \frac{1}{B_m}}{s^n + \frac{A_{n-1}}{A_n}s^{n-1} + \cdots + \frac{1}{A_n}} \tag{A.5}$$

$$= K\,\frac{B_m}{A_n}\,\frac{(s-z_n)(s-z_{n-1})\cdots(s-z_1)}{(s-p_m)(s-p_{m-1})\cdots(s-p_1)} \tag{A.6}$$

$$= K\,\frac{(T_{z_n}s+1)(T_{z_{n-1}}s+1)\cdots(T_{z_1}s+1)}{(T_{p_m}s+1)(T_{p_{m-1}}s+1)\cdots(T_{p_1}s+1)} \tag{A.7}$$

The quantity B_m/A_n is often called the level factor. The quantity z_j is called a zero of the system since the transfer function goes to zero when $s = z_j$. The quantity p_j is called a pole of the system since the transfer function becomes infinite when $s = p_j$. T_{p_j} is the time constant of pole j and T_{z_j} is the time constant of zero j. The poles and zeros may be real or complex quantities. If they are complex they must occur in conjugate pairs for the transfer function polynomial coefficients to be real numbers. If a pole or zero is real then it is referred to as a simple pole or a simple zero.

A1.3 System response to forcing

If the input e_i is sinusoidal then the output e_o will also be sinusoidal after a sufficient time for the transients to decay. In this case the system response can be calculated by putting $s = j\omega$ where ω is the forcing frequency in rad/s. This gives a complex number for $(\hat{\epsilon_o}/\hat{\epsilon_i})(\omega)$. A plot of the amplitude versus frequency is known as the Bode diagram.

The response to a more general class of inputs was considered by Perry (1982) using

$$e_i = E_i H(t) e^{\lambda t} \tag{A.8}$$

where E_i and λ are in general complex quantities. The Heaviside step function $H(t)$ ensures that initial conditions are zero. The Laplace transform of the input is given by

$$\hat{\epsilon_i}(s) = \frac{E_i}{(s-\lambda)}.$$

Therefore the output of the system described by (A.4) is given by

$$\hat{\epsilon_o}(s) = \frac{K E_i B(s)}{A_n(s-p_n)\cdots(s-p_1)(s-\lambda)} \tag{A.9}$$

where $B(s) = B_m s^m + B_{m-1}s^{m-1} + \cdots + 1$. Once the denominator has been factorized the equation can be expressed as partial fractions,

$$\hat{\epsilon_o}(s) = \frac{C_n}{(s-p_n)} + \frac{C_{n-1}}{(s-p_{n-1})} + \cdots + \frac{C_1}{(s-p_1)} + \frac{C_\lambda}{(s-p_\lambda)} \tag{A.10}$$

The coefficients $C_n \cdots C_1$ and C_λ can be found by equating coefficients of (A.9) and (A.10). By allowing s to approach $p_n, p_{n-1}, \cdots p_1$ and p_λ in turn then the appropriate term in (A.10) will dominate. Hence

$$C_j = \lim_{s \to p_j} \left\{ \frac{E_i F(s)}{(s-\lambda)} (s - p_j) \right\} \tag{A.11}$$

$$C_\lambda = \lim_{s \to \lambda} \left\{ E_i F(s) \right\} \tag{A.12}$$

where $F(s)$ is the full transfer function as given in (A.4) to (A.7). The partial fractions in equation (A.10) allow the inverse transform to be obtained rather simply so that the output can be expressed as a function of time

$$\frac{e_o(t)}{E_i} = \sum_{j=1}^{n} \lim_{s \to p_j} \left\{ \frac{F(s)(s-p_j)}{(s-\lambda)} \right\} e^{p_j t} + F(\lambda) e^{\lambda t} \tag{A.13}$$

It can be seen that the solution consists of two parts. The first part is the complimentary function and the time constants depend on the poles. The second part is the particular integral. The response rate depends on λ which is a property of the input. Equation (A.13) is a slightly generalized version of the Heaviside expansion theorem and is given by Perry (1982).

The full transient response of the system to the sinusoid

$$e_i(t) = E_i H(t) e^{j\omega t} \tag{A.14}$$

can be found from (A.13) by putting $\lambda = j\omega$. The square-wave response i.e. the response to the step input

$$e_i(t) = E_i H(t) \tag{A.15}$$

can be found by putting $\lambda = 0$ which leads to

$$\frac{e_o(t)}{E_i} = \sum_{j=1}^{n} \lim_{s \to p_j} \left\{ \frac{F(s)}{s} (s - p_j) \right\} e^{p_j t} + F(0). \tag{A.16}$$

The response to a delta function $e_i = E_\delta \delta(t)$ can be found by writing this as

$$e_i = E_\delta H(t) \lim_{q \to 0} \left\{ \frac{e^{-t/q}}{q} \right\} \tag{A.17}$$

which gives

$$\frac{e_o(t)}{E_i} = \sum_{j=1}^{n} \lim_{s \to p_j} \left\{ F(s)(s - p_j) \right\} e^{p_j t} + \lim_{q \to 0} (1/q) F(-1/q) e^{-t/q} \tag{A.18}$$

REFERENCES

Davis, M.R. and Davies, P.O.A.L. (1968), "The physical characteristics of hot-wire anemometers", ISVR Tech. Report 2, Institute of Sound and Vibration, Southampton University.

Miller, I.S., Shah, D.A. and Antonia, R.A. (1987), "A Constant Temperature Hot-wire Anemometer", J. Phys. E: Sci. Intsr. 20: 311-314.

Perry, A.E. (1982), "Hot-wire Anemometry", Oxford: Clarendon Press.

Perry, A.E. and Morrison, G.L. (1971), "A study of the Constant Temperature Hot-wire Anemometer", J. Fluid Mech. 47: 577-599.

Smits, A.J. and Perry, A.E. (1980), "The effect of varying resistance ratio on the behaviour of constant-temperature hot-wire anemometers", J. Phys. E: Sci. Instr. 13: 451-456.

Smits, A.J., Perry, A.E. and Hoffman, P.H. (1978), "The Response to Temperature Fluctuations of a Constant-current Hot-wire Anemometer", J. Phys. E: Sci. Instr. 11: 909-914

Watmuff, J.H. (1987), "Some Higher-order Effects in the Behaviour of Constant Temperature Hot-wire Anemometer Systems", ASME Symposium on Thermal Anemometry, Cincinnati, Ohio, June 1987.

Watmuff, J.H. (1989), "The effects of Feedback Amplifier Characteristics on Constant Temperature Hot-wire Anemometer Systems". Tenth Australasian Fluid Mechanics Conference, Melbourne, Australia, December, 1989.

Wood, N.B. (1975), "A method for determination and control of the frequency response of the constant-temperature hot-wire anemometer", J. Fluid Mech. 67: 769-86.

REPORT DOCUMENTATION PAGE

Form Approved
OMB No. 0704-0188

1. AGENCY USE ONLY *(Leave blank)*	2. REPORT DATE	3. REPORT TYPE AND DATES COVERED
	August 1994	Contractor Report

4. TITLE AND SUBTITLE

A High-Performance Constant-Temperature Hot-Wire Anemometer

5. FUNDING NUMBERS

NCC2-698

6. AUTHOR(S)

Jonathan H. Watmuff

7. PERFORMING ORGANIZATION NAME(S) AND ADDRESS(ES)

MCAT Institute
3933 Blue Gum Dr.
San Jose, CA 95127

8. PERFORMING ORGANIZATION REPORT NUMBER

A-94126

9. SPONSORING/MONITORING AGENCY NAME(S) AND ADDRESS(ES)

National Aeronautics and Space Administration
Washington, DC 20546-0001

10. SPONSORING/MONITORING AGENCY REPORT NUMBER

NASA CR-177645

11. SUPPLEMENTARY NOTES

Point of Contact: Jonathan H. Watmuff, Ames Research Center, MS 260-1, Moffett Field, CA 94035-1000; (415) 604-4150

12a. DISTRIBUTION/AVAILABILITY STATEMENT

Unclassified-Unlimited
Subject Category – 35

12b. DISTRIBUTION CODE

13. ABSTRACT ***(Maximum 200 words)***

A high-performance constant-temperature hot-wire anemometer has been designed based on a system theory analysis that can be extended to arbitrary order. A motivating factor behind the design was to achieve the highest possible frequency response while ensuring overall system stability. Based on these considerations, the design of the circuit and the selection of components is discussed in depth. Basic operating instructions are included in an operator's guide. The analysis is used to identify operating modes, observed in all anemometers, that are misleading in the sense that the operator can be deceived by interpreting an erroneous frequency response. Unlike other anemometers, this instrument provides front panel access to all the circuit parameters which affect system stability and frequency response. Instructions are given on how to identify and avoid these rather subtle and undesirable operating modes by appropriate adjustment of the controls. Details, such as fabrication drawings and a parts list, are provided to enable the instrument to be constructed by others.

14. SUBJECT TERMS

Frequency response, Instability, Printed circuit board

15. NUMBER OF PAGES

91

16. PRICE CODE

A05

17. SECURITY CLASSIFICATION OF REPORT	18. SECURITY CLASSIFICATION OF THIS PAGE	19. SECURITY CLASSIFICATION OF ABSTRACT	20. LIMITATION OF ABSTRACT
Unclassified	Unclassified		